# EFFECTS OF SUBSURFACE DAMAGE ON THE PHOTOLUMINESCENCE OF ZnO

By

DAVID WILLIAM HAMBY

Bachelor of Science
Mechanical Engineering
Oklahoma State University
Stillwater, Oklahoma
1991

Master of Science
Mechanical Engineering
Virginia Polytechnic Institute and State University
Blacksburg, Virginia
1993

Submitted to the Faculty of the
Graduate College of the
Oklahoma State University
in partial fulfillment of
the requirements for
the Degree of
DOCTOR OF PHILOSOPHY
December, 2003

EFFECTS OF SUBSURFACE DAMAGE ON THE

PHOTOLUMINESCENCE OF ZnO

Thesis Approved:

Don A. Lucca

Thesis Advisor

Dean of the Graduate College

ACKNOWLEDGMENTS

I would like to genuinely thank Dr. D. A. Lucca for his guidance and support. I am grateful for the opportunity to have worked in his lab on exciting and interesting problems. I would also like to thank him for his encouragement to set high goals and his unending help to achieve those goals. His confidence in me will serve as a constant inspiration. A special thank you is extended to Dr. L. H. Robins and Dr. S. W. S. McKeever for their helpful comments regarding the design and specifications of the photoluminescence (PL) system used in this study. Many thanks to Mr. G. Cantwell and Mr. B. Haskins for their hard work and contributions to this work. I wish to thank each of my committee members -Dr. C. E. Price, Dr. E. A. Misawa and Dr. S. W. S. McKeever- for their helpful comments and commitment to this work. I would also like to thank Dr. M. Nastasi and Dr. J. -K. Lee for their contributions to this research. A thank you is also extended to Dr. Cheville for his assistance with our research and for the use of his plasma cleaner in our hydrogen-treated ZnO work.

A genuine thank you is extended to Robert W. and Jean M. Schuetz for their generous financial support via the Distinguished Graduate Fellowship program. It is a tremendous honor to receive such a fellowship and I will always be grateful to them for their support. I would like to thank Matt Klopfstein for his help with all of the PL experiments and his willingness to discuss the entire spectrum of PL topics. I would also like to thank him for his help in the preparation of this document. A thank you is also extended to each of the members of the Ultraprecision Surfaces Laboratory, both past and present, for their participation in this research. I wish to acknowledge Los Alamos National Lab, Eagle-Picher Technologies, the National Science Foundation and the Oklahoma Center for the Advancement of Science and Technology for their support.

I would like to extend a most sincere thank you to my wife, Jennifer, for her patience, support, encouragement, and for her understanding of the long hours and difficult schedule. I would also like to thank her for all of her hard work, without which none of this would be possible. Additionally, I would like to say thank you to her and my daughter, Emily, for their inspiration and love. This achievement is ours not mine.

TABLE OF CONTENTS

1 **Introduction** 1

1.1 Motivation . . . . . 2

1.2 Literature Review . . . . . 4

1.2.1 Characterization of Subsurface Damage in Semiconductors . . . . . 4

1.2.2 Luminescence Studies of ZnO . . . . . 10

1.3 Research Overview . . . . . 16

1.3.1 Objective . . . . . 16

1.3.2 Research Plan . . . . . 16

2 **Photoluminescence of Semiconductors** 17

2.1 Band Structure . . . . . 18

2.2 Radiative and Nonradiative Recombination . . . . . 19

2.3 Excitons . . . . . 21

2.3.1 Free-exciton Luminescence . . . . . 23

2.3.2 Bound-exciton Luminescence . . . . . 27

2.3.3 Exciton-electron Luminescence . . . . . 29

2.3.4 Hot-exciton Luminescence . . . . . 30

2.3.5 Exciton-polariton Theory . . . . . 32

2.4 Phonon-assisted Luminescence . . . . . 34

2.4.1 LO Phonon-assisted Free-exciton Luminescence . . . . . 35

2.4.2 Temperature-dependent LO Phonon-assisted Free-exciton Luminescence . . . 37

2.5 Donor-acceptor-pair Luminescence . . . . . 37

2.6 Deep-level Luminescence . . . . . 39

3 **Experimental** 40

3.1 ZnO Structure and Growth . . . . . 40

3.2 Sample Preparation . . . . . 41

3.3 Photoluminescence System . . . . . 42
3.3.1 Laser . . . . . 43
3.3.2 Spectrometer . . . . . 43
3.3.3 Charge Coupled Device (CCD) Array . . . . . 44
3.3.4 Cryostat . . . . . 44
3.4 Estimated Depth of Investigation Using PL . . . . . 44

**4 Results and Discussion** **45**
4.1 Etched ZnO . . . . . 45
4.2 Chemomechanically Polished ZnO . . . . . 52
4.2.1 Sample-to-sample Variation of the 4.2 K PL . . . . . 53
4.2.2 Aging Effects . . . . . 54
4.2.3 Temperature-dependent Exciton Luminescence . . . . . 54
4.2.4 Comparison of Low Temperature PL from Etched and Chemomechanically Polished Surfaces . . . . . 60
4.2.5 Comparison of RT PL from Etched and Chemomechanically Polished Surfaces 66
4.3 Mechanically Polished ZnO . . . . . 67
4.3.1 Hot-exciton Luminescence . . . . . 67
4.3.2 Mechanical Damage Induced Luminescence . . . . . 70
4.3.3 Comparison of RT PL from Mechanically Polished and Chemomechanically Polished Surfaces . . . . . 79
4.4 Hydrogen-treated ZnO . . . . . 82
4.4.1 Hydrogen-Implanted ZnO . . . . . 82
4.4.2 Hydrogen/Argon Plasma-treated ZnO . . . . . 83
4.4.3 He-implanted ZnO . . . . . 84

**5 Conclusions and Possible Future Work** **86**
5.1 Conclusions . . . . . 86
5.2 Possible Future Work . . . . . 88

**Bibliography** **90**

**A ZnO Properties** **110**

**B RT PL of As-grown ZnO** **111**

**C PL of Ion Channeled ZnO** **112**

**D RT PL of Etched CdS** **113**

**E Operation of PL System** **114**

E.1 $Ar^+$ Laser . . . . . 114

E.2 Monochromator . . . . . 115

E.3 Cryostat . . . . . 117

E.4 Low Temperature PL Procedure . . . . . 119

**F Arrhenius Plot** **121**

**G FX Line Broadening** **122**

G.1 Lorentzian Lineshape . . . . . 122

G.2 Gaussian Lineshape . . . . . 123

**H Temperature Dependent LO Phonon-assisted FX Luminescence** **125**

H.1 One LO Phonon-assisted FX Luminescence . . . . . 125

H.2 Two LO Phonon-assisted FX Luminescence . . . . . 126

**I Photoelectrochemical Etching** **128**

I.1 Literature Review . . . . . 128

I.2 Preliminary Results . . . . . 131

**J PL of Si Implanted $SiO_2$** **134**

J.1 Literature Review . . . . . 134

J.2 Preliminary Results . . . . . 135

**K List of Abbreviations** **136**

LIST OF TABLES


4.1 Summary of 4.2 K PL peak assignments for etched (0001) ZnO . . . . . . . . . . . . . . 49

4.2 Comparison of FX (A) values from the literature . . . . . . . . . . . . . . . . . . . . . 56

A.1 ZnO material properties . . . . . . . . . . . . . . . . . . . . . . . . . . . . . . . . . . 110

LIST OF FIGURES

2.1 Simplified direct band gap showing some electronic energy transitions which can result in photoluminescence, from [109] . . . . . 20
2.2 Some of the possible Auger effect recombination mechanisms, after [100] . . . . . 21
2.3 Exciton energy levels and excited states shown on simplified energy diagram for direct band gap semiconductor, after [100]. . . . . 22
2.4 Exciton dispersion on two-particle diagram, after [101]. Shown are exciton dispersion curves for $n = 1, 2, \infty$, where $n = \infty$ represents the bottom of the conduction band. Also shown is a photon dispersion curve ($\hbar ck$) superimposed on the exciton model. . 23
2.5 Effect of line broadening on measured PL position of free exciton peak, after [102]. . 25
2.6 Hot exciton model, after [136]. Shown is (a) indirect photon absorption, (b) exciton kinetic energy relaxation, and (c) phonon-assisted exciton luminescence. . . . . 30
2.7 Resonant Raman scattering model, after [136]. Shown is the phonon scattering of photons. As a result, the photon is not absorbed in the crystal. . . . . 31
2.8 Polariton dispersion curves (solid lines), after [102]. Also shown is the free-exciton dispersion (dotted line) assuming no radiation field superimposed on a photon dispersion (dotted line) curve. The interaction of excitons and photons results in the upper polariton branch (UPB) and the lower polariton branch (LPB). . . . . 33
2.9 Polariton dispersion showing range of energy ($\Delta E_m$) for mixed photon and exciton states. . . . . 34
2.10 Exciton dispersion model depicting a 1LO phonon-assisted recombination, after [154]. The initial state is given by ($\hbar K_i$). Whereas the resulting energy of the photon emission is decreased by the LO phonon energy, its final energy is dependent on the amount of initial free-exciton kinetic energy. . . . . 36
2.11 Simplified energy band gap depicting donor-acceptor-pair (DAP) recombination. . . 38

2.12 Simplified energy diagram illustrating some of the possible electronic transitions leading to the observation of DL luminescence. Shown are three possible recombination paths resulting in three different photon energies, $E_{DL1}$, $E_{DL2}$, and $E_{DL3}$. . . . . . . 39

3.1 Crystal structure (a) and stacking sequence of atoms along the c axis (b) for wurtzite ZnO, from [101]. . . . . . . . . . . . . . . . . . . . . . . . . . . . . . 41

3.2 PL System Schematic . . . . . . . . . . . . . . . . . . . . . . . . . . . . . . 43

4.1 4.2 K PL of etched (0001) ZnO. . . . . . . . . . . . . . . . . . . . . . . . . 46

4.2 4.2 K PL of etched (0001) ZnO. Inset illustrates detailed free A-valence exciton, FX (A), and lower A-valence polariton, LPB (A), emission. . . . . . . . . . . . . . 46

4.3 4.2 K PL of etched (0001) ZnO. Inset illustrates detailed emission from 3.35 to 3.37 eV. PL in this energy range is dominated by the collapse of excitons bound to defect pair complexes which simulate neutral donors [82]. . . . . . . . . . . . . . . . . . 47

4.4 4.2 K PL of etched (0001) ZnO. Inset illustrates detailed emission from 3.30-3.35 eV. PL in this energy range has been attributed to two-electron satellites of bound excitons [82,87]. . . . . . . . . . . . . . . . . . . . . . . . . . . . . . . . . 48

4.5 4.2 K PL of etched (0001) ZnO. Inset illustrates detailed emission from 3.10-3.30 eV. The lower energy PL in this range is typically from DAP recombination or phonon replicas of higher energy transitions. . . . . . . . . . . . . . . . . . . . . . . . 48

4.6 Comparison of a 4.2 K PL spectrum from an etched (0001) ZnO sample to that collected from the same sample about ten weeks after the initial characterization. Inset shows detail of exciton emission. . . . . . . . . . . . . . . . . . . . . . . . 50

4.7 Comparison of 4.2 K PL spectra collected from the two polar faces of the same sample. Inset shows detail of exciton emission. . . . . . . . . . . . . . . . . . . . . . . . 51

4.8 RT PL from etched (a) (0001) and (b) (000$\bar{1}$) ZnO. Shown is free-exciton (FX) luminescence at 3.26 eV, a second clearly resolved peak at 3.12 eV, and deep level (DL) emission at about 2.5 eV. . . . . . . . . . . . . . . . . . . . . . . . . . . . . 51

4.9 Temperature dependence of FX-2LO and S peaks. Also shown is the predicted temperature dependence of (a) FX, (b) FX-2LO, and (c) exciton-electron luminescence. 52

4.10 Comparison of the 4.2 K PL spectra for (0001) chemomechanically polished and (0001) etched ZnO. Inset shows detail of exciton emission. . . . . . . . . . . . . . . . . 53

4.11 Comparison of the 4.2 K PL from two different (0001) ZnO samples prepared by chemomechanical polishing. . . . . . . . . . . . . . . . . . . . . . . . . . . . . 54

4.12 Comparison of an initial 4.2 K PL spectrum from a chemomechanically polished (0001) ZnO sample to one collected seven months after the initial characterization. Seven months aging in atmospheric conditions is seen to significantly affect the bound-exciton luminescence spectrum. . . . . . . . . . . . . . . . . . . . . . . . . . . . . . 55

4.13 20 K PL spectrum of (0001) ZnO. Six bound-exciton peaks are identified from 3.358-3.368 eV. $LPB_A$ (3.374 eV) and FX (A) (3.378 eV) peaks are also shown. . . . . . . . 56

4.14 Photoluminescence spectra of (0001) ZnO at selected temperatures. Zero-, one-, and two-LO phonon-assisted FX (A) transitions are indicated by arrows for the 77 K spectrum and labeled as FX (A), FX (A)-1LO and FX (A)-2LO, respectively. . . . . 57

4.15 Temperature-dependent exciton peak position for (0001) ZnO. Individual FX (A) (▲) and FX (B) (△) peaks are not resolvable above 150 K. The 300 K FX (A) peak position (■) is based on the band gap energy of ZnO (3.37 eV (see Ref. [17])). The FX (A) data were fit using (MW). Also shown are the measured energy positions for the 1LO-(▽) and 2LO-(□) phonon assisted FX (A) transitions and the predicted temperature dependence for both peaks (see Ref. [102]). The 3.364 eV bound-exciton peak ($D^0X$) (∘) is not observed at temperatures above 150 K. . . . . . . . . . . . . . 59

4.16 Natural logarithm of the normalized total intensity (peak intensity times FWHM) of the 3.364 eV $D^0X$ peak as a function of 1/T. The thermal activation energy ($E_A$) was determined to be approximately 14 meV. Inset: Temperature dependence of FX (A) to $D^0X$ intensity ratio. . . . . . . . . . . . . . . . . . . . . . . . . . . . . . . . . . . 60

4.17 77 K PL spectra for (a) chemomechanically polished and (b) wet etched (0001) ZnO samples. Spectra are normalized using the 3.360 $D^0X$ peak. . . . . . . . . . . . . . . . 61

4.18 100 K PL spectra from (a) chemomechanically polished and (b) wet etched (0001) ZnO. Spectra are normalized using the 3.360 $D^0X$ peak. . . . . . . . . . . . . . . . . . . . . 62

4.19 100 K PL spectrum from chemomechanically polished (0001) ZnO (solid line). Shown are the predicted energies and lineshapes for both FX-1LO (dashed line) and FX-2LO (dotted line) transitions using Eqns. (2.9) and (2.10), respectively. . . . . . . . . . . 63

4.20 100 K PL spectrum from etched (0001) ZnO (solid line). Shown are the predicted energies and lineshapes for both FX-1LO (dashed line) and FX-2LO (dotted line) transitions using Eqns. (2.9) and (2.10), respectively. Also shown is the measured energy difference (55 meV) between the $D^0X$ and $D^0X$-1TO peaks which is consistent with the reported TO phonon energy of 51.2 meV for ZnO [110] . . . . . . . . . . . . 64

4.21 Temperature-dependent PL of experimentally observed FX-1LO peak for chemomechanically polished (0001) ZnO. Shown are theoretical predictions for (a) FX(E) from Ref. [171], (b) FX-1LO(E) using Eqn. (2.12), (c) $D^0$X-1TO(E) assuming a temperature independent TO phonon energy of 51 meV and the experimentally observed temperature dependence of the FX-1LO peak. . . . . . . . . . . . . . . . . . . . . . . . 64

4.22 Temperature-dependent PL of experimentally observed $D^0$X-1TO peak for etched (0001) ZnO. Shown are theoretical predictions for (a) FX(E) from Ref. [171], (b) FX-1LO(E) using Eqn. (2.12), (c) $D^0$X-1TO(E) assuming a temperature independent TO phonon energy of 51 meV, (d) exciton-electron predicted energy from Eqn. (2.7) with $\gamma$=7.74. Also shown is the temperature dependence of the FX-1LO peak observed at temperatures between about 120-150 K. . . . . . . . . . . . . . . . . . . . . . . . . . 65

4.23 Comparison of 115 K and 120 K PL spectra for etched (000$\bar{1}$) ZnO. . . . . . . . . . 66

4.24 Normalized RT PL intensities for (a) etched (000$\bar{1}$), (b) etched (0001), (c) polished (000$\bar{1}$) and (d) polished (0001) ZnO surfaces. All spectra have been normalized by their FX peak intensity. . . . . . . . . . . . . . . . . . . . . . . . . . . . . . . . . . . 67

4.25 4.2 K PL of 1 $\mu$m mechanically polished (a) (0001) and (b) (000$\bar{1}$) ZnO. In addition to donor-bound exciton ($D^0$X) and two-electron satellite ($D^0X_{n=2}$) emission, three hot-exciton peaks are observed at 3.458 (HX-1LO), 3.385 (HX-2LO) and 3.312 (HX-3LO) eV. The laser excitation energy is 3.532 eV. . . . . . . . . . . . . . . . . . . . . . . . 68

4.26 PL of 1 $\mu$m mechanically polished (0001) ZnO for the following temperature: (a) 4.2 K, (b) 100 K, (c) 200 K and (d) 300 K. Inset: Normalized PL intensity of HX-2LO emission for (□) (0001) and (▲) (000$\bar{1}$) as a function of temperature. . . . . . . 69

4.27 4.2 K PL for (0001) ZnO. Shown are spectra for samples prepared by (a) 1 $\mu$m diamond abrasive mechanical polishing and (b) chemomechanical polishing. Each spectrum is normalized by the bound-donor exciton ($D^0$X) peak at 3.364 eV (not shown). . . . . 70

4.28 4.2 K PL for (000$\bar{1}$) ZnO. Shown are spectra for samples prepared by (a) 1 $\mu$m diamond abrasive mechanical polishing and (b) chemomechanical polishing. Each spectrum is normalized by the bound-donor exciton ($D^0$X) peak at 3.364 eV (not shown). . . . . 71

4.29 4.2 K PL spectra of (a) mechanically polished (0001) and (000$\bar{1}$) ZnO and (b) chemomechanically polished (0001) ZnO. Spectra in (a) are normalized using the 3.364 eV $D^0$X peak. Insets for both (a) and (b) show detail of (0001) exciton emission. . . . 73

4.30 Temperature-dependent PL spectra of (0001) ZnO prepared by 1 $\mu$m diamond abrasive mechanical polishing. Shown are spectra recorded at 4.2, 10, 25, 50 and 77 K. Each spectrum is normalized by its maximum intensity. . . . . . . . . . . . . . . . . 74

4.31 Temperature dependence of the 3.211 eV peak position for both (0001) (□) and (000$\bar{1}$) (◇) surfaces prepared by 1 $\mu$m diamond abrasive mechanical polishing. Also shown is the temperature dependence of the 3.364 eV $D^0X$ peak for the (0001) (△) and (000$\bar{1}$) (▼) mechanically polished samples and the MW fit of the free A exciton (FX (A)) temperature-dependent peak position [171] for a chemomechanically polished (0001) ZnO sample. . . . . . . . . . . . . . . . . . . . . . . . . . . . . . . . . . 75

4.32 Natural logarithm of the normalized total intensity (peak intensity times FWHM) of the 3.211 eV peak as a function of 1/T for the (0001) Zn-terminated 1 $\mu$m mechanically polished surface. The inset shows the same analysis for the (000$\bar{1}$) O-terminated 1 $\mu$m mechanically polished surface. A fit of the linear portion of the data (first four data points) yields thermal activation energies for the (0001) and (000$\bar{1}$) surfaces of 52 and 54 meV, respectively. . . . . . . . . . . . . . . . . . . . . . . . . . . . . . . . 76

4.33 4.2 K PL of three different (0001) 1 $\mu$m mechanically polished samples normalized by the $D^0X$ peak at 3.364 eV (not shown). Variation in 3.211 eV peak intensity relative to its $D^0X$ intensity suggests that it may be related to damage present in the crystal. Curve (a) is from a sample that had been polished twice prior to the PL measurement. Inset: Enlarged view of (c). Dotted lines are from the deconvolution of (b) using Lorentzian lineshapes and illustrate the possibility that both the 3.211 and 3.22 eV peaks are present in the PL of 1 $\mu$m mechanically polished (0001) ZnO. 77

4.34 4.2 K PL of (0001) ZnO. Shown are PL from samples prepared by (a) 1 $\mu$m diamond abrasive mechanical polishing, (b) 1/4 $\mu$m diamond abrasive mechanical polishing, and (c) chemomechanical polishing. Each spectrum is normalized by the $D^0X$ peak at 3.364 eV (not shown). Inset: Enlarged view of (b) and (c). Dotted lines are from the deconvolution of (b) using Lorentzian lineshapes and illustrate the possibility that both the 3.211 and 3.22 eV peaks are present in the PL of 1/4 $\mu$m mechanically polished (0001) ZnO. . . . . . . . . . . . . . . . . . . . . . . . . . . . . . . . . . 78

4.35 4.2 K PL of $(000\bar{1})$ ZnO. Shown are PL from samples prepared by (a) 1 $\mu$m diamond abrasive mechanical polishing, (b) 1/4 $\mu$m diamond abrasive mechanical polishing, and (c) chemomechanical polishing. Each spectrum is normalized by the $D^0X$ peak at 3.364 eV (not shown). Inset: Enlarged view of (b) and (c). No peak was observed at 3.211 eV for (b) or (c). . . . . . 79
4.36 Relative PL intensities for polished surfaces, (a) chemomechanically polished-O face, (b) chemomechanically polished-Zn face, (c) mechanically polished surfaces for comparison. . . . . . 80
4.37 Normalized PL intensities for mechanically polished surfaces, (a) 1/4 $\mu$m-O face, (b) 1/4 $\mu$m-Zn face,(c) 1 $\mu$m-O face, (d) 1 $\mu$m-Zn face. . . . . . 81
4.38 4.2 K PL spectra for: (a) unimplanted and (b) H-implanted (0001) ZnO. . . . . . 83
4.39 4.2 K PL spectra for the sample: (a) before and (b) after plasma exposure. . . . . . 84
4.40 Comparison of 4.2 K PL spectra for H-implanted, He-implanted, and untreated ZnO. The spectra are normalized using the 3.364 eV peak. . . . . . 85

B.1 Comparison of RT PL from as-grown (0001) and chemomechanically polished (0001) ZnO . . . . . . 111

C.1 Comparison of RT PL for channeled and chemomechanically polished $(000\bar{1})$ ZnO. . . 112

D.1 RT PL comparison between etched (0001) ZnO and etched (0001)-oriented CdS. . . 113

H.1 Temperature dependent FX, FX-1LO and FX-2LO peak positions for 0-300 K. The FX curve is from Ref. [171], the FX-1LO and FX-2LO curves are from Eqns. (H.4) and (H.7), respectively. . . . . . 127

I.1 PEC setup . . . . . . 132

J.1 RT PL comparison of four Si implanted, annealed $SiO_2$ samples. . . . . . 135

LIST OF SYMBOLS

| | |
|---|---|
| $a$ | Lattice parameter |
| BX | Bound-exciton transition |
| $c$ | Speed of light in vacuum ($2.998 \times 10^8$ m/s);<br>lattice parameter |
| $\mathbf{c}$ | Optical axis of hexagonal (wurtzite) crystal |
| $D^0$ | Neutral donor |
| $D^0X$ | Neutral-donor-bound-exciton transition |
| $(D^0X_{n=2})_{1LO}$, TES-1LO | One LO phonon replica of a two-electron<br>satellite for neutral-donor-bound exciton luminescence |
| $D^0X$-1TO | One TO phonon-assisted transition of neutral-donor-bound-exciton |
| $E$ | Energy; modulus of elasticity |
| $\mathbf{E}$ | Electric field vector |
| $E_0$ | Energy of band gap at 0 K |
| $E_A$ | Thermal activation energy corresponding to ionization<br>of electron (hole) from shallow donor (acceptor) in<br>DAP transition or ionization of exciton from donor or acceptor |
| $E_a$ | Energy of acceptor level in direct band gap semiconductor |
| $E_b$ | Exciton binding (localization) energy to defect |
| $E_c$ | Energy of the bottom of the conduction band |
| $E_d$ | Energy of donor level in direct band gap semiconductor;<br>energy of defect/impurity level |
| $E_D$ | Binding energy of electron to donor ion |
| $E_{DAP}$ | Energy of donor-acceptor-pair recombination |
| $E_{DL}$ | Energy from deep level radiative recombination of EHP |
| $E_{ex}$ | Exciton binding energy |
| $E_g$ | Energy of direct band gap semiconductor |
| $E_{kin}$ | Kinetic energy of free exciton |

| | |
|---|---|
| $E_L$ | Longitudinal exciton energy; energy of laser |
| $E_{LT}$ | Splitting energy between longitudinal and transverse excitons, $E_{LT} = E_L - E_T$ |
| $E_n$ | Excited energy levels for donor electrons |
| $E_T$ | Transverse exciton energy |
| $E_v$ | Energy of top of the valence band |
| $E_x$ | Energy of free exciton |
| EHP | Electron-hole pair |
| $F(E_{kin})$ | Distribution of free excitons with kinetic energy |
| FX | Free-exciton transition |
| FX-1LO | One LO phonon-assisted transition of free exciton |
| FX-2LO | Two LO phonon-assisted transition of free exciton |
| FX(A) | Energy of A valence band free exciton luminescence |
| $G$ | Shear modulus |
| HX | Hot exciton transition |
| HX-1LO | Hot-exciton transition separated from the excitation laser energy by an amount equal to the energy of one LO phonon |
| HX-2LO | Hot-exciton transition separated from the excitation laser energy by an amount equal to the energy of two LO phonons |
| HX-3LO | Hot-exciton transition separated from the excitation laser energy by an amount equal to the energy of three LO phonons |
| $h$ | Planck's constant ($4.135 \times 10^{-15}$ eV s) |
| $\hbar$ | Normalized Planck's constant ($h/2\pi$) |
| $K$ | Exciton wavevector |
| $k$ | Photon wavevector |
| $k_B$ | Boltzmann's constant ($8.62 \times 10^{-5}$ eV/K) |
| $L_m$ | Lineshape function for phonon-assisted free exciton luminescence ($m = 1, 2$) |
| $\mathrm{LPB}_A$, LPB (A) | Luminescence from lower polariton branch of the A valence band |
| $M$ | Sum of electron and hole effective masses |
| $m$ | Free electron rest mass ($9.11 \times 10^{-31}$ kg) |
| $n$ | Excited levels for free excitons (n=1,2,...,$\infty$); |

| | |
|---|---|
| | index of refraction |
| $P_m$ | Radiative probability for phonon-assisted free exciton recombination ($m = 1, 2$) |
| $q, e$ | Electronic charge ($1.60 \times 10^{-19}$ C) |
| $R$ | Distance between ionized donor and acceptor in crystal |
| $S(\hbar\omega - E_x)$ | Lineshape function of absorption peak |
| $T$ | Temperature (K) |
| TES, $D^0X_{n=2}$ | Two-electron satellite of bound-exciton transition |
| $U, V, s, \theta$ | Fitting parameters for Manoogian-Woolley equation |
| $\alpha, \beta$ | Fitting parameters for Varshni equation |
| $\alpha_L$ | Mean thermal expansion coefficient |
| $\Gamma$ | Full-width at half-maximum of absorption peak |
| $\gamma$ | Coefficient in exciton-electron model |
| $\Delta E_m$ | Range of energies for which excitons and photons are better described as polaritons |
| $\delta$ | Energy redshift of free exciton luminescence relative to the actual transition energy as measured by absorption |
| $\epsilon_s$ | Static dielectric constant |
| $\epsilon_0$ | Permittivity of free space ($8.85 \times 10^{-12}$ F/m) |
| $\Theta$ | Fitting parameter for both the modified Bose-Einstein and Pässler equations |
| $\theta_D$ | Debye Temperature (K) |
| $\nu$ | Frequency |
| $\tau$ | Exciton lifetime |
| $\omega$ | Frequency ($\omega = 2\pi\nu$) |
| $\hbar\omega_{LO}$,$h\nu_{LO}$,$E_{LO}$ | Energy of longitudinal optical phonon |
| $(\hbar\omega)^{Ex-El}$ | Energy of exciton-electron interaction spontaneous luminescence peak |

# Chapter 1

# Introduction

The blue-light-emitting diode (LED) has been described as "the holy grail of opto-electronics" by Waguih Ishak, an optics research director at Hewlett-Packard [1]. Short-wavelength (blue, UV) light emitters are a necessary precursor to the development of white-light LEDs [2] –anticipated as potential replacements for incandescent, fluorescent and halogen bulbs– with a potential global market estimated at around $12 billion [3]. While GaN-based materials have had some commercial success in short-wavelength light-emitting applications, the need for high-quality scalable native substrates has precluded further development of high-power, high frequency devices [4]. ZnO has been proposed as a potential substrate for GaN-based devices due to the availability of high-quality 50 mm wafers and its minimal lattice mismatch (about 2%) to GaN [4]. Additionally, with the recent announcement of *p*-type ZnO layers [5] and its superior material properties (Appendix A) compared to GaN, homoepitaxial ZnO is currently being pursued as an alternative to GaN as the blue-light-emitting material [4]. The focus of this study, however, will be limited to the continued development of ZnO substrates. This work seeks to contribute to a fundamental understanding of the effect of crystalline defects resulting from ultrafine finishing processes on the optical performance of bulk, hexagonal (wurtzite) ZnO. This understanding will aid in identifying the processing conditions which show promise for producing high-quality substrates for use in the homoepitaxial growth of ZnO or the heteroepitaxial growth of GaN thin films.

This introductory chapter is organized into three sections with the first section providing a more detailed motivation for this study, namely, the need for development of epitaxy-ready ZnO substrates. The second section provides a review of the literature regarding: 1) subsurface damage studies of semiconductors and 2) luminescence studies of ZnO. The third section presents the objective of this study and a brief overview of the research plan.

## 1.1 Motivation

The announcement of $p$-type doping of ZnO epilayers [5] has led to a tremendous research effort to develop ZnO/ZnO based short wavelength light emitters in an attempt to capture some of the estimated $3 billion potential market for blue light emitting diode (LED) and laser diode (LD) applications [1]. The potential for ZnO in LD applications has been demonstrated by several researchers with their observations of room temperature (RT) lasing from ZnO thin films using optical excitation [6–10], where the principal lasing mechanism was reported to be exciton-exciton interaction. Recently it has been shown that low power threshold (2 mW) room temperature polariton lasers can be realized with ZnO-based microcavities [11]. These results are encouraging and clearly demonstrate the potential of ZnO for short wavelength light emitters, however much work remains. Before considering some of the current research issues in the development of ZnO-based devices, a brief comparison of ZnO to existing technology for blue LEDs and LDs, namely GaN, is provided. ZnO has many advantages when compared to GaN and may serve as an excellent alternative for short wavelength light emitters and other applications. One significant advantage is the availability of large bulk single crystal ZnO substrates for homoepitaxial growth. By comparison, all of the GaN-based LEDs are heteroepitaxially grown on SiC or sapphire substrates due to the lack of commercially available large bulk single crystal GaN [12]. Lattice mismatch and differences in thermal expansion coefficients between the GaN epilayer and either the SiC (3.3% lattice mismatch [4]) or sapphire (14.8% mismatch [4]) substrate yield very high dislocation densities that significantly reduce electron mobility, doping efficiency and the lifetime of the subsequent devices [12]. Threading dislocation densities as high as $10^9$ to $10^{10}$ cm$^{-2}$ have been reported for GaN/(SiC or sapphire) systems [13]. Availability of large bulk single crystal ZnO presents the opportunity to grow ZnO/ZnO devices with low defect densities and subsequently long lifetime (typically, LED lifetimes are targeted to be greater than 10,000 hrs). The significance of homoepitaxial growth for thin films is best illustrated by the work of Kamp et al. [13] who demonstrated that homoepitaxy thin films exhibited dislocation densities approximately six orders of magnitude lower than those prepared with heteroepitaxy methods. Material property advantages of ZnO include a higher exciton binding energy (60 meV) than GaN (28 meV) and a higher optical gain (300 cm$^{-1}$) than GaN (100 cm$^{-1}$) [14]. A large exciton binding energy results in excitons which are stable at elevated temperatures [15]. As mentioned previously, Bagnall et al. [6] have reported the room temperature optically pumped lasing of ZnO thin films. Their results suggest that laser emission threshold intensities for ZnO compare favorably with GaN. Specifically, ZnO has a room temperature lasing threshold that ranges from

40-240 kW/cm$^2$, whereas the room temperature threshold for GaN is greater than 400 kW/cm$^2$ [16]. Because ZnO is one of the hardest materials in the II-VI compound family, degradation of the material due to the generation of dislocations during device operation is thought to be minimal [17]. With its large bond strength, ZnO also ensures a large damage threshold for laser irradiation [18]. In addition to its potential as an efficient, low threshold, excitonic blue laser, ZnO also shows promise for flat panel displays, surface acoustic wave (SAW) devices and oxygen gas sensors [19]. ZnO has also been shown to be more resistant than GaN to radiation damage [20] and therefore a better potential candidate for space applications [21]. While ZnO appears to have many advantages when compared to GaN, several research issues remain. For one, realization of a commercially viable alternative to GaN-based devices requires the development of epitaxy-ready (epi-ready) ZnO substrates for homoepitaxial growth. The successful growth of defect-free epitaxial layers, and subsequently long-lasting devices, depends entirely on a clean, well-defined and defect-free substrate surface [22]. Epi-ready substrates have surfaces which enable high quality film growth without any prior chemical pretreatment [23]. Hong et al. [24] reported that epi-ready (001) GaAs substrates were critical to achieving the 2D layer-by-layer growth of ZnSe thin films and subsequent suppression of stacking faults that are detrimental to device performance. Epi-ready substrates have also been reported for InP [23]. The potential for epi-ready ZnO substrates is not limited to ZnO/ZnO systems. ZnO has also been proposed as an alternative substrate for the growth of GaN thin films due to its small lattice mismatch (about 2% [4]) [25, 26]. In either case, successful epitaxy requires substrates with clean, smooth surfaces and minimal near surface damage resultant from finishing processes.

While a clean, smooth surface may be an obvious prerequisite for high quality film growth, the detrimental effect of subsurface damage in the substrate, resulting from ultrafine finishing processes such as polishing, is not so apparent. Caldwell et al. [27] examined the effects of substrate polishing on subsequent device performance and reported the presence of "buried defects" associated with polishing of the substrate negatively influenced the epitaxial layers and resulting devices. Using TEM, Ponce et al. [28] were able to demonstrate the presence of dislocations in a GaN epilayer originating from dislocation loops in the near surface of a mechanically polished substrate. Tournie et al. [29] also point to the critical nature of substrate preparation and its effect on the photoluminescence (PL) properties of the subsequently grown thin film. Reports on the successful growth of GaN epilayers using mechanically polished GaN substrates point to the need for additional pregrowth steps, such as chemically assisted ion beam etching (CAIBE) [30] or reactive ion etching [31], to remove the subsurface damage due to polishing and to approximate epi-ready surfaces. In contrast, ZnO has a well-established chemomechanical polishing process [21]. Whereas this process is sufficient

for surface smoothness (with typical rms surface roughness values less than 1 nm [32]), it requires modifications to the current process parameters (e.g., slurry pH, slurry constituents, etc.) to further minimize the subsurface damage introduced during polishing. As an aside, the use of wet etching as a final finishing process to remove the subsurface damage in the polished substrate is precluded by the introduction of etch pits. Therefore, chemomechanical polishing appears to be a necessary final ultrafine finishing process for ZnO substrates. Central to proper selection of polishing parameters (and improved polishing techniques) and thus successful development of epi-ready ZnO substrates is the need to characterize the subsurface damage in a rapid, inexpensive, reliable and nondestructive manner. The fundamental aim of this research is to characterize the effects of near-surface damage, resulting from ultrafine finishing processes, on the PL of ZnO substrates.

## 1.2 Literature Review

The following review is separated into two parts: 1) characterization of subsurface damage in semiconductors using various techniques including PL and 2) luminescence studies of ZnO. The former is important for demonstrating the breadth of research that has been conducted regarding subsurface damage in semiconductors. It is also intended to convey the usefulness of PL as a tool for characterizing subsurface damage in semiconductors. The latter illustrates that while research on the luminescence of ZnO is extensive there is very little information regarding the effects of near surface damage on the PL of ZnO substrates.

### 1.2.1 Characterization of Subsurface Damage in Semiconductors

Several characterization techniques have been used to assess subsurface damage in semiconductors resulting from finishing processes. The following is a collection of results from some of those techniques reported in the literature. While this review will focus primarily on the use of luminescence techniques such as CL and PL to characterize the near surface damage in semiconductors resulting from polishing, it is useful to first examine other possible techniques and discuss observations from these methods to better understand the types of damage associated with final finishing processes. Many of these techniques are costly and destructive; nevertheless they provide a detailed assessment of the nature of the subsurface damage in single crystalline materials introduced by polishing.

Transmission electron microscopy (TEM) has provided information for both the nature and extent of subsurface damage in single crystal materials resulting from polishing. Black et al. [33] in an

extensive investigation of polished (0001) sapphire substrates used TEM in conjunction with polarized light microscopy, X-ray diffraction topography and Raman spectroscopy in an effort to develop noninvasive methods for the characterization of subsurface damage of high performance optics. No details regarding the polishing procedure were given. From TEM results, it was reported that the "damaged layer" of the polished substrate exhibited a network of dislocation half loops with no observable cracks extending to about 100 nm below the surface. By comparing the results of each of the techniques listed above with TEM results, it was determined that Raman spectroscopy showed the most promise for the relative measurement of strain fields in the near surface resultant from polishing. In another study, George et al. [34] used 300 K Raman spectroscopy to investigate polished (100) GaAs and compared their results to images obtained by cross-sectional TEM. Polishing was performed using a slurry of 0.05 $\mu$m alumina powder and studies were conducted to determine the effect of polishing time on the amount of near surface damage introduced to the crystals. TEM results showed that the near surface of the 2.5-minute polished sample exhibited a high dislocation density that extended to about 75 nm beneath the surface. It was reported that the damage depth increased with increased polishing time and was observed to be more than 500 nm for the 30- and 60-minute polishing times. The polish-induced strain damage depth, as determined by Raman spectroscopy, was observed to follow a similar trend as the dislocation damage depth, as determined by TEM. In a more recent TEM study, Zarudi et al. [35] investigated the effect of polishing on the near surface of (110) Si. Surfaces were prepared with successive polishing processes using 15 $\mu$m, 9 $\mu$m, 5 $\mu$m and 1 $\mu$m mean diameter abrasives. Fine polishing was performed using an oxide slurry with 0.025 $\mu$m particles. TEM results for the surface prepared with the 5 $\mu$m abrasive indicated dislocations and microcracks which extended approximately 1-3 $\mu$m from the surface. After the final (fine-) polishing process, the near surface damage was reportedly "completely removed".

Another technique for the characterization of polish-induced subsurface damage in semiconductors is axial ion channeling. Studies using this technique on polished CdS, ZnSe [36] and ZnO [37] have been reported. Results show a significant variation of subsurface damage between CdS, ZnSe and ZnO for the same polishing processes. To illustrate, for surfaces prepared by mechanical polishing with a 1 $\mu$m diamond abrasive slurry, the approximated damage depths were 235 nm for (0001) and $(000\bar{1})$ ZnO, 147 nm for (0001) CdS and 424 nm for (100) ZnSe. Data from surfaces prepared by mechanical polishing with a 1/4 $\mu$m diamond abrasive slurry showed a similar trend. The subsurface damage depth for (0001) and $(000\bar{1})$ ZnO was reported to be 115 nm, whereas the damage depths for (0001) CdS and (100) ZnSe were 105 nm and 377 nm, respectively. These results clearly demonstrate that near surface damage does not necessarily scale with grit size. It does appear, however, that the

amount of subsurface damage is strongly dependent on the material being polished. Results from chemomechanically polished ZnO showed that the depth of damage resulting from polishing was less than the depth resolution of the technique. Other characterization tools for the assessment of subsurface damage in semiconductors have also been reported. These include X-ray photoelectron spectroscopy (XPS) [38], absorption [39], and infrared (IR) reflectance with attenuated total reflection spectroscopy [40]. These methods, however, have not been as widely reported as luminescence techniques such as CL and PL.

Borovich et al. [41] used CL to study the damage imparted to CdS single crystals by mechanical and chemomechanical polishing. It was reported that the pattern of integrated CL had a strong dependence on the surface treatment. Each process yielded its own characteristic luminescence pattern. The differences in patterns were attributed to the formation of a "disturbed layer" whose depth was a function of the surface treatment. The distribution of the damage was reported to be heterogeneous and the subsurface damage was greater for the mechanically polished samples as compared to the chemomechanically polished samples. Borovich et al. [41] noted that the chemomechanical polishing of CdS samples best satisfied the requirements for surface finish while minimizing the subsurface damage. Kozlovskii et al. [42] also used CL to investigate the defects introduced in single crystal CdS by mechanical polishing. Specifically, CL was used to assess a technique of passivating the damage by annealing in atomic hydrogen. It was reported that the depth of the polish-induced damage layer was a function of the grain size used for polishing, namely, the samples polished with 1 $\mu$m grain size resulted in shallower damage than those samples polished with 10 $\mu$m grains. Their measurements showed that annealing in atomic hydrogen produced a significant increase in CL intensity. They proposed that the dislocations from mechanically polished samples could be thought of as local sinks of nonequilibrium electron hole pairs (EHP) with a particular rate of nonradiative recombination which depends on the state of the broken bonds on dislocations. During annealing, the atomic hydrogen diffuses into the sample, completes broken bonds of the dislocations, and reduces the nonradiative recombination by several orders of magnitude. CL has also been instrumental in characterizing specific types of point and extended defects. Myhajlenko et al. [43] investigated the luminescence of individual dislocations and related defects in metal-organic chemical vapor deposition (MOCVD) ZnSe thin films. Initial TEM characterization of the sample revealed a high density of stacking faults bounded by partial dislocations. "Unusual" luminescence bands at 2.60 eV (Y) and at 2.52 eV (S) were observed and attributed to dislocations. The occurrence of the Y emission band was found to be dependent on the growth conditions, in particular, the cleanliness of the reactor. They reported that it was not the dislocations alone that resulted in the Y emission, rather an

association of impurities with dislocations that led to a luminescence band at 2.60 eV. It was also reported that the Y emission was associated with complex dislocation tangles and not caused by stacking faults. In a separate CL investigation, Negrii and Osip'yan [44, 45] studied the effect of various dislocations on the low temperature (10-77 K) CL of CdS. Particular interest was paid to the radiative recombination processes in the blue and green parts of the spectrum. Using four-point bending and indentation, a dislocation density of $10^7$-$10^8$ cm$^{-2}$ was achieved. The orientation of the crystal in the bending deformation was such that the preferential glide of the dislocations occurred in the (0001) planes (basal) or the $(10\bar{1}0)$ and $(1\bar{2}10)$ planes (prismatic). Relative measurements were conducted on those parts of the crystal that were characterized by high dislocation density, such as regions with dislocation rosettes, with other parts of the crystal that were relatively free of dislocations. It was discovered that, in addition to the quenching of the exciton bands, there were strong luminescence bands in the green part of the spectrum (2.447, 2.439, 2.430 eV) emitted from those parts of the crystal with a high dislocation density. The "new" bands were attributed to the presence of dislocations. In addition, the 2.439 eV peak was observed only in the presence of dislocations in the basal (0001) plane. The 2.430 and 2.447 eV peaks were common to both types of dislocations. Studies were also conducted on the effect of deformation temperature (300-600 K) and storage time after deformation and it was concluded that they had the same influence, namely that the intensities of the three characteristic peaks decreased and the structure of the spectrum flattened out. This led to the conclusion that the degradation of the dislocation luminescence spectrum in regions where dislocations exist resulted from a redistribution of point defects in an elastic field and their migration to dislocations. The mechanism suggested for the 2.430 eV peak was a recombination of the electron and hole of the main dislocation state, whose formation may be attributed to the deformation potential field of the basal or prismatic dislocation binding the electron and hole. The 2.439 eV peak was explained by the existence of a dislocation state that is characterized by a small electron binding energy in the electric field of a charged dislocation. Lastly, the 2.447 eV band was attributed to radiative recombination of an electron excited from any of the dislocation states to the conduction band with a trapped hole on the dislocation. These results demonstrate the competition between radiative and nonradiative mechanisms and demonstrate that mechanical damage can result in a reduction of the overall luminescence efficiency of the semiconductor.

PL has also been routinely used for the characterization of defects in semiconductors resulting from polishing. Akimova et al. [46] used PL spectroscopy and periodic wet etching to study the depth of subsurface damage due to mechanical and chemomechanical polishing of (0001)-oriented CdS. They suggested that spatial inhomogeneities in the bulk crystal may lead to erroneous results

when determining the depth of damage using photoluminescence. However, it was reported that one advantage of PL is that it gives a simple and rapid means of testing the effects of surface treatment on the basis of the radiative properties of the material. Additionally, they reported that chemomechanically polished semiconductors yielded the highest quality surface finish with the least amount of subsurface damage. In another subsurface damage PL study, Laczik et al. [22,47] investigated the polishing damage on (100) InP using total light, room-temperature scanning PL and a technique of chemically angle-polished surfaces [48,49]. For this technique, a small-angle bevel is formed on part of the surface of the wafer by chemical dipping. The bevel allowed a more detailed examination of the subsurface damage. A lateral resolution of <2 mm and a depth resolution of <10 nm were reported. For the as-polished wafers, it was observed that there was a layer extending from the surface down to ~10 nm that seemed relatively undamaged. Beneath that "good" surface layer was a damaged layer extending to ~50 nm. The amount and distribution of damage, identified as dislocations and cracks, were different in each of the wafers examined. A subsequent defect etch revealed shallow etch pits (S-pits) on the beveled region to a depth of ~50 nm with no S-pits on the unbeveled region. Based on the PL and defect etch information, Laczik proposed two competing explanations for the "good" surface layer. The first possibility reported was that there was damage in the first ~10 nm of the wafer, but was not observed because it had been passivated. The minority carriers either recombine radiatively at the damage or they do not recombine at the damage in the first 10 nm of the material. The passivation could be caused by a chemical effect from the polishing procedure. This same chemical effect could have passivated the damage against chemical etching attack as well. An alternative explanation was that there was no damage in the "good" zone. In addition to the "large" pressure on the wafer surface (during polishing) which causes damage down to a depth of ~50 nm, there is a "small" pressure that removes damage down to a depth of ~10 nm. This could be due to either smearing or amorphisation of the surface layer. One additional observation made by Laczik was that most of the measured emitted PL light came from material <10 nm deep in both the beveled and unbeveled regions. One consequence of this observation, as reported by Laczik, is that if the PL technique is used to investigate as-polished InP wafers without beveling the specimen, polishing damage below the 'good' zone will not be observed. It was also reported that the subsurface damage could adversely affect epitaxial growth, initiating S-pits in the layers above the substrate.

Whereas most often the near surface disorder introduced by polishing leads to decreased luminescence efficiency owing to competitive nonradiative recombination, there are examples in the literature of mechanical damage resulting in new PL peaks. These include PL studies of mechani-

cally polished GaAs [50]and InP [51,52]. In each case point defects resultant from dislocation motion were implicated as the source of luminescence. Swaminathan et al. [50] used low temperature (10-70 K) PL spectroscopy to study GaAs with the following surface conditions: as-cut, mechanically polished with a 600 grit SiC paper, scribed with a carbide tipped tool and chemically ($Br_3$-$CH_3OH$) polished. For those wafers subjected to surface damage from either saw cutting, polishing or scribing, a new luminescence band (~1.4 eV) at low temperature (10 K) was observed. It was reported that this new band was thermally quenched above about 30 K. For the chemically polished samples, no band at 1.4 eV was observed. The ~1.4 eV band was observed in all mechanically damaged crystals regardless of whether they were grown by horizontal Bridgman or by liquid encapsulated Czochralski technique, whether they were doped or undoped and whether they were semi-insulating or not. This new band was attributed to point defects created by limited dislocation motion at or near the surface. The point defects, which serve as radiative centers, had relatively shallow energy levels and were demonstrated to be stable at room temperature with high annealing temperatures ($\geq$ 400°C). These results indicated that the radiative centers were defect clusters rather than simple point defects. They also noted that the scratches from polishing and scribing appeared 'dark' in luminescence images, suggesting that the dislocations produced by the mechanical damage resulted in nonradiative recombination centers. In fact, the PL intensity of as-cut samples, near the band edge, was approximately an order of magnitude less than the polished samples, suggesting that the as-cut samples exhibited more severe mechanical damage. Similar observations have been reported by other researchers. Bohm and Fischer [53] reported that the overall intensity of the PL spectra is lowered by about 30% in a region of 5-10 mm around dislocations, but the shape of the spectra remains unchanged. Tuck [54] also reported a correlation between PL degradation and dislocation etch-pit density in crystals that had been mechanically polished. The total damage depth of the as-cut wafers was 10-20 $\mu$m. This result was determined by etching the wafer at various times until the band at ~1.4 eV had subsided. Swaminathan et al. recommended chemical polishing to remove approximately 20 $\mu$m of mechanical damage before any subsequent device application. Other sources of point defects resulting in new radiative centers include etching and aging under atmospheric conditions. Amirtharaj et al. [55] used PL spectroscopy in the temperature range of 8-40 K to study the effects of $Br_2/CH_3OH$ etching and aging in atmospheric conditions on In-doped CdTe. The dominant effect of etching was the introduction of a distinct peak at 1.5896 eV. This peak was interpreted as arising from the introduction of Cd vacancies in the chemically etched region. The effect of aging (approximately 10 weeks) produced similar results, namely, the presence of the 1.5896 eV peak, whereas the freshly cleaved sample exhibited no peak at this energy. The presence of this peak

strongly suggested Cd vacancies at the surface of the aged face. The Cd vacancies were attributed to an inherent surface reactivity and/or instability as well as reaction with atmospheric oxygen. It was suggested that the formation of Cd vacancies could interfere with successful fabrication of devices and could negatively impact those devices that contain exposed surfaces. Low temperature PL has also been used for evaluation of homoepitaxial films to infer the quality of the growth method and the substrate [28, 56]. Ponce et al. [28] investigated the MOCVD growth of GaN on mechanically polished single crystal GaN using low temperature (2 K) PL and TEM. They reported the growth of high quality homoepitaxial GaN films with a measured upper limit for the dislocation density of $10^8$ $cm^{-2}$. The observed dislocations, primarily dislocation loops, were reported to originate from the surface condition of the substrate. PL data from the substrate exhibited very strong "yellow luminescence" indicative of many defects in the crystal. The authors indicated that improved surface conditions for the substrate could eliminate the observed dislocations altogether. In another GaN homoepitaxy study [56], CAIBE was used to remove subsurface damage from the polished bulk substrate to improve the growth quality. The CAIBE-treated substrate showed improved PL emission with higher signal and reduced linewidths. The metal-organic vapor-phase epitaxy (MOVPE) grown films showed clear, intense and narrow PL spectral emission indicating very high quality.

From these results, two very general observations can be made: 1) point defects can be associated with radiative centers leading to new bands in the PL emission and 2) the presence of extended defects, such as dislocations, in the near surface introduces nonradiative recombination sites that reduce the overall luminescence efficiency of the material. It is apparent that near surface mechanical damage significantly affects the PL of semiconductors. Very little information was found specifically regarding the effects of polish-induced subsurface damage on the luminescence of ZnO, however, there are several fundamental studies concerning the PL and CL of ZnO reported in the literature.

### 1.2.2 Luminescence Studies of ZnO

ZnO exhibits hexagonal (wurtzite) crystalline structure with asymmetric stacking sequences of atomic layers along its optical axis (**c**) which results in two distinct polar surfaces, namely the (0001) Zn-terminated face and the $(000\bar{1})$ O-terminated face [57]. Differences for the two polar faces have been observed for: wet-etch patterns [58], radiation damage thresholds [20] and PL [57]. These polar surfaces are also known to exhibit significantly different material removal rates for polishing [59].

Some debate still exists regarding the RT band gap energy for ZnO. While the most commonly reported value is 3.37 eV [17], other values have been reported. Srikant and Clarke [60] documented

values ranging from 3.1 to 3.3 eV. In their study, based on reflection and transmission absorption, Fourier transform infrared spectroscopy and PL measurements, it was concluded that the RT bandgap for ZnO was 3.3 eV. They attributed the scatter of RT values to a valence band-donor transition at ~3.15 eV. Additional ZnO material properties such as lattice parameters, exciton binding energy, and Debye temperature are presented in Appendix A.

To date, very little information is available regarding the PL resulting from various surface treatments for ZnO, though there have been some damage-related studies performed for this material. Czernuszka et al. [61] reported the CL of dislocations around indentations on (0001) and $\{1\bar{1}00\}$ surfaces. Look et al. [20, 62] investigated defect production from high-energy electron beam irradiation using Hall-effect measurements and PL. Studies of subsurface damage for polished bulk ZnO have been performed using axial ion channeling [37], however PL of these surfaces has not been addressed. This review includes some of the important research that has established the identification of much of the luminescence from ZnO in addition to some very recent PL results reported for bulk ZnO produced by Eagle-Picher (EP). These results are relevant because the material used for this study is provided by EP.

Thomas [63] is generally credited with establishing the excitonic spectrum of ZnO using absorption and reflection measurements from 4.2-300 K. The material used was grown from the vapor phase and assumed the form of "hexagonal needles" several mm long and less than one mm thick. Owing to a degeneracy in its valence band, ZnO exhibits three valence band excitons. The 4.2 K energies of the three exciton peaks as measured by reflection were reported to be 3.3770 eV for the A valence exciton, 3.3845 for the B valence exciton and 3.4225 eV C valence exciton. To observe the A and B exciton reflectivity, the light was polarized perpendicular to the optical axis of the crystal ($\mathbf{E} \perp \mathbf{c}$) and to observe the C valence exciton, the light was polarized parallel to the optical axis ($\mathbf{E} \parallel \mathbf{c}$). Surface irregularities associated with etching reduced the reflectivity of the crystal and polishing the crystal altered both reflection and absorption data. As an example, the absorption line at 3.3758 eV was observed to be nearly obscured in the polished crystal, but was restored after etching. Sharp polarized luminescence lines were reported between 3.35 and 3.3758 eV. Similar research was performed, using absorption and reflection techniques, by Park et al. [64] to characterize the exciton spectrum of ZnO. They reported results that differed slightly with Thomas [63] for the three valence excitons, however they also reported the presence of several bound-exciton transitions.

Klingshirn [65] reported the PL of ZnO platelets for temperatures between 4-300 K using one- and two-photon excitation. The ZnO platelets used were grown from the vapor phase. Results included observations of free-exciton and longitudinal optical (LO) phonon-assisted free-exciton luminescence.

Klingshirn [65] mapped the temperature-dependent luminescence of these peaks as well as several bound exciton and LO phonon-assisted bound-exciton peaks. Also reported was the observation of spontaneous emission from the inelastic interaction between excitons and electrons at temperatures higher than 70 K. This particular emission peak exhibited a strong shift to lower energy with increasing temperature. Luminescence from bound excitons and their phonon replicas were observed as well as a two-electron satellite, measured at 3.322 eV, of a bound-exciton peak measured at 3.361 eV. For high one-photon excitation intensity, stimulated emission resultant from exciton-exciton interaction was also observed. Klingshirn [66] has also published a useful "rule of thumb" to be used as a first approximation for the identification of the individual 4.2 K PL peaks of ZnO. To illustrate, peaks that fall within the range of energies of $E_1$-$E_2$ are identified as ionized donor bound-exciton peaks. Luminescence within $E_3$-$E_4$ are identified as neutral donor bound-exciton peaks and so on. Whereas this model is not sufficient as an absolute identification of the PL peaks from bulk ZnO, it does provide a guide to narrow the possible choices for the individual luminescence peaks. Other early PL research of ZnO includes the work by Tomzig and Helbig [67] who reported observations of bound-exciton luminescence associated with Li and Na acceptor levels in their study of Li and Na doped ZnO and Hvam [68] who reported on the exciton-exciton interaction in stimulated emission from ZnO platelets at 1.9 K using 5-500 $kW/cm^2$ laser excitation.

In a recent study of polycrystalline ZnO, Studenkin et al. [69] investigated the 1.7 K near-band-edge PL of thin films prepared by spray pyrolysis. In their study, two types of samples were used: 1) high conductivity, annealed and 2) low conductivity, as-grown. They used Klingshirn's "conventional classification" model [66], discussed above, to aid in the identification of some of the PL peaks in their study. For the high-conductivity samples that were annealed prior to PL, luminescence from several bound-exciton complexes together with LO phonon replicas were reported. In contrast, the as-grown low-conductivity samples exhibited broader, less resolved bound-exciton peaks with a lower energy periodic structure spaced by 108 meV. This periodicity was attributed to a resonant two-transverse optical (TO) phonon assisted luminescence of two-electron satellite peaks. No observation of free-exciton luminescence was reported. In a low temperature PL study of single crystalline ZnO thin films grown by radical-beam epitaxy, Butkhuzi et al. [70] reported the observation of free-exciton luminescence and the absence of any visible luminescence and attributed this result to high structural subsurface quality and negligible amounts of defects or impurities. Each of the valence-band free excitons was observed and their energies were reported as 3.369 eV, 3.378 eV and 3.416 eV for the A, B and C excitons, respectively.

Much attention has been paid to the role of defects in ZnO and their effect on device perfor-

mance [71]. In particular, those defects that result in mid-band-gap-energy or deep level (DL) luminescence have been studied due to their effect on the efficiency of near-band-edge luminescence [72, 73]. Using ZnO powder, Vanheusden, et al. [74] studied the mechanisms responsible for the broadband deep level emission, commonly referred to as green luminescence in ZnO, using electron paramagnetic resonance (EPR), optical absorption, and PL. Their results showed a good correlation between the green PL emission, free carrier concentration and the density of singly ionized oxygen vacancies. It was suggested that the electrons associated with the oxygen vacancies recombine with photoexcited holes in the valence band resulting in green emission. Vanheusden [75] proposed that depletion caused by band bending at the surface also plays an important rôle in the green luminescence of ZnO. Reynolds et al. [76, 77] compared the green emission of single crystal ZnO to the analogous yellow emission of single crystal GaN. It was reported that both emissions are defect related and share common mechanisms. As an example, the yellow emission (in GaN) only occurs in high conductivity (N deficient) GaN. Similarly, the green emission (in ZnO) occurs only in high conductivity (Zn rich) crystals. Point defects were reported as the likely candidates for the deep level emission in ZnO. The possible defects listed were: oxygen vacancies, zinc interstitials and zinc antisites. Based on theoretical calculations for the defects responsible for the yellow emission in GaN, the authors hypothesized that the Zn antisites were the defects responsible for the green emission in ZnO [76]. In a subsequent study [77], the authors reported that the green emission was due to a transition between a shallow donor and a deep level. It was hypothesized that the deep level in ZnO might be a complex consisting of a zinc vacancy and a substitutional chlorine at an oxygen site. Sekiguchi et al. [78] demonstrated that the green emission was strongly passivated in a hydrogen plasma. The passivation resulted in enhanced band-edge luminescence further demonstrating the competitive nature of the nonradiative recombination mechanisms associated with defects. The ratio of the band-edge peak to the green peak has been used as an assessment of material quality, where a larger ratio indicates higher material quality. Ratios reported in the literature range from about 1:1 [60] to 23:1 [79].

Turning our attention to luminescence studies of EP material, Ohashi et al. [80] investigated the temperature-dependent (20-300 K) CL of a chemomechanically polished ZnO sample produced by EP. For this study, CL of the EP sample provided a baseline for comparison to an Al-doped sample produced by a chemical vapor transport method. In addition to bound-exciton and phonon-assisted free-exciton luminescence, an unidentified "extra" luminescence peak was observed at approximately 3.375 eV from the 40 K CL spectrum of the EP sample. The nature of this extra peak was speculated to be luminescence from a bound-exciton state. No free-exciton luminescence was observed below 50

K. They suggested that the RT CL from the EP sample was not from the collapse of free excitons. This result is in contradiction with other RT PL studies [15, 81] which attribute the principal RT luminescence of ZnO to free-exciton emission. Ohashi's article underscores the difficulty encountered in luminescence research to adequately and accurately identify the individual peaks. From the intermediate temperature (150-300 K) CL spectra presented, convolution of multiple peaks is seen to restrict analysis above 150 K, however, Ohashi maps the temperature dependence of all of the observed peaks through this temperature range extending to 300 K.

Reynolds et al. [82] investigated the bound-exciton peaks observed at 2 K, for material produced by EP, using PL. The bound excitons were attributed to defect-pair complexes. Specifically, it was reported that the defect pairs exhibited properties of neutral donors and the luminescence was the result of the collapse of excitons bound to these complexes. Studies were conducted for as-grown and annealed (350-800°C) samples. Significant spectral differences were observed between as-grown crystals and those that were annealed prior to the PL measurement. Annealing was observed to transfer all of the bound-exciton emission into the lowest energy peak. Energy-level diagrams were presented to describe the PL transitions involving the neutral-donor states for as-grown and 800°C annealed samples. From the PL spectra presented, the neutral-donor-bound excitons provided the strongest emission at 2 K. Luminescence from excited states and two-electron satellites of the bound excitons were also observed. In another luminescence study of EP material, Sherriff et al. [57] used 2 K PL to compare the luminescence from the two polar faces of (0001)-oriented ZnO. Differences between the Zn-terminated (0001) and O-terminated $(000\bar{1})$ chemomechanically polished surfaces were reported. First, whereas free-exciton luminescence was observed for the $(000\bar{1})$ surface, it was described as "essentially absent" from the (0001) surface. Second, two specific phonon replicas of the bound-exciton luminescence were observed to be dominant for the $(000\bar{1})$ surface over the same energy positions for the (0001) surface. These phonon replicas were identified as a TO-phonon assisted recombination of a bound-exciton complex and a TO-LO assisted transition of the same complex. Comparisons of the 2 K PL were also made for wet-etched and cleaved polar surfaces to demonstrate the intrinsic nature of the differences between the PL of the $(000\bar{1})$ and (0001) surfaces. In a separate PL study of EP material, Boemare et al. [83] presented temperature-dependent (14-300 K) luminescence data and Rutherford backscattering (RBS) for bulk ZnO. As many as 14 peaks were observed in the exciton region of the 15 K PL spectrum. Free-, ionized-donor-bound-, and neutral-donor-bound-exciton luminescence transitions were identified. Three separate models for the temperature dependence (14-200 K) of free-exciton luminescence were developed based on: 1) Varshni [84], 2) modified Varshni [85] and 3) Pässler [86]. Good agreement was observed for all

models, however the best agreement was reported for the Pässler model. In another low temperature PL study of EP-grown ZnO, Thonke et al. [87] reported observations of donor-acceptor pair (DAP) transitions in addition to several of the previously reported bound-exciton peaks. Much like the Reynolds work [82], the observation of two-electron satellites of the neutral-donor-bound-exciton peaks was reported. From this observation, Thonke estimated a donor binding energy of 40 meV. From the DAP peak, a binding energy for the acceptor was approximated to be 195 meV. Thonke hypothesized the acceptor to be nitrogen and the donor to be hydrogen.

Very recently, research on ZnO has focused on the possible identification of hydrogen as the principal donor in ZnO [88–97] which leads to the unintentionally doped $n$-type behavior of the as-grown material. Initially, it was believed that native defects such as O vacancies and Zn interstitials were the cause of this conductivity, however, researchers have reported [88,89] that native point defects, known to give rise to deep level emission, do not exhibit the necessary characteristics of shallow donors and thus are unlikely candidates as the source of high concentration donors in ZnO. Van de Walle [88] provided theoretical evidence to demonstrate that, unlike many other semiconductors, hydrogen is not amphoretic (precluded as a source of conductivity) in ZnO and, as a result, H occurs only as a donor in ZnO. This theoretical prediction was confirmed experimentally by Cox et al. [90]. Using a muon spin rotation technique, they were able to show that the muons behaved as shallow donors based on their hyperfine interaction and ionization energies. Further experimental evidence of H as a shallow donor in ZnO has been reported [91,96]. PL [93] and CL [94] have also been used as characterization tools for the identification of H as the principal donor. From the PL study [93], luminescence was reduced by more than 2 orders of magnitude from the PL of the unimplanted samples. For the CL study, the H irradiation was observed to passivate deep donor and acceptor states, thus increasing the luminescence efficiency. Spectral variations in the low temperature PL resulting from H implantation could provide further experimental evidence that H is the likely shallow donor in ZnO. These results suggest that proper control of H content in the growth process could result in a significant reduction of the RT conductivity for as-grown ZnO [98]. Van de Walle [98] has also reported that simultaneous incorporation of H with N may assist in the development of $p$-type doping of ZnO.

PL has been used to investigate material quality for both polycrystal and single crystal ZnO, where exciton emission, both free and bound, has been shown to be sensitive to the near surface integrity of the crystal. It has also provided information on shallow and deep level defects introduced during growth, however the effects of polishing on the PL of ZnO has not been addressed.

## 1.3 Research Overview

### 1.3.1 Objective

Critical to the further development of bulk single-crystal ZnO epi-ready substrates is the ability to characterize the lattice disorder in the near surface layers of the material. Subsurface defects in substrates have been shown to contribute to poor quality films (and subsequent short lifetime devices). Many of the defects associated with the degradation of device performance are generated in the final finishing processes of the substrates, such as saw cutting, mechanical and chemomechanical polishing. This work seeks to contribute to a fundamental understanding of the effect of crystalline defects resulting from ultrafine finishing processes on the optical performance of bulk, hexagonal (wurtzite) ZnO. This understanding will aid in identifying the processing conditions which show promise for producing high-quality ZnO substrates.

### 1.3.2 Research Plan

In this study, comparisons of PL from: wet-etched, chemomechanically polished, mechanically polished, and H-treated surfaces are made for both polar faces of (0001)-oriented ZnO. Spectrally-resolved and peak-intensity differences in the PL from these surfaces are investigated to determine the effects of near-surface damage in bulk ZnO. In addition to RT PL, characterization of these surfaces includes temperature-dependent (4.2-300 K) PL to assist in the identification of individual peaks and to further illustrate differences in the near surfaces of the various prepared surfaces. Included in the Appendix are results from additional PL studies by our group such as: comparisons of as-grown and ion-channeled ZnO surfaces to chemomechanically polished ZnO surfaces (Appendices B and C), RT PL of etched CdS (Appendix D), and PL of Si implanted $SiO_2$ (Appendix J). A short review of the physics of PL is presented in the next chapter.

# Chapter 2

# Photoluminescence of Semiconductors

Photoluminescence (PL) is a fast, nondestructive technique for the characterization of both intrinsic and extrinsic properties of semiconductors [99]. PL is the result of optical excitation where photons are absorbed, creating electron-hole pairs which after recombining result in new photons characteristic of the photo-excited material [100]. Much has been written regarding the physics of PL of semiconductors. Excellent overviews on optical processes in semiconductors such as those by Yu and Cardona [101], Pankove [100], Bebb and Williams [102] and Basu [103] include discussions of photoluminescence mechanisms, some of which are summarized here.

The process of a material absorbing energy from incident radiation and then re-emitting light of a lower energy (Stoke's Law) is called luminescence [104]. For luminescence resulting from absorption of photons, the process is labeled photoluminescence. Electrons as the source of excitation results in cathodoluminescence (CL). Whereas other types of excitation are possible, such as mechanical (triboluminescence) and thermal (thermoluminescence), PL and CL are two of the most important in device applications [105]. PL consists of three fundamental processes [99]: 1) absorption or electron-hole pair (EHP) excitation, 2) EHP thermalization and 3) EHP recombination. EHP recombination may or may not result in the emission of light or luminescence. These three processes are discussed further in Section 2.2. The photons resulting from EHP recombination can be described as either fluorescent or phosphorescent emission. Fluorescence is the term used to describe nearly instantaneous emission, whereas phosphorescence describes the process where there is some delay in the emission of light after absorption. Phosphorescent emission can continue for periods of seconds or minutes after the excitation is removed [105]. In each of these processes, allowed energy levels within the band gap determine to some degree the characteristic time and energy of luminescence. These energy levels also influence the luminescence efficiency (i.e., how many absorbed photons are

converted into emitted photons) of the material. A review of the band structure which gives rise to the various energy levels participating in the emission of photons is discussed below.

## 2.1 Band Structure

Much of the phenomenological electronic behavior observed for metals, insulators and semiconductors can be explained by band theory (i.e., the band structure of the material). In this section, a brief review of band structure is presented as the basis for a simplified model to describe PL of semiconductors.

As two atoms are brought together, the Pauli exclusion principle dictates that no two electrons in a given system may have the same quantum state. The result is splitting of the discrete electron energy levels for the two isolated atoms into new electron energy levels belonging to the pair of atoms rather than to the individual atoms [105]. For the case of a solid, many atoms are brought together, so that the split energy levels form essentially continuous bands of energies. For this collection of atoms, assembled into some periodic array, the continuous energy bands can be separated by an energy gap or band gap ($E_g$) [100]. For semiconductors, the lower energy band (valence band) is filled at 0 K and the higher energy band (conduction band) is empty. As a result, semiconductors do not conduct at 0 K. As the temperature is increased, electrons are thermally excited from the valence band into the conduction band (according to Fermi-Dirac probability [106]) resulting in higher conductivity. The size of the band gap and availability of electrons determine the electronic behavior of the material (i.e., whether it is an insulator, metal, or semiconductor) [100]. Metals are generally characterized by either a partially filled conduction band at 0 K or overlapping conduction and valence bands [107]. While no agreement exists as to the "cutoff" value of the band gap energy to differentiate insulators from semiconductors, insulators generally exhibit energy gaps larger than $\sim$5 eV [106], whereas semiconductors typically have band gaps ranging from $0^+$ to $\sim$4-5 eV. Semiconductors exhibit one of two types of band structures: direct or indirect. For a direct band gap material, an excited electron in the conduction band can fall directly to an empty state in the valence band, emitting a photon equal to the band gap energy $E_g$. An electron in the conduction band of an indirect semiconductor, however, cannot fall directly to the valence band. It must undergo a momentum change in addition to changing its energy [105]. For direct band gap semiconductors such as ZnO, PL is the result of photoexcited electrons returning to their ground state and emitting photons. Only direct band gap semiconductors will be considered in this discussion as the probability of a band-to-band radiative transition in an indirect band gap material is regarded as an inefficient

luminescence process [107]. For an ideal semiconductor, the band gap contains no allowed energy states [105]. However, imperfections in the crystal such as impurities and defects introduce allowed energy states or traps within the "forbidden" band gap. Participation of these allowed intermediate states in the collapse of the photoexited electrons to their ground state may result in either sub-band gap radiative or nonradiative recombination of EHP. The following section provides a discussion for some of these radiative and nonradiative mechanisms of EHP recombination.

## 2.2 Radiative and Nonradiative Recombination

PL is routinely used for the identification of many types of impurities or defects in a semiconductor [108]. PL has been used extensively to investigate optical properties and electronic band structure of semiconductors [60]. Because the band structure of a semiconductor is sensitive to the presence of defects and impurities, the PL response is altered according to the type and density of defects or impurities. While defects or impurities in the crystal may result in new PL spectral peaks resultant from the recombination of electrons and holes at the defect [50], they may also introduce nonradiative mechanisms that do not result in photons (e.g., an Auger process). Such nonradiative mechanisms compete with the radiative luminescence and effectively lower the relative intensity of the spectral peaks. As a result, the spectral content of PL measurements and the overall PL intensity can provide important information regarding the crystalline quality of the semiconductor [108]. To better understand the processes involved in luminescence, consider the excitation and emission of a hypothetical material with discrete allowed energies shown in Fig. 2.1, from [109]. The figure shows some of the possible electronic energy transitions which can result in photoluminescence on a simplified energy level diagram for a direct band gap semiconductor. The valence ($E_v$) and conduction ($E_c$) bands separated by the band gap energy $E_g$ are shown, where the vertical scale is energy. The far right side of Fig. 2.1 shows the PL emission spectrum which might result from the radiative processes. In process (a), a photon of sufficient energy, i.e., $h\nu_1 > E_g$ where $h$ is Planck's constant and $\nu$ is frequency, is absorbed by the material and results in the excitation of an electron into the conduction band, and the creation of a hole in the valence band. The photoexcited electron nonradiatively releases energy to the lattice by scattering events (thermalization) until it reaches the bottom of the conduction band (b), where it recombines with a hole in the top of the valence band (c), resulting in the emission of a photon with energy approximately equal to the band gap, $h\nu_2 \approx E_g$. The peak in PL intensity which results (c) is shown at the far right of Fig. 2.1. Other transitions are possible. After excitation to the conduction band the combination of (d) scattering

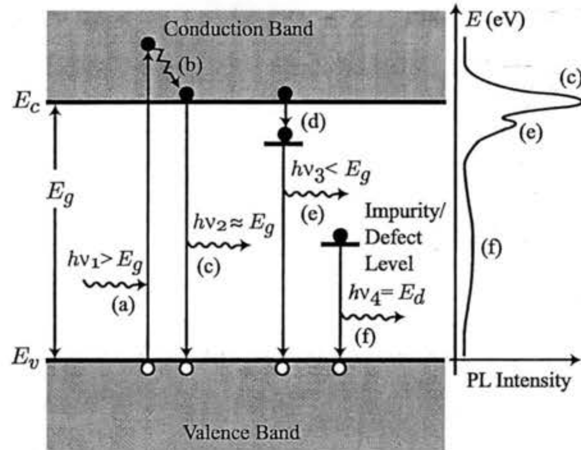


Figure 2.1: Simplified direct band gap showing some electronic energy transitions which can result in photoluminescence, from [109]

from lattice vibrations (phonon scattering) which results in energy loss and (e) a radiative transition which results in a photon of $h\nu_3 < E_g$ can occur, and is referred to as a phonon-assisted transition. Impurities or defects can result in allowed energy levels within the band gap. The recombination of an electron from this energy level and a hole may result in (f) a radiative recombination at some energy $h\nu_4 = E_d$, or may result in a nonradiative recombination. Whereas these defect/impurity levels may result in new spectral peaks, the principal effect of the introduction of damage to the room temperature PL is to increase the nonradiative paths for recombination which results in a lower PL intensity. Examples of nonradiative recombination of electrons and holes include: Auger effect, surface recombination, phonon emission and recombination mediated by defects [100]. In this review, discussion of the nonradiative processes is limited to the Auger effect. For Auger recombination processes, the energy from the collapse of an EHP is transfered to another free carrier, either an electron or hole, effectively raising the energy of the free carrier by an amount equal to the energy of the absorbed photon or EHP. Figure 2.2 illustrates some of the possible Auger effect processes in a simplified band gap diagram, after [100]. These processes are typical for $n$-type semiconductors such as ZnO. Shown are processes which illustrate EHP recombination for (a) band-to-band and (b-d) intermediate donor and acceptor levels. In each case the energy from the EHP collapse is transfered to a nearby electron. Such three-body collisions result in no net photon emission [100]. All nonradiative recombination paths for nonequilibrium EHPs compete with the radiative paths. An increased density of defects, which introduce nonradiative recombination paths for nonequilibrium EHPs, results in a reduction in the radiative emission following photoexcitation, i.e., decreased luminescence efficiency. Now that a simplified approximation of the PL process has been presented,

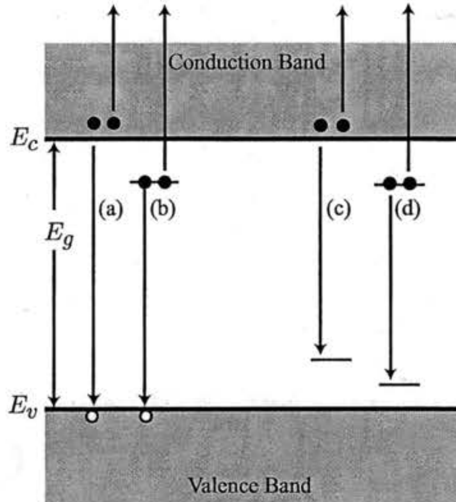


Figure 2.2: Some of the possible Auger effect recombination mechanisms, after [100]

some modifications are required to improve the accuracy of this model.

Band-to-band recombination of EHPs is generally precluded by Coulombic interaction between the electron and hole. This correlated EHP is referred to as an exciton [101]. The bound EHP, or exciton, has less energy than when the electron and hole are far apart [104]. The reduction in energy is equal to the binding energy of the electron and hole, known as exciton binding energy ($E_{ex}$). This binding energy is a material property and varies according to the dielectric constant and reduced electron and hole masses of the material. For ZnO, the exciton binding energy is 60 meV [17]. Coulombic interaction between the electron and hole is the reason the emitted photon shown in Fig. 2.1 (c) is labeled with an energy approximately equal to $E_g$. The following section provides a more detailed discussion of excitons and their luminescence characteristics.

## 2.3 Excitons

Proximate electrons and holes experience a Coulombic attraction effectively binding an electron to a hole in a hydrogen-like orbit. This coupled electron-hole pair, or exciton, can move freely through the crystal with no net charge carrying energy equivalent to the band gap less the Coulombic binding energy. More specifically, if the exciton is free to move about the crystal, it is called a free exciton. Several excellent reviews of exciton theory are available. Examples include Bebb and Williams [102] who present exciton topics relevant to the PL of III-V compound semiconductors and Reynolds and Collins [110] who provide a broader treatment of the basic properties of excitons and emphasize their use as a tool in understanding properties of semiconductors. This section provides a brief

introduction of excitons and exciton luminescence particularly as it relates to ZnO.

Some texts [100, 104] illustrate exciton energy levels on a simplified energy band gap diagram as shown in Fig. 2.3 where the exciton energy levels are shown below the conduction band. In the figure, $n = 1$ represents the lowest energy state for the exciton and $n = 2, 3...$ represent excited states for the same exciton. The exciton binding energy is proportional to $1/n^2$, so therefore, $n = \infty$ represents the continuum or the bottom of the conduction band. While useful for illustrating exciton energy levels in a simplified manner, this model is not rigorously correct [101]. The problem arises from representing a two-particle entity using one-electron energy levels when a more appropriate model of the allowed energy states of an exciton is given by Fig. 2.4, after [101]. This two-particle representation of exciton energy dispersion is given in momentum space rather than real space as with the simplified band gap diagram. From the figure, the abscissa ($K$) is the exciton wavevector and the ordinate ($E$) is energy. With the origin representing the ground state of the crystal, the bottom of the conduction band, $E_c$ also represents the band gap energy, $E_g$. The total energy of the exciton is given by two terms: a Coulomb interaction energy $E_x$ which is the energy of the band gap less the exciton binding energy and an exciton kinetic energy term, $\frac{\hbar^2 K^2}{2M}$, where $M$ is the sum of the electron and hole effective masses. One excited state ($n = 2$) is shown in addition to the lowest level ($n = 1$) free-exciton dispersion curve. The continuum is represented by ($n = \infty$). Also shown is a photon dispersion curve given by $\hbar ck$. The model illustrates that free excitons have a range of quasi-continuous allowed energies. However, only those free excitons with momentum equal to the photon momentum can recombine and emit photons [102]. From Fig. 2.4, the collapse of an ($n = 1$) exciton with negligible momentum ($K \sim 0$) results in a photon with an energy of $E_x$. This emission

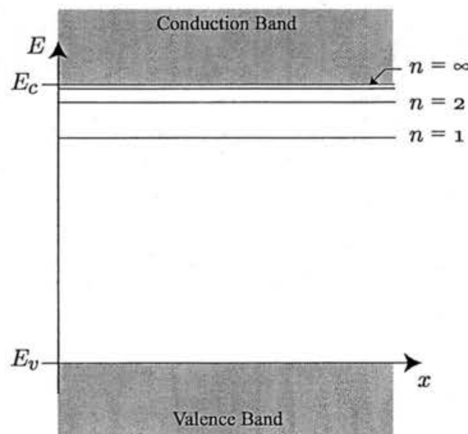


Figure 2.3: Exciton energy levels and excited states shown on simplified energy diagram for direct band gap semiconductor, after [100].

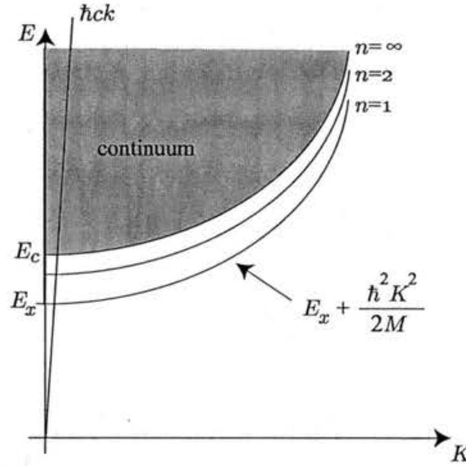


Figure 2.4: Exciton dispersion on two-particle diagram, after [101]. Shown are exciton dispersion curves for $n = 1, 2, \infty$, where $n = \infty$ represents the bottom of the conduction band. Also shown is a photon dispersion curve ($\hbar ck$) superimposed on the exciton model.

is referred to as free-exciton luminescence.

### 2.3.1 Free-exciton Luminescence

Before discussing free-exciton luminescence in detail, a brief overview of the entire luminescence spectrum is presented. As reported by Pavesi and Guzzi [99], the PL spectrum from a semiconductor can be divided into three principle energy regions where the range of each region depends on the particular material. While the general regions reported here are from Pavesi, the specific ranges reported are not ( [99] reported regions for GaAs); the energies reported here are approximations for ZnO.

1. Near band gap emission ($E_x \geq \hbar\omega \geq E_x - 20$ meV). This region includes luminescence from free-excitons and donor-bound-excitons, discussed in a later section. Other than hot-carrier effects, excited-exciton states, Raman scattering and band-to-band EHP recombination, free-exciton luminescence represents the highest possible energy emission for a given photoexcited semiconductor.

2. Shallow impurity emission ($E_x - 20 \geq \hbar\omega \geq E_x - 30$ meV). This region is characterized by acceptor-bound exciton recombination. For ZnO, no significant acceptor-bound exciton luminescence has been observed, so this region is not particularly useful.

3. Deep level emission ($\hbar\omega \leq E_x - 30$ meV). In this region, luminescence is characterized by

recombination of free carriers involving deep level traps resultant from defects and impurities in the crystal. This type of emission is presented in Section 2.6.

Observations of many of the transitions described above require very low sample temperature (e.g., 4.2 K). At higher temperatures, line broadening and thermal ionization diminish resolution and quench luminescence peaks. Phonon interaction at higher temperatures can also significantly affect luminescence. Phonon participation can reduce overall luminescence efficiency, but may also assist in the luminescence of additional low-energy peaks. This topic is discussed in Section 2.4.

Free-exciton luminescence provides an indicator of material quality. Many researchers have identified material to be of high quality based solely on the observation of free-exciton luminescence at low temperatures [70,111]. Given the importance of free excitons in ZnO, two additional topics associated with their luminescence, namely free-exciton line broadening and the temperature dependence of free-exciton luminescence, are presented.

**Free-exciton Line Broadening**

Because momentum selection rules restrict recombination of free excitons to those with a wavevector of $K \sim 0$, one might expect a discrete line with energy $E_x$ for free-exciton emission. Such discrete luminescence, however, is not observed experimentally. Instead, the luminescence exhibits a non-zero line width ($\sim$ 1 meV for GaAs at 1.4 K [100]) at an energy slightly red shifted in energy compared to the absorption value. We begin with a discussion of the observed line broadening. Toyozawa [112,113] first demonstrated that the free-exciton line (luminescence) is 'lifetime broadened' as a result of the short time the exciton remains in the $K \sim 0$ state prior to being scattered to other momentum states by phonon interaction [102]. For this review of free-exciton line broadening, discussion is limited to a summary of the information presented in Refs. [99,102]. Free exciton "lifetime broadening" is a direct result of the Heisenberg uncertainty principle ($\Delta E \Delta \tau > \hbar$). Excitons (eigenstates) with infinite lifetime exhibit perfectly sharp emission peaks. Finite exciton lifetimes, on the other hand, introduce some uncertainty in energy. As a result, all of the processes which limit the time an exciton resides at $K \sim 0$, such as phonon scattering, determine the free-exciton line width [102]. Presence of impurities and lattice defects may also contribute to line broadening of exciton luminescence [99]. Line broadening also introduces a redshift to lower energy for free-exciton luminescence. To better understand this phenomenon, we begin by assuming an arbitrary absorption lineshape of $S(\hbar\omega - E_x)$ centered at a free-exciton energy of $E_x$ (after [102]), shown as a solid line in Fig. 2.5 (top). Because the spontaneous-emission lineshape ($R_{sp}$) is seen to vary

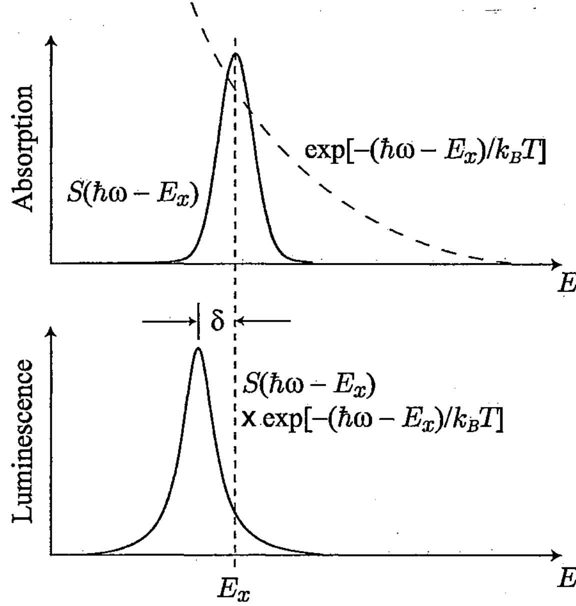


Figure 2.5: Effect of line broadening on measured PL position of free exciton peak, after [102].

exponentially with energy ($R_{sp} \sim \exp(-(\hbar\omega - E_x)/k_BT)$) near the band gap [102], an exponential curve (dashed line) is superimposed on the absorption profile. The spontaneous emission (luminescence) is proportional to the product of the absorption profile and the exponential term as shown in Fig. 2.5 (bottom). This product necessarily introduces some redshift in energy ($\delta$) from the original absorption value. The magnitude of $\delta$ is determined by the specific absorption lineshape and sample temperature. Two limiting cases of absorption lineshape have been reported for weak exciton-phonon coupling (Lorentzian) and strong exciton-phonon coupling (Gaussian) [99]. For a Gaussian absorption curve, the estimated redshift in energy for the observed luminescence peak is $\delta = \sigma^2/k_BT$ where $\sigma = 0.425$(full width at half maximum (FWHM) of absorption peak) [99]. For a Lorentzian profile, the redshift is given by $\delta = k_BT + \sqrt{(k_BT)^2 - \left(\frac{\hbar\Gamma}{2}\right)^2}$ where $\Gamma$ is the FWHM of the absorption peak. From this, it can be seen that the magnitude of redshift is not only a function of the absorption lineshape, but also varies with temperature. Derivations of these values for $\delta$ are given in Appendix G. In this study, free-exciton luminescence will be symbolized using FX. For emission specifically from the A valence band, FX(A) is used.

#### Temperature-dependent Free-exciton Luminescence

The energy of free-exciton luminescence (FX) is observed to decrease with increasing temperature. This behavior can be traced directly to the shrinkage of the band gap with increasing temper-

ature. For a temperature-independent value of exciton binding energy, the FX luminescence can be assumed to follow the shrinking energy of the band gap with increasing temperature. As a result, temperature-dependent FX luminescence can be used to estimate the temperature dependence of the band gap. Temperature-dependent variation in the band gap is attributed to two main factors [84]: 1) lattice dilatation and 2) electron-phonon interaction. Each of these is believed to shift the relative position of the conduction and valence bands with increasing temperature thus lowering the band gap energy. While techniques such as absorption and reflection/transmission spectroscopy provide more reliable data for the temperature dependence of the band gap, researchers have used luminescence to construct empirical models of the shrinking band gap with increasing temperature. Varshni's [84] seminal work reported a generalization for the temperature dependence of an energy gap as follows: for $T << \theta_D$, $\Delta E_g \propto T^2$, and for $T >> \theta_D$, $\Delta E_g \propto T$ where $\theta_D$ is the Debye temperature of the material. From this, Varshni developed an empirical relation for the temperature dependence of the energy gap in semiconductors:

$$E_g(T) = E_0 - \frac{\alpha T^2}{T + \beta} \tag{2.1}$$

where $E_g$ is the energy of the band gap, $E_0$ is the energy of the band gap at 0 K and $\alpha$, $\beta$ are constants. This relationship adequately approximates the linear behavior of the band gap at higher temperatures and the quadratic dependence at lower temperatures. Varshni's relationship has been widely used in a number of publications as a model for the temperature-dependent band gap for such materials as GaN [114, 115], CdTe [116] and InP [117] to name a few, however complications arise when using this model with limited data sets (0-300 K) for materials with high Debye temperatures (i.e., $\theta >> 300$ K) [118,119]. Pässler [118,120,121] addressed these limitations by developing another three-parameter model:

$$E_g(T) = E_0 - \frac{\alpha\Theta}{2}\left(\left[1 + \frac{\pi^2}{6}\left(\frac{2T}{\Theta}\right)^2 + \left(\frac{2T}{\Theta}\right)^4\right]^{1/4} - 1\right) \tag{2.2}$$

In contrast to the Varshni model, the fitting parameters $\alpha$ and $\Theta$ were given physical significance. $\Theta$ reportedly represented the effective (average) phonon temperature ($\Theta = \hbar\bar{\omega}/k_B$ where $\bar{\omega}$ is an average phonon frequency) and $\alpha$ was said to be the limiting slope of the $E_g(T)$ curve. Other models have been used to describe the temperature-dependent band gap including variations of the Bose-Einstein model, such as [121]:

$$E_g(T) = E_0 - \frac{\alpha\Theta}{2}\left[\coth\left(\frac{\Theta}{2T}\right) - 1\right] \tag{2.3}$$

where $\Theta$ is an average phonon energy and $\alpha$ again represents a limiting gap shrinkage coefficient. While each of these models have been used in the literature to describe the shrinking band gap

with some success, none include specific parameters for the individual contributions from lattice dilatation and electron-phonon interaction. A model that does separate lattice dilatation effects from electron-phonon interaction was developed by Manoogian and Woolley (MW) [119]:

$$E_g(T) = E_0 + UT^s + V\theta \left[\coth\left(\frac{\theta}{2T}\right) - 1\right] \tag{2.4}$$

In this model, $U, s, V$, and $\theta$ are temperature independent constants. The MW equation consists of three terms [119]: (i) $T = 0\ K$ intercept, $E_0$, (ii) lattice dilatation, $UT^s$, and (iii) electron-phonon interaction, $V\theta\left[\coth\left(\theta/2T\right) - 1\right]$. Manoogian and Woolley showed that Varshni's equation is actually a second order approximation of the electron-phonon term in the MW equation and is only applicable for data sets that extend well beyond the Debye temperature (i.e., $\theta_D/T << 1$). Additionally, it was reported that the fitting parameter $\theta$ could be related to the Debye temperature of the material by $\theta = (3/4)\theta_D$. In the present study, assuming a temperature independent exciton binding energy, the temperature dependence of the free-exciton peak position for ZnO was fit using the MW equation and the coefficients obtained show reasonable agreement both with first-principle theoretical calculations and empirical values of the coefficients for other II-VI semiconductors such as CdS [122] and CdTe [123].

### 2.3.2 Bound-exciton Luminescence

For many semiconductors at low temperature it is energetically favorable for the free exciton, as it moves through the crystal, to become trapped or bound to a defect, such as an impurity [102]. An emitted photon from the collapse of an exciton bound to a defect radiates energy lower than that of the free exciton by an amount equal to the binding (or localization) energy ($E_b$) of the exciton to the defect. As a result, emission from bound excitons (BX) is at slightly less energy (~5-20 meV) than the luminescence of free excitons. BX emission is also characterized by very narrow peaks (0.1 meV widths have been reported [100]) and strong intensity. Most often the dominant low temperature PL emission of semiconductors is from the recombination of bound excitons. Depending on the type of defect, the exciton can be categorized as bound to a neutral donor, a neutral acceptor, an ionized donor or an ionized acceptor. However, it has been reported [101] that excitons cannot be bound to both ionized donors and acceptors in the same material. The bound exciton actually forms a complex consisting of a donor or acceptor (either neutral or ionized), one or two electrons, and one or two holes determined by the valence of the donor (acceptor) [102]. Low temperature bound-exciton luminescence has been shown to be a very useful tool for the identification of crystalline defects in ZnO [70]. At very low temperatures, there is no thermalization of the bound-exciton complexes. As

a result, ZnO exhibits a variety of bound-exciton peaks due to the efficient binding of excitons to structurally different neutral impurities [124].

### Neutral-donor-bound-exciton Luminescence

Whereas excitons can be trapped by neutral acceptors as well as ionized donors and acceptors, it is the neutral donors which are most important to the low temperature exciton PL of ZnO [82]. As many as seven or eight neutral-donor-bound-exciton peaks in the energy range of 3.357-3.366 eV have been reported for EP-produced bulk ZnO [125]. Multiple bound excitons owing to various chemical identities are well-known for II-VI semiconductors [104]. The specific complex formed by an exciton bound to a neutral donor consists of a neutral donor ion ($D^0$), two electrons, and a hole [102]. Luminescence from the collapse of this neutral-donor-bound-exciton complex is given the symbol $D^0X$. Bound excitons can be modeled after the hydrogen molecule $H_2$ with different binding energies [101] where the bound exciton exhibits significantly smaller binding energies than $H_2$ because the effective mass of the hole (for the exciton) is much smaller than the proton [101]. As the sample temperature is raised, the exciton can be thermally liberated (ionized) from the defect. Dissociation of the bound exciton into a free exciton and a neutral donor ($D^0X \rightarrow FX + D^0$) has been reported [126] and can provide information about the specific type of donor participating in PL emission. Specific donors can also be implicated by two-electron satellite luminescence discussed below.

### Two-electron Satellite of Bound-exciton Luminescence

Two-electron satellite (TES or $D^0X_{n=2}$) luminescence is the result of radiative recombination of a bound exciton that leaves the neutral donor electron in an excited state [127]. This type of luminescence is characteristic of neutral-donor bound-exciton radiation [82]. Detailed assessment of the TES luminescence can yield information about the specific donor that traps the exciton. This emission has been reported for the low temperature PL of EP-grown bulk ZnO [82, 87], however questions remain regarding the identification of the individual donors. Analysis of the TES spectrum from GaN was used to identify Si and O as the neutral donors in the low temperature bound-exciton luminescence [128]. Analogous to TES luminescence is two-hole satellite emission of neutral-acceptor-bound excitons. Analysis of the two-hole satellite emission has been used to implicate specific shallow acceptors in ZnTe [129]. In both cases, the excited state is assumed to be hydrogenic [82]. That is, exciting the donor electron (or acceptor hole) from a ground state ($n_1 = 1$) to the $n_2 = 2$ state requires 3/4 of the donor binding energy ($E_D$) [130]. To derive this result, consider Bohr's atomic

model for hydrogen which gives the energy difference between orbits $n_1$ and $n_2$ as [105]:

$$E_{n2} - E_{n1} = \frac{mq^4}{2K^2\hbar^2}\left(\frac{1}{n_1^2} - \frac{1}{n_2^2}\right) \tag{2.5}$$

where $m$ is the mass of the electron, $q$ is the electronic charge, $K$ equals $4\pi\epsilon_0$ and $\epsilon_0$ is the permittivity of free space. This energy difference can be used to determine the binding energy of the shallow donor [130]. The donor binding energy ($E_D$) can be written as [131]:

$$E_D = \frac{4}{3}\left(E_{D^0X} - E_{TES}\right) \tag{2.6}$$

The computed $E_D$ value can then be compared to values computed from an effective mass approximation to determine a possible donor candidate.

When discussing bound-exciton emission, several "binding energies" are of interest [102]. To review, the Coulombic interaction between the electron and hole giving rise to an exciton is given the name exciton binding energy ($E_{ex}$). Binding (localization) energy which traps an exciton to a defect is called localization energy ($E_b$) and the binding energy of a donor electron to the donor ion (resulting in a neutral donor) is referred to as the donor-binding energy ($E_D$).

### 2.3.3 Exciton-electron Luminescence

Klingshirn [65] initially reported the observation of a spontaneous emission peak due to the inelastic interaction of excitons and electrons at higher temperatures (T > 70 K) from the PL of ZnO. This exciton-electron (*Ex-El*) peak was characterized by a strong shift to lower energy with increasing temperature. The temperature dependence of this peak was modeled as [65]:

$$E_x - (\hbar\omega)^{Ex-El} = \gamma k_B T \tag{2.7}$$

where $E_x$ is the free-exciton energy and $(\hbar\omega)^{Ex-El}$ is the energy of the exciton-electron peak. Klingshirn [65] computed a value of $\gamma = 7.74$ based on a ratio of exciton and electron masses. This peak was observed to exhibit stimulated emission under high density optical excitation. Similar spontaneous luminescence has been observed for other II-VI semiconductors, such as CdS [132, 133] and CdSe [134]. Other values for $\gamma$ have also been reported. From a fit of the temperature-dependent data, a value of $\gamma = 7$ was reported in [132] and a value of $\gamma = 9.11$ from [134]. Exciton-electron collision has been reported as the mechanism responsible for the strong temperature shift of stimulated emission for CdS [133]. In all cases, the *Ex-El* luminescence exhibits a much stronger decrease in energy with increasing temperature than the band gap.

## 2.3.4 Hot-exciton Luminescence

The radiative recombination of non-thermalized excitons (i.e., excitons with kinetic energy exceeding both the thermal energy of the photoexcited sample and the exciton binding energy [135]) in the crystal can be regarded as hot excitons. These excitons are characterized by very short lifetimes usually due to interaction with defects in the material and are typically scattered by longitudinal optical (LO) phonons [136] prior to radiative recombination. Hot-exciton luminescence has been reported for several compound semiconductors including SiC [137], CdS [138, 139], ZnTe [140] and GaSe [141], however, the most interesting observation was reported for mechanically polished CdSe [136]. This result suggests near-surface disorder can play an important role in the evolution of hot-exciton luminescence. Figure 2.6 illustrates the hot-exciton luminescence mechanism, after [136]. Shown is the exciton dispersion superimposed on the photon dispersion with the energy of the incident photons from the laser ($E_L$) and the subsequent LO phonon energy levels (i.e., $E_L$-1LO, $E_L$-2LO, etc.). For this figure, the incident excitation photons are assumed to have an energy of 3.532 eV, consistent with the 351 nm line from an $Ar^+$ laser. The figure illustrates the indirect photon absorption, process (a), mediated by phonons or defects. After absorption, excitons

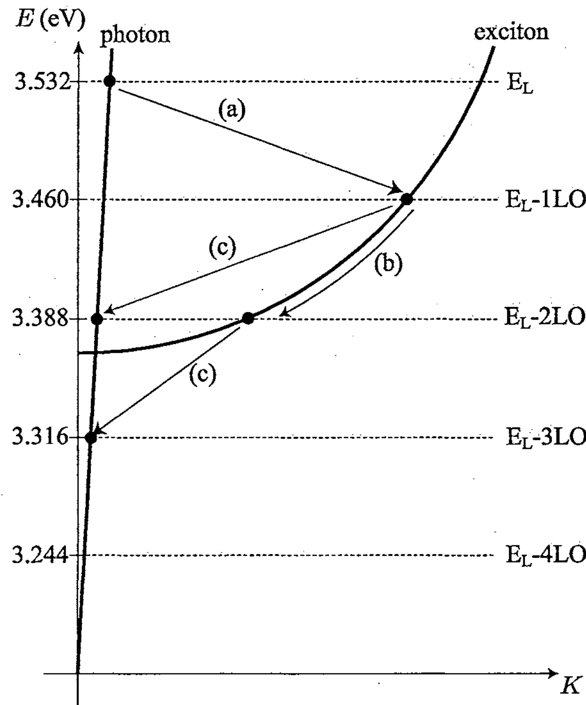


Figure 2.6: Hot exciton model, after [136]. Shown is (a) indirect photon absorption, (b) exciton kinetic energy relaxation, and (c) phonon-assisted exciton luminescence.

can either release kinetic energy by moving down the dispersion curve (i.e., kinetic energy relaxation), process (b), or they can be scattered by phonons to the photon dispersion curve, resulting in photon emission (i.e., phonon-assisted exciton luminescence), process (c). This type of luminescence exhibits a set of emission lines differing in energy from the incident excitation photons by an integer multiple of the energy of an LO phonon [142]. Based on this model, one would not expect to see any luminescence at an energy $E_L$-1LO, however emission at this energy is observed experimentally. Such observations have been explained as the breakdown in momentum conservation in the disordered near-surface layer [139]. This suggests the possibility that defects, rather than phonons, may participate in the photon absorption process. All of the hot-exciton peaks (except the $E_L$-1LO peak) exhibit very similar intensities owing to the predicted equal population of the different hot exciton levels in the dispersion model [143]. Hot-exciton luminescence closely resembles resonant Raman scattering (RRS). In this process, shown as Fig. 2.7, the photons are not absorbed, but rather scattered directly by LO phonons to subsequent lower energies.

Distinction between hot-exciton luminescence and RRS has generated some controversy [101]. Quoting from Martin and Falicov [144] in their work on RRS in semiconductors, "...hot luminescence

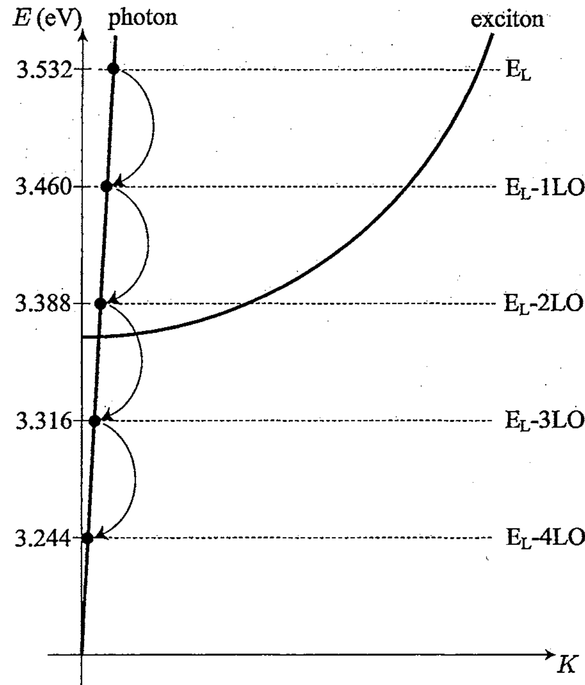


Figure 2.7: Resonant Raman scattering model, after [136]. Shown is the phonon scattering of photons. As a result, the photon is not absorbed in the crystal.

is hard to distinguish from RRS, and the criteria used to differentiate one from the other are mostly operational, based on theoretical formalisms or experimental convenience; (which) vary widely from researcher to researcher". We will defer to the interpretation of Yu et al. [101] who stated that a measurement of the coherence of the scattered photons for a well-defined set of scattering phonons is necessary to distinguish between the two processes. Since this measurement is not typically performed, declaration of the emission process is reduced to semantics [101]. In our study, radiation observed to be a function of the excitation energy will be recognized as hot-exciton luminescence.

### 2.3.5 Exciton-polariton Theory

To this point the interaction of excitons and photons has been neglected when discussing the exciton dispersion. The assumption has been that when representing the free-exciton dispersion it is unperturbed by any radiation field. A more rigorous approach is to consider the radiative recombination of excitons in terms of exciton-polaritons or simply polaritons [101]. Excitons traveling in a sample radiate electromagnetic waves which, in turn, can excite excitons, thus making it impossible to distinguish the exciton from the photon [101]. This coupled electromagnetic and polarization wave traveling in the sample is then given the name polariton [101]. Polaritons are complexes which result from the polarizing interaction between electromagnetic waves (photons) and oscillators (excitons) resonant at the same frequency [100]. For materials such as ZnO which exhibit strong exciton-photon coupling, the propagation of electromagnetic waves through the sample is more correctly regarded as a mixture of the electronic polarization and electromagnetic waves [102]. This mixing of photons and excitons is illustrated in Fig. 2.8. The mixing of states results in the splitting of the exciton dispersion curve into two separate polariton branches. Shown is the upper polariton branch (UPB) (solid line) and lower polariton branch (LPB) (solid line), where the knee in the LPB is called the polariton "bottleneck" and represents the region where polaritons have the longest lifetime [101]. Lower polaritons above the bottleneck exhibit a large exciton component and as a result of strong phonon scattering have shorter lifetimes [101]. Polaritons below the bottleneck principally behave as photons and can easily escape from the sample and as a result are also short-lived [101]. From Fig. 2.8, those excitons on the UPB that recombine (with nearly zero momentum) are regarded as longitudinal excitons ($E_L$) and those from the flat portion of the LPB are called transverse excitons ($E_T$). There exists a polariton dispersion for each of the valence excitons (e.g., A, B, and C valences for ZnO). As a consequence, the luminescence from a particular valence will be identified accordingly (e.g., LPB (A) is luminescence from the lower polariton branch of the A valence band). The energy

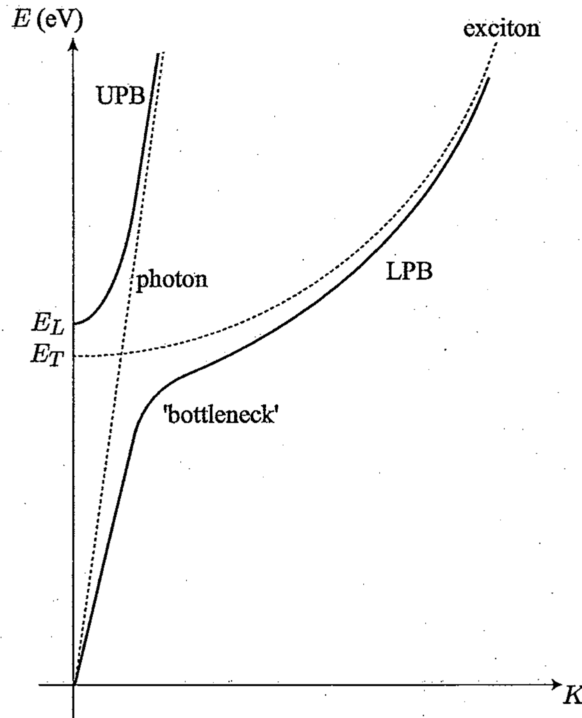


Figure 2.8: Polariton dispersion curves (solid lines), after [102]. Also shown is the free-exciton dispersion (dotted line) assuming no radiation field superimposed on a photon dispersion (dotted line) curve. The interaction of excitons and photons results in the upper polariton branch (UPB) and the lower polariton branch (LPB).

range over which the mixing of states is significant can be estimated by $\Delta E_m = \sqrt{E_T \cdot E_{LT}}$ where $\Delta E_m$ is the range of energy, centered at $E_T$, over which the radiation can be considered the result of polariton emission and $E_{LT} = E_L - E_T$ [145]. This range of mixing is illustrated in Fig. 2.9. Within $E_m$, the transverse excitons and photons are coupled to form polaritons. Much research has been published on the luminescence of polaritons [139, 146–149]. Reynolds et al. [125] reported the observation of luminescence from the "bottleneck" region of the LPB (A) in addition to free-exciton-like emission for ZnO. They also reported the observation of luminescence from the UPB (A) for $K = 0$ (longitudinal excitons, $E_L$). In all cases, observations of polariton emission were made at low temperature where $k_B T$ is smaller than the interaction energy between the excitons and photons and the observation of polaritons is possible [102].

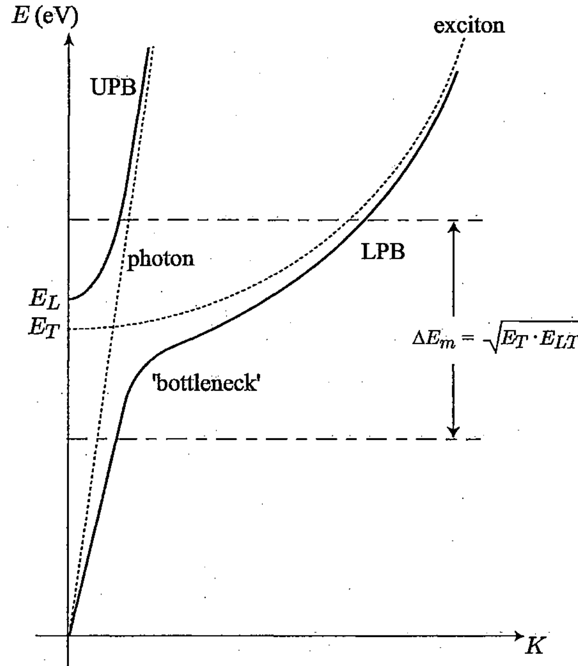


Figure 2.9: Polariton dispersion showing range of energy ($\Delta E_m$) for mixed photon and exciton states.

## 2.4 Phonon-assisted Luminescence

In addition to scattering events involving acoustic and optical phonons which lead to the thermalization (energy relaxation) of free carriers and excitons, phonons can also participate in the luminescence process. To illustrate their importance, phonon-assisted free-exciton transitions have been shown to exhibit stimulated emission for high-quality ZnO [150]. Whereas momentum selection rules dictate that only those excitons with nearly zero kinetic energy can radiatively recombine, these rules do not preclude excitons from possessing kinetic energy [102]. In fact, excitons with nonzero kinetic energy can also recombine radiatively via phonon interaction [102]. For polar semiconductors, such as ZnO, excitons predominantly couple to LO phonons as compared to other phonon types (e.g., transverse optical (TO) phonons) [151]. The LO phonons provide the necessary additional momentum to satisfy the conservation rules and allow excitons with nonzero kinetic energy to radiatively recombine [102]. While complexes such as bound excitons can couple to LO phonons resulting in luminescence, this section will focus on LO phonon-assisted free-exciton luminescence. LO phonon-assisted free-exciton luminescence has been shown to be strongly influenced by the presence of defects [151]. This is best illustrated by the work of Verbin et al. [152]. They showed that

for high quality or "perfect" (hence, low defect density) ZnO samples, the ratio of intensities for the 1LO- and 2LO-assisted free-exciton peaks was 0.1. However, for those samples known to have a high concentration of defects, the ratio increased to 2 [152]. Another important aspect of the LO phonon-assisted free-exciton emission is that the spectral lineshape provides information regarding the kinetic energy distribution of the free excitons [151]. This is illustrated below. Because multi-phonon luminescence intensities strongly decrease with increasing order [151], the discussion will be limited to the special cases of 1LO- and 2LO-phonon assisted transitions.

### 2.4.1 LO Phonon-assisted Free-exciton Luminescence

LO phonon-assisted luminescence of free excitons (abbreviated as FX-$m$LO, where $m = 1, 2$) exhibits a lineshape which can be adequately described by a Maxwellian distribution of the free-exciton kinetic energies $F(E_{kin}) \propto E_{kin}^{1/2} \exp(-E_{kin}/k_B T)$ where $E_{kin}$ is the kinetic energy of the free exciton [151]. For the general case of $m$LO phonon-assisted emission, the transition probability $P_m(\hbar\omega)$ for radiative recombination can be written as [153]:

$$P_m(\hbar\omega) \propto (\hbar\omega + m\hbar\omega_{LO} - E_x)^{5/2-m} \exp^{-(\hbar\omega + m\hbar\omega_{LO} - E_x)/k_B T} \tag{2.8}$$

where $m\hbar\omega_{LO}$ is the energy of the $m$LO phonon ($m = 1, 2$) and $E_x$ is the energy of the free exciton. We will assume that the transition probability function ($P_m$) also provides a good approximation of the emission lineshape ($L_m$). From this, the 1LO phonon-assisted transition lineshape function can be written as [153]:

$$L_1 \sim (\hbar\omega + \hbar\omega_{LO} - E_x)^{3/2} \exp^{-(\hbar\omega + \hbar\omega_{LO} - E_x)/k_B T} \tag{2.9}$$

and, similarly, the 2LO phonon-assisted lineshape is approximated by [153]:

$$L_2 \sim (\hbar\omega + 2\hbar\omega_{LO} - E_x)^{1/2} \exp^{-(\hbar\omega + 2\hbar\omega_{LO} - E_x)/k_B T} \tag{2.10}$$

These equations have been shown to closely approximate experimental results for both the FX-1LO and FX-2LO peaks for ZnO [153].

Experimental studies have shown that the 2LO phonon-assisted free-exciton peak lineshape directly reproduces the kinetic energy distribution of free excitons because its transition probability is independent of the exciton kinetic energy [151]. In contrast, the 1LO assisted transition probability is directly proportional to the exciton kinetic energy [102]. Additionally, the integrated intensity of the FX-2LO peak is proportional to the free-exciton concentration in the photoexcited sample and can be used for its measurement [151].

Intuitively, one would expect the energy separation between the FX, FX-1LO, and FX-2LO peaks

to be equal to the LO phonon energy of ZnO. However, this is not observed experimentally. Free exciton kinetic energy results in phonon replicas separated by energy less than an integer multiple of the LO phonon energy [102] as illustrated in Fig. 2.10, after [154]. Shown is a 1LO-phonon-assisted transition from an initial state ($\hbar K_i$) to the ground state represented by processes (a) and (b). The creation of an LO phonon results in decreased energy for the emitted photon, however this energy reduction is not from the zero momentum state, but from the initial state which contains some kinetic energy. As a result, the emitted photon has some final energy equal to $E_x - m\hbar\omega_{LO}$ plus a kinetic energy term. This kinetic energy term is a function of the sample temperature. As a result, the energy separation between the FX, FX-1LO, and FX-2LO peaks is also a function of temperature. This temperature-dependent energy separation between the three peaks is discussed below.

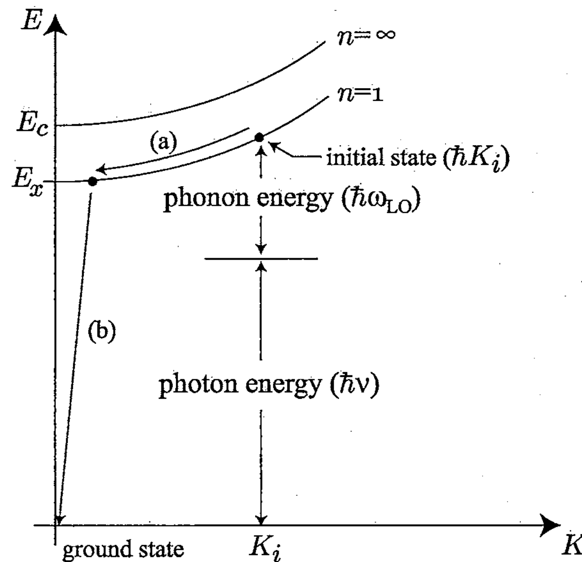


Figure 2.10: Exciton dispersion model depicting a 1LO phonon-assisted recombination, after [154]. The initial state is given by ($\hbar K_i$). Whereas the resulting energy of the photon emission is decreased by the LO phonon energy, its final energy is dependent on the amount of initial free-exciton kinetic energy.

### 2.4.2 Temperature-dependent LO Phonon-assisted Free-exciton Luminescence

The emitted photon energy ($\hbar\omega$) of an LO phonon-assisted free-exciton recombination is equal to $E_x - \hbar\omega_{LO}$ plus a temperature-dependent kinetic energy term ($uk_BT$). This can be written as [102]:

$$\hbar\omega = E_x - m\hbar\omega_{LO} + uk_BT \tag{2.11}$$

The coefficient $u$ is calculated for both the 1LO-phonon and the 2LO-phonon assisted peaks by differentiating Eqns. (2.9) and (2.10), respectively, and setting them equal to zero. This is done in Appendix H with the results summarized here. For the 1LO-phonon-assisted peak, the temperature-dependent separation from the free-exciton peak can be written as:

$$(\hbar\omega)_{FX-1LO} = E_x - \hbar\omega_{LO} + \frac{3}{2}k_BT \tag{2.12}$$

and for the 2LO-phonon-assisted peak:

$$(\hbar\omega)_{FX-2LO} = E_x - 2\hbar\omega_{LO} + \frac{1}{2}k_BT \tag{2.13}$$

These results indicate that the phonon replica peak is separated from the zero phonon peak not by an integer multiple ($m = 1, 2$) of the energy of an LO phonon, but rather an integer multiple of the energy of an LO phonon less a thermal kinetic energy term ($uk_BT$), where $u = 3/2$ for a one LO process and $u = 1/2$ for a two LO phonon assisted transition. One consequence of the temperature-dependent FX line broadening (Appendix G) and LO phonon-assisted FX luminescence is that the zero- and one-LO phonon-assisted FX peaks merge into one convoluted peak at higher temperatures. From results later presented, this convolution occurs at about 200 K.

## 2.5 Donor-acceptor-pair Luminescence

The presence of donors and acceptors in a material can lead to radiative recombination of electrons and holes from these levels as shown in Fig. 2.11. Such luminescence has been reported for many semiconductors including CdS [155], GaN [156,157], ZnSe:N [158–160], and GaS [161] to name a few. This emission is commonly referred to as donor-acceptor-pair (DAP) luminescence. From Fig. 2.11, one might expect the emitted photon to exhibit an energy equal to $E_g - E_a - E_d$, however this assumption does not include the Coulombic interaction between the ionized donors and acceptors [101]. The amount of interaction is dependent on the separation between the individual donor and acceptor ions. Whereas exciton Coulombic interaction is determined by quantum mechanics,

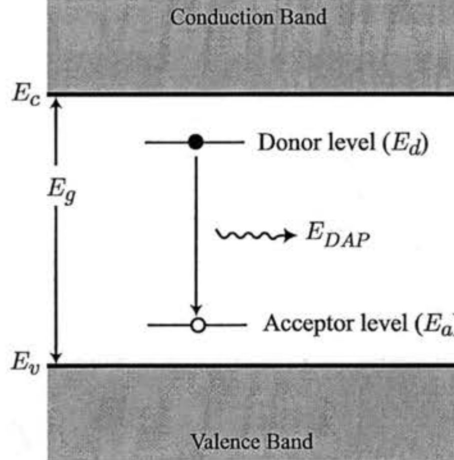


Figure 2.11: Simplified energy band gap depicting donor-acceptor-pair (DAP) recombination.

the distance between ionized impurities, $R$, is determined by the crystal structure [101]. The DAP complex consists of a donor ion, an acceptor ion, a free electron and a free hole and can be identified as either (i) distant DAP pairs or (ii) associated DAP pairs based on the spacing between the donor and acceptor ions [102]. For the case of distant pairs, $R$ is considered to be much larger than the lattice constant and the emitted photon energy from the DAP recombination, $E_{DAP}$, can be written as [101]:

$$E_{DAP} = E_g - E_a - E_d + \frac{e^2}{\epsilon R} \tag{2.14}$$

where the last term represents the Coulombic interaction between the donors and acceptors, $e$ is the electron charge and $\epsilon$ is the static dielectric constant. For the case of closely-spaced (associated) pairs such as at nearest neighbor sites, Eqn. (2.14) remains essentially the same, but the static dielectric constant is replaced by the high frequency dielectric constant for the material [102]. At low temperatures, the individual contributions from closely spaced pairs for discrete values of $R$ have been observed in GaP [101]. The luminescence is characterized by several sharp, closely spaced peaks converging toward the limiting case of $E_g - E_a - E_d$ for $R \to \infty$ [101].

Luminescence from distant pairs is characterized by the presence of multiple LO phonon replicas [159], a blue shift of the DAP peak with increased optical excitation intensity [159, 162] and increased temperature [156, 157, 161]. The intensity of the DAP peak, $I_{DAP}$, varies with temperature as $\exp[-E_A/(k_B T)]$ where $E_A$ is the thermal activation for either the donor electron or acceptor hole. This activation energy can be determined from a plot of $\ln[I_{DAP}]$ versus $1/(k_B T)$ (See Appendix F).

## 2.6 Deep-level Luminescence

Deep-level luminescence (DL) is a general description for a variety of EHP recombination processes including radiative recombination from DAP. Most of the participating impurities in DL emission have large ionization energies and as a result form traps deep in the energy gap [100]. Figure 2.12 illustrates some of the possible transitions involving these deep states. Shown are processes for donor-acceptor recombination, conduction band-to-acceptor recombination and donor-to-valence band recombination with each resulting in photons of energy, $E_{DL}$. Deep impurities have been shown to negatively affect II-VI semiconductor devices [101]. As discussed previously, DL emission is characteristic of ZnO and also for a similar wide band gap material, GaN. Recently, Colton et al. [163], in a DL PL study of GaN, were able to demonstrate that selectively excited (below band gap energy) DL emission involves associated DAP complexes whereas above band gap excitation resulted in the recombination of distant pairs. For ZnO, the DL emission has been identified as the result of point defects such oxygen vacancies [164] and Zn interstitials or antisites [76].

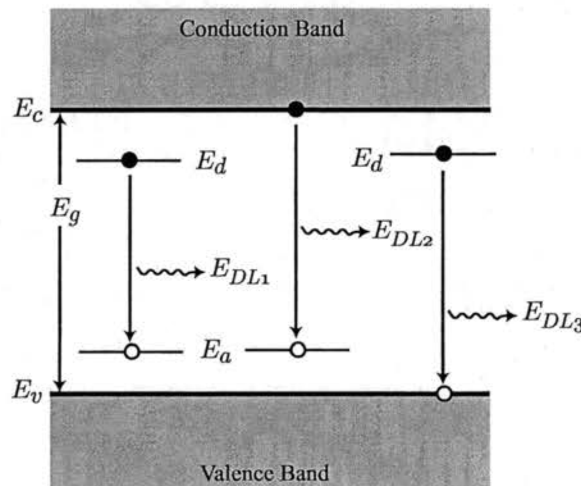


Figure 2.12: Simplified energy diagram illustrating some of the possible electronic transitions leading to the observation of DL luminescence. Shown are three possible recombination paths resulting in three different photon energies, $E_{DL1}$, $E_{DL2}$, and $E_{DL3}$.

# Chapter 3

# Experimental

## 3.1 ZnO Structure and Growth

Figure 3.1 shows both the (a) three-dimensional crystal structure and (b) atomic stacking sequence (viewed along the optical axis) for wurtzite ZnO, from [101]. The asymmetric stacking sequence (A(Zn)B(O)B(Zn)A(O)A(Zn)B(O)B(Zn)...) of atomic layers along the **c** axis which gives rise to the two distinct polar faces –the (0001) Zn-terminated face and the $(000\bar{1})$ O-terminated face– can be seen. The wurtzite lattice is a variation of the zincblende structure with the tetrahedral nearest-neighbor bonding described as "eclipsed" [101]. A description of the seeded chemical vapor transport (SCVT) method used to grow the ZnO crystals used in this study is given in Look et al. [165]. A brief summary of the growth method follows. The vapor-phase technique uses a nearly-closed horizontal tube with pure ZnO powder as the source at the hot (1150°C) end of the tube. Hydrogen is used as the carrier gas to transport the material to the cooler end of the tube. The reaction at the hot end is:

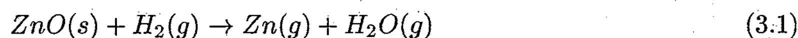

$$ZnO(s) + H_2(g) \rightarrow Zn(g) + H_2O(g) \tag{3.1}$$

Using a single crystal seed and a small amount of water vapor to maintain the proper stoichiometry, ZnO is formed by the reverse of the reaction (3.1) at the cool end end of the tube. The growth time required to produce 2-inch-diameter crystals of about 1 cm thickness is about 150-175 hours. The purity of the vapor-grown crystals is typically 99.9999% or better as measured by glow discharge mass spectrometry (GDMS) [166]. Typical defects resulting from the growth process include Zn interstitials [77], O vacancies [164], impurities such as Si and N [166] and dislocations. Dislocation density for these samples, as estimated from etch pit density, ranges from 1 to 2x10$^5$ cm$^{-2}$ [167].

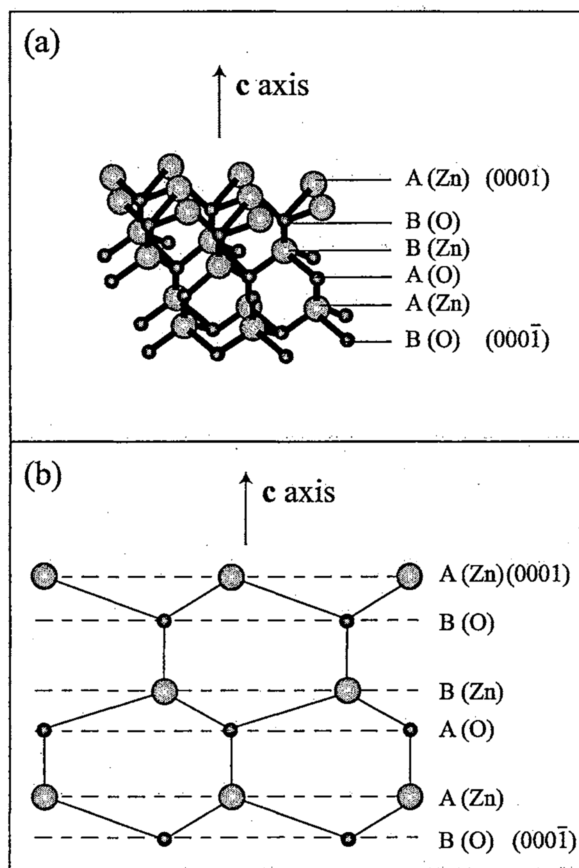


Figure 3.1: Crystal structure (a) and stacking sequence of atoms along the c axis (b) for wurtzite ZnO, from [101].

Estimates of impurity concentration as determined from GDMS are 528 parts per billion atomic (ppba) for Si and 98 ppba for N. Using an I.D. saw, 1 mm thick wafers are sawn from the boule and then lapped and polished as described in the following section.

## 3.2 Sample Preparation

Wurtzite structure ZnO produced by Eagle-Picher and grown by the SCVT method [165] was used in the study. Both the (0001) Zn-terminated face and the (000$\bar{1}$) O-terminated faces were studied. The (0001)-oriented wafers were sawn from the boule and then etched in 5 vol % trifluoroacetic acid ($F_3CCOOH$) and de-ionized $H_2O$ ($\geq$15 $\Omega$-cm) to remove about 25 $\mu$m from the saw-damaged surface. The wafers were processed on both sides by first lapping and then chemomechanical polishing. This provided flat, minimally damaged surfaces which could be then further processed. Lapping was performed using a commercial lapping machine with a cast iron wheel and a 9 $\mu$m $Al_2O_3$/de-ionized

$H_2O$ slurry resulting in an additional 50 $\mu m$ of material removal from each side. This was followed by chemomechanical polishing using a commercial polishing machine and a slurry of a 1:8 ratio of sodium hypochlorite:colloidal silica (9.1 pH). (0001) and (000$\bar{1}$) wafers were then prepared with one of the following polishing preparations: 1) mechanical polishing with 1 $\mu m$ diamond abrasive/de-ionized $H_2O$ slurry, 2) mechanical polishing with 1/4 $\mu m$ diamond abrasive/de-ionized $H_2O$ slurry and 3) chemomechanical polishing as described above. Mechanical polishing was performed using a nylon pad and a pressure of 1.4 x $10^{-2}$ MPa.

For the H-treated ZnO studies, the (0001) face of one sample was implanted with 0.3 x $10^{15}$ H/cm$^2$ at 12 keV in the Ion Beam Materials Laboratory at Los Alamos National Laboratory. The (0001) face of another sample was exposed to a 200 W rf 95% Ar/5% $H_2$ plasma for 1 minute at 167 mTorr using a commercial plasma-cleaning instrument. An estimate of the hydrogen concentrations in the untreated and treated samples was made by elastic recoil detection (ERD) at Los Alamos. The H concentration in the untreated samples was below the detection limit of our technique. An analysis of the ion-implanted sample using a combination of ERD data and TRIM simulations [168] showed that the hydrogen had a Gaussian distribution with a peak approximately 57 nm below the surface and that the average concentration within the variance of the distribution was 1.0 x $10^{20}$ H/cm$^3$. In the plasma-etched sample, the ERD data showed the presence of a near uniform distribution of H within the first 1 $\mu m$ of the sample surface (the depth limit of the technique) with an average concentration of 4.2 x $10^{20}$ H/cm$^3$.

## 3.3 Photoluminescence System

The PL system used in this study was conventional in design and typical of many systems reported in the literature. A simplified schematic of the system is shown in Fig. 3.2. PL was excited using the 351 nm (3.532 eV) line from an $Ar^+$ laser with a typical power density of about 50 mW/cm$^2$ to minimize carrier interaction. PL studies were performed on the (0001) Zn-terminated and (000$\bar{1}$) O-terminated faces with the electric field vector perpendicular to the optical axis of the sample ($\mathbf{E} \perp \mathbf{c}$). The emitted light was dispersed by a 0.5 m monochromator with a 2400 g/mm grating and detected with a $LN_2$-cooled CCD camera. The spectral resolution of the system with the 2400 g/mm diffraction grating and the CCD detector is 0.5 meV at 3.37 eV. The sample temperature was varied from 4.2 to 300 K using a continuous flow liquid He optical cryostat. The following is a detailed list and specifications for each of the subsystems used to measure PL from ZnO. Appendix E provides a checklist for the operation of each subsystem.

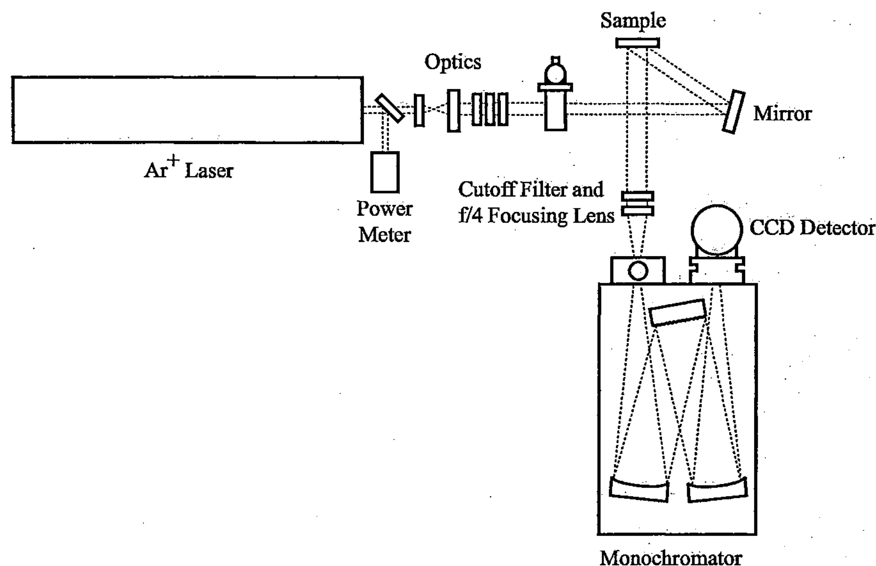


Figure 3.2: PL System Schematic

### 3.3.1 Laser

The continuous wave (cw) excitation source used in these experiments was a Beamlok 2065-7S Argon ion laser from Spectra-Physics. The output power of the Gaussian ($TEM_{00}$) beam is rated for 7 W all lines and 250 mW at 351.1 nm (3.532 eV). To enable the selection of the 351.1 nm line from the laser, an ultraviolet (UV) prism was used with a UV output coupler mirror. The nominal beam diameter (1/e) was 1.7 mm. However, using a Keplerian beam expander, the typical spot size at the sample was about 3 mm. The laser is water cooled using a closed-loop heat exchanger (Model no. 315A). Within the secondary loop of the heat exchanger (the water flowing through the laser frame) is a bypass loop that conditions the cooling water using a deionizing/deoxygenation filter. The output power was monitored using an Ultima Labmaster power meter manufactured by Coherent Auburn Group with a cw power range of 10 nW - 10 W. Experiments were also conducted using an Omnichrome HeCd multimode laser operating at 325 nm with a maximum output power of 20 mW.

### 3.3.2 Spectrometer

Luminescence from ZnO was dispersed using a 0.5 m focal length spectrometer (Model no. 500M) from Jobin-Yvon (ISA/SPEX) with a 2400 g/mm diffraction grating holographically blazed at 400 nm. The f/4 aperture, Czerny-Turner spectrometer with 2400 g/mm grating has a mechanical range of 0-750 nm with an accuracy of 0.05 nm, a repeatability of 0.005 nm, and a resolution of 0.01 nm.

### 3.3.3 Charge Coupled Device (CCD) Array

The CCD used in these experiments was a 1024 × 128 pixel (26.6 mm × 3.3 mm) back-illuminated, UV-enhanced, liquid nitrogen cooled array from Jobin/Yvon (ISA/SPEX). The individual pixel size is 26 × 26 $\mu$m. The detection range is 1.55-4.96 eV (800-250 nm). The resolution of this detector coupled with the 500M spectrometer and 2400 g/mm grating is about 0.5 meV at 3.37 eV.

### 3.3.4 Cryostat

The sample temperature was varied using a continuous flow liquid He cryostat (Model no. ST-100) manufactured by Janis Research and a Lakeshore autotuning (PID) temperature controller (Model no. 330) with a silicon diode thermometer and a 25 $\Omega$ control heater in the copper sample mount (cold finger). The system has a temperature range of 4.2-325 K with a 50 mK stability. The sample chamber and annular volume of the He transfer line were evacuated using a turbomolecular pump (Model no. EXT70-H) manufactured by BOC Edwards. Typical vacuum pressure for each evacuated volume was about 15 $\mu$Torr as measured by an active inverted magnetron (AIM) gage (Model no. AIM-S-NW25) also manufactured by BOC Edwards.

## 3.4 Estimated Depth of Investigation Using PL

The depth of investigation below the surface was estimated by considering the absorption coefficient, defined by the relationship $I(z)/I_o = exp(-\alpha z)$, where $I(z)/I_o$ is the intensity at depth $z$ below the surface relative to the incident intensity $I_o$ and $\alpha$ is the absorption coefficient. Reported values for $\alpha$ for wurtzite structure ZnO at 3.5 eV include $1.55 \times 10^5$/cm [25] and $1.8 \times 10^5$/cm [169]. If the average of these two values is used, 90% absorption of the excitation energy would be accomplished at a depth of 137 nm. To allow for surface-normal collection of PL, the excitation laser beam was directed at the sample with a glancing angle of approximately 63 degrees relative to the surface normal. In light of this glancing angle of the beam relative to the sample surface, the depth for 90% absorption would be about 60 nm from the polished surface.

# Chapter 4

# Results and Discussion

PL results presented here are organized according to surface preparation (e.g., etched, chemomechanically polished, etc.). The first three sections are presented in order of increasing near surface damage (from wet-etched to mechanically polished) as determined by axial ion channeling [37]. Low temperature, RT and temperature-dependent PL are used to compare the effects of subsurface damage on the luminescence of ZnO for each of the surface preparations. In some cases, comparisons are also made between the two polar surfaces of ZnO for a given surface preparation. The final section presents a low temperature PL study of H-treated ZnO. All of the spectra presented are typical and represent data which has not been filtered, smoothed or corrected for detector response. Results not specific to this study are included in the Appendix. PL observations from etched ZnO provide the best approximation of bulk PL response. These can be used as a baseline for comparison to subsequent PL results for other surface preparations.

## 4.1 Etched ZnO

Figure 4.1 shows a typical 4.2 K PL spectrum from etched (0001) ZnO. Shown is the spectrally-resolved PL intensity, given in arbitrary units (a.u.), as a function of energy, in units of electron-volts (eV). Some general comments can be made regarding this spectrum. First, these results are consistent with previous reports for the PL of etched EP-grown bulk ZnO initially reported by Sherriff et al. [57]. Second, whereas the 4.2 K PL spectrum is seen to be dominated by very narrow peaks near 3.365 eV, there are many peaks which require identification. For this discussion, the PL spectrum is divided into smaller energy regions. For example, the inset of Fig. 4.2 is from the 3.37-3.40 eV range of the full spectrum and shows the A valence band free-exciton peak, FX (A), and a

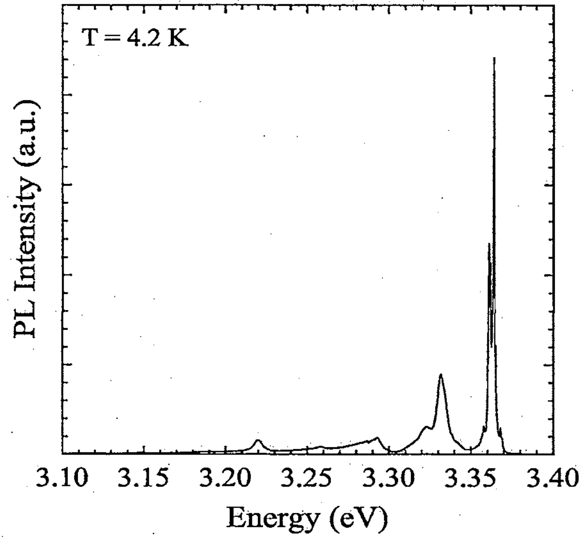


Figure 4.1: 4.2 K PL of etched (0001) ZnO.

slight peak from the lower polariton branch from the same A valence band, LPB (A) as identified in a study by Reynolds et al. [125]. In their study, the LPB (A) was specifically identified as emission from the "bottleneck" region of the lower polariton branch of the A valence band. The high quality ZnO used in this study is evidenced by the observation of free-exciton luminescence at 4.2 K. The next lower energy region in the PL spectrum is the bound-exciton emission.

The inset of Fig. 4.3 shows the peaks observed in the energy range 3.35 to 3.37 eV. In a separate

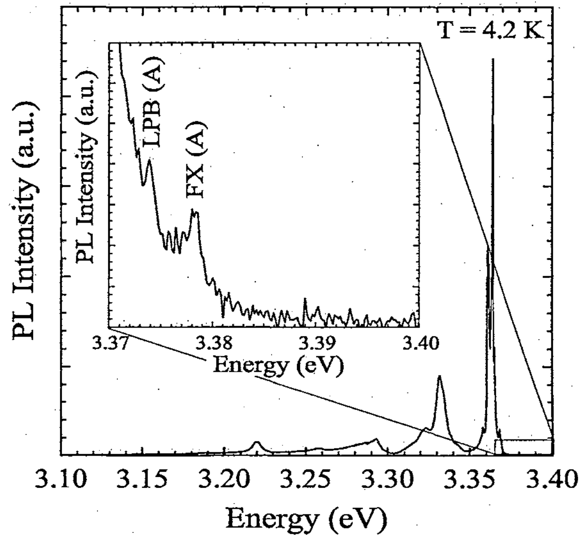


Figure 4.2: 4.2 K PL of etched (0001) ZnO. Inset illustrates detailed free A-valence exciton, FX (A), and lower A-valence polariton, LPB (A), emission.

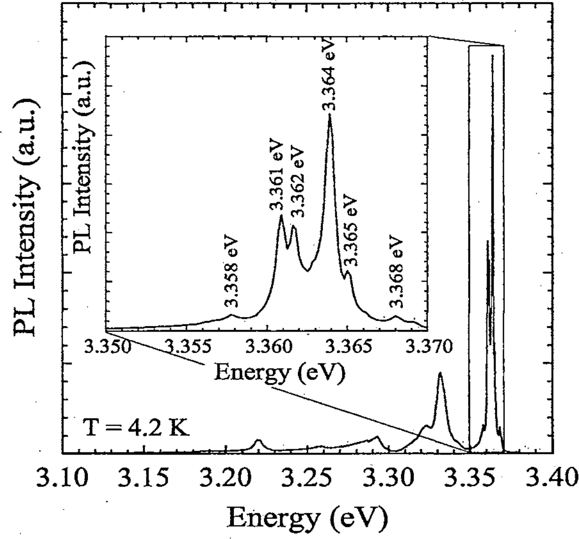


Figure 4.3: 4.2 K PL of etched (0001) ZnO. Inset illustrates detailed emission from 3.35 to 3.37 eV. PL in this energy range is dominated by the collapse of excitons bound to defect pair complexes which simulate neutral donors [82].

study of ZnO, also produced by Eagle-Picher, Reynolds et al. [82] attributed the peaks in this energy range to excitons bound to neutral donor complexes ($D^0X$). We identify six clearly resolved $D^0X$ peaks located at 3.368, 3.365, 3.364, 3.362, 3.361 and 3.358 eV. The full-width at half maximum (FWHM) of the 3.364 eV peak, the strongest of the six peaks, is observed to be about 0.9 meV. Such narrow emission is consistent with luminescence from bound excitons. As will be shown later, the FWHM of these bound excitons is significantly altered by the introduction of near-surface damage.

The inset of Fig. 4.4 shows the detailed emission in the range 3.30-3.35 eV. PL from ZnO in this energy range has been previously identified by other researchers as two-electron satellite (TES) emission [82,87]. Based on this information, we also identify the peaks at 3.323 eV and 3.332 eV as the result of TES emission. While it is difficult to determine which of the $D^0X$ peak(s) results in the satellite peaks, the following analysis assumes the collapse of the 3.364 eV bound exciton leads to the 3.332 eV luminescence. Based on this assumption and Eqn. (2.6), we compute a donor-binding energy ($E_D$) of 42.6 meV. This value is in good agreement with Thonke et al. [87] who reported a value of 39.9 meV for EP-grown ZnO. They hypothesized that H is the shallow donor based on their value of donor-binding energy.

Figure 4.5 shows the detailed emission in the range 3.10-3.30 eV. We identify the peaks at 3.292 eV, 3.220 eV and 3.146 eV as zero-, one-, and two-LO-phonon assisted transitions of associated donor-acceptor pairs, respectively, and the peaks at 3.258 eV and 3.187 eV as one- and two-LO

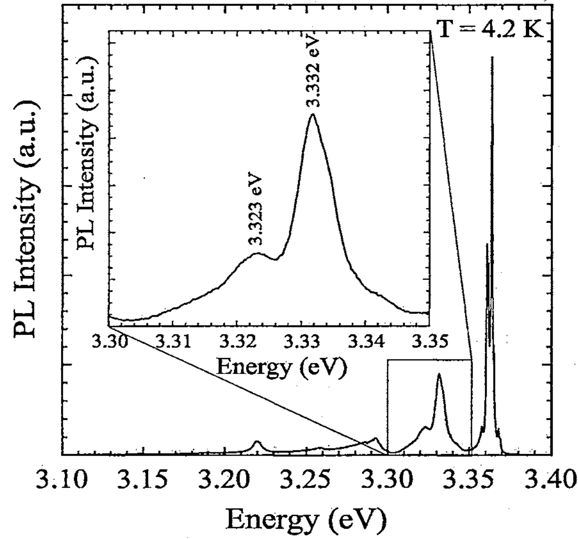


Figure 4.4: 4.2 K PL of etched (0001) ZnO. Inset illustrates detailed emission from 3.30-3.35 eV. PL in this energy range has been attributed to two-electron satellites of bound excitons [82, 87].

phonon replicas of the TES peak at 3.332 eV, respectively. Notice that the spacing of these peaks is consistent with an integer multiple of the LO phonon energy for ZnO (72 meV) from the zero-phonon peak. The identification of the zero-phonon-assisted DAP peak is based principally on its asymmetric

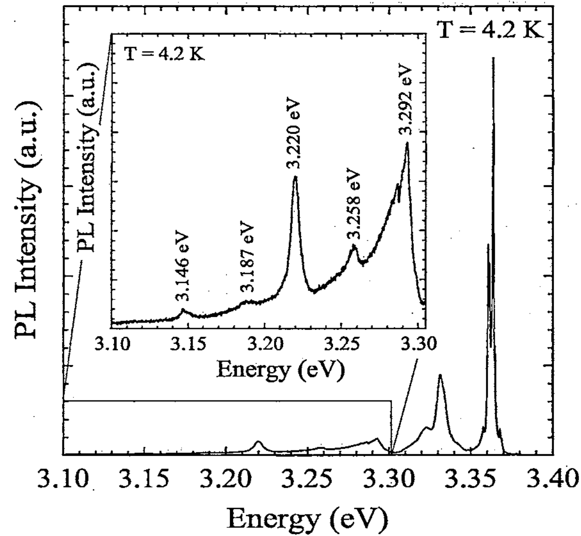


Figure 4.5: 4.2 K PL of etched (0001) ZnO. Inset illustrates detailed emission from 3.10-3.30 eV. The lower energy PL in this range is typically from DAP recombination or phonon replicas of higher energy transitions.

lineshape. As discussed previously, for associated pairs, the luminescence is characterized by several sharp, closely spaced peaks converging toward the limiting case of $E_g - E_a - E_d$ for $R \rightarrow \infty$ [101]. We are unable to resolve the individual sharp lines, but we see a convolution of each of the near-spaced pairs resulting in a low-energy tail. The limiting energy of the near-spaced pairs is then 3.292 eV. The identification of this DAP peak is in contradiction with Thonke et al. [87] who identified the 3.22 eV peak as the zero-phonon-assisted DAP peak. Table 4.1 summarizes the identification of each of the 4.2 K PL peaks observed from etched (0001) ZnO. In addition to the observed asymmetric

| **PL Energy (eV)** | **Assignment** | **Reference** |
|---|---|---|
| 3.378 | FX (A) | present work |
| 3.374 | LPB (A) | [125] |
| 3.368, 3.365, 3.364, 3.362, 3.361, 3.358 | $D^0X$ | [82] |
| 3.332, 3.323 | TES | [82,87] |
| 3.292 | $D^0X$-1LO | [87] |
| | DAP | present work |
| 3.258 | TES-1LO | present work |
| 3.220 | DAP | [87] |
| | DAP-1LO | present work |
| 3.187 | TES-2LO | present work |
| 3.146 | DAP-1LO | [87] |
| | DAP-2LO | present work |

Table 4.1: Summary of 4.2 K PL peak assignments for etched (0001) ZnO.

lineshape of the 3.292 eV peak, we also believe its assignment as zero-phonon DAP emission (rather than $D^0X$-1LO as reported by Thonke et al. [87]) is based on the fact that there are no previous reports of LO phonons coupling to neutral-donor-bound excitons for ZnO at low temperature (see for example Ref. [57]). Based on our identification of the 3.292 eV peak as zero-phonon-assisted DAP luminescence, our identification of each of the phonon replicas is shifted relative to Thonke's assignments by the energy of 1 LO phonon. For example, Thonke et al. [87] identifies the 3.220 eV peak as a zero-phonon DAP peak while we identify this same peak as a 1LO phonon-assisted DAP peak.

Apart from slight differences in absolute intensity, the 4.2 K PL from these etched substrates exhibits good repeatability. Figure 4.6 shows a comparison between two spectra collected from the

same sample about ten weeks apart, where the spectra are normalized using the 3.364 eV peak. There are no observed differences between the two spectra. Additionally, the 4.2 K PL from $(000\bar{1})$ ZnO is observed to be similar to that for (0001) ZnO as shown in Fig. 4.7, where the spectra are normalized using the 3.364 eV peak. Differences observed for the PL from these two etched polar surfaces have been previously reported by Sherriff et al. [57]. Having established a low temperature PL spectrum as a baseline for bulk ZnO, we now turn our attention to the RT PL response of the same etched surfaces.

The RT PL for both polar faces of etched (0001)-oriented ZnO is shown in Fig. 4.8, where the spectra are normalized using the FX peak at 3.26 eV. For both the (0001) and $(000\bar{1})$ etched surfaces, shown in Fig. 4.8 as curves a and b, respectively, the RT PL spectra were found to exhibit three distinct peaks. The identification of the peak at 3.26 eV is uncertain. Recent reports have attributed this emission to LO phonon-assisted free-exciton (FX-1LO) luminescence [170] or bound-exciton luminescence [80]. We tentatively identify this peak as the collapse of free excitons (FX) based on the consistency with previous reports for high-quality (0001) ZnO films [15]. Whereas this assignment results in a RT band gap energy (3.32 eV) less than the accepted value of 3.37 eV [17], we believe this 50 meV difference may be attributed to FX line broadening, as described in Bebb and Williams [102]. Convolution of the presumed FX peak with LO phonon-assisted FX luminescence precludes an accurate measure of its linewidth and lineshape. A second broad peak

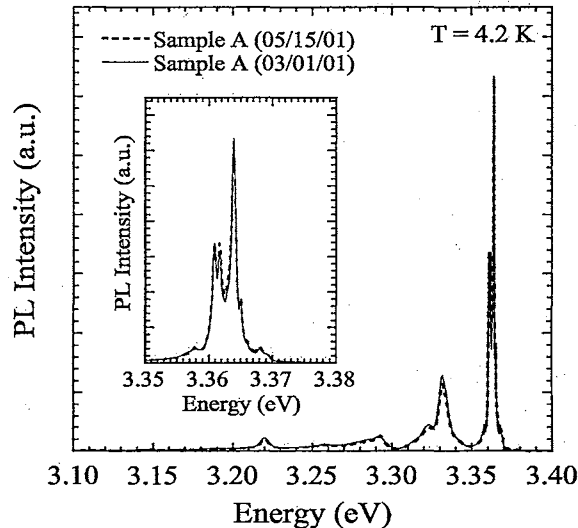


Figure 4.6: Comparison of a 4.2 K PL spectrum from an etched (0001) ZnO sample to that collected from the same sample about ten weeks after the initial characterization. Inset shows detail of exciton emission.

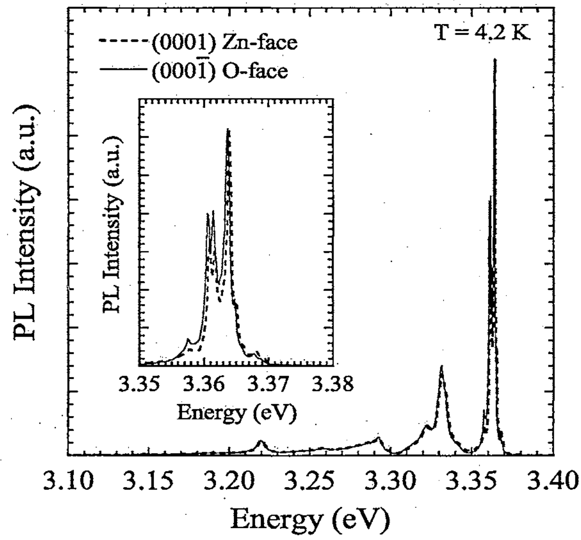


Figure 4.7: Comparison of 4.2 K PL spectra collected from the two polar faces of the same sample. Inset shows detail of exciton emission.

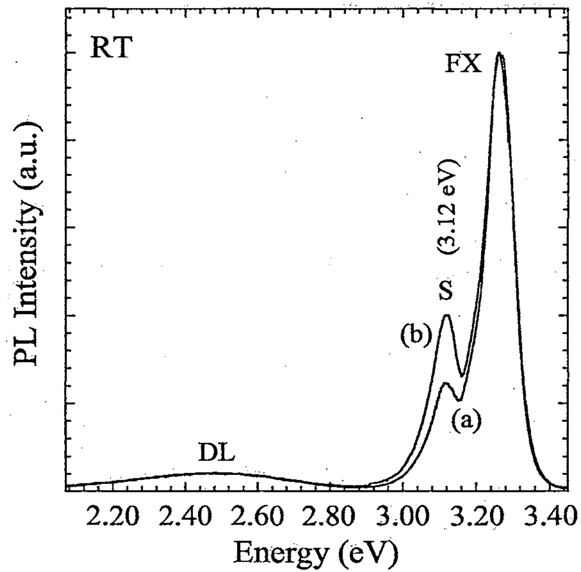


Figure 4.8: RT PL from etched (a) (0001) and (b) (000$\bar{1}$) ZnO. Shown is free-exciton (FX) luminescence at 3.26 eV, a second clearly resolved peak at 3.12 eV, and deep level (DL) emission at about 2.5 eV.

is observed at about 2.5 eV and is commonly associated with deep level (DL) emission in ZnO. A recent study on similar ZnO attributes this DL emission to oxygen vacancies [164]. A third distinct peak is observed at 3.12 eV, referred to by the designation "S". To the best of our knowledge, this is the first report of this peak for etched bulk ZnO. Identification of the S peak is uncertain. One plausible explanation for this peak is exciton-electron interaction. This assignment is supported by the temperature-dependent (0-300 K) PL energies of the FX-2LO and S peaks shown in Fig. 4.9. The predicted FX temperature dependence, shown as curve (a), is from Ref. [171]. The measured FX-2LO peak is shown with a theoretical model based on Eqn. (2.13), shown as curve (b). Also shown is the measured temperature dependence of the S peak. Curve (c) is a model for luminescence from inelastic interaction between excitons and electrons (Eqn. (2.7) with $\gamma = 7.74$), from Ref. [65]. The agreement observed between the measured temperature dependence of the S peak and the predicted temperature dependence of exciton-electron luminescence for 200-300 K is evidence that the S peak is luminescence resulting from exciton-electron interaction.

## 4.2 Chemomechanically Polished ZnO

The 4.2 K PL spectrum from a chemomechanically polished surface closely resembles the PL from an etched surface as shown in Fig. 4.10, where the two spectra are normalized using the 3.364 eV peak. The relative intensity of the lower energy features such as TES and DAP emission is seen to be higher

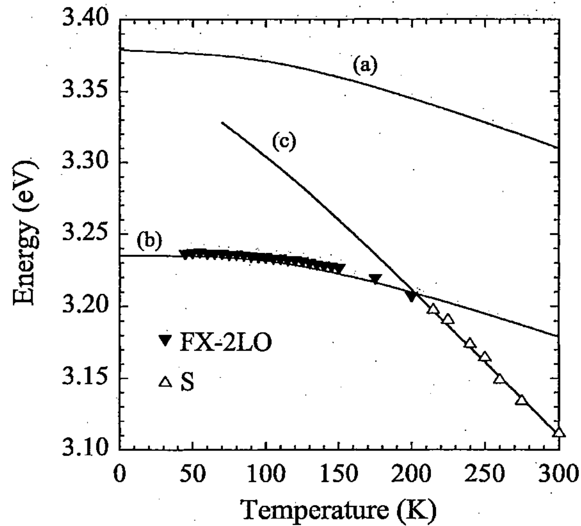


Figure 4.9: Temperature dependence of FX-2LO and S peaks. Also shown is the predicted temperature dependence of (a) FX, (b) FX-2LO, and (c) exciton-electron luminescence.

for the etched material as compared to the polished surface. Otherwise, no significant differences are observed between the two spectra at this temperature. The difference in observed FX peak position for the samples prepared by chemomechanical polishing and those etched in trifluoroacetic acid/deionized $H_2O$ falls within the resolution of the detection system. The bound-exciton luminescence was nearly identical for these two surfaces. PL results from chemomechanically polished ZnO are organized into five sections. Results from Sections 4.2.3 and 4.2.5 have been reported in the literature and can be found in Refs. [171] and [172], respectively.

### 4.2.1 Sample-to-sample Variation of the 4.2 K PL

Because the growth and final processing of compound semiconductors such as ZnO is an inexact science, there necessarily is some variation in the growth conditions as well as polishing parameters in production of the material. These variations can significantly affect the optical properties of the material. An example of this can be seen in a comparison of the 4.2 K PL from two different samples (labeled sample 1 and 2) cut from two different boules, shown in Fig. 4.11. For this comparison, the spectra are limited to the bound-exciton emission and normalized using the 3.363/3.364 eV $D^0X$ peak. Differences in the number and intensity of the bound-exciton peaks can be seen. Additionally, the free-exciton and lower polariton emission is observed to be much stronger for sample 2, suggesting a much higher quality (e.g., fewer impurities or defects) for this sample as compared to sample 1. In addition to quality variation from boule-to-boule, we also observe sample-to-sample variation in

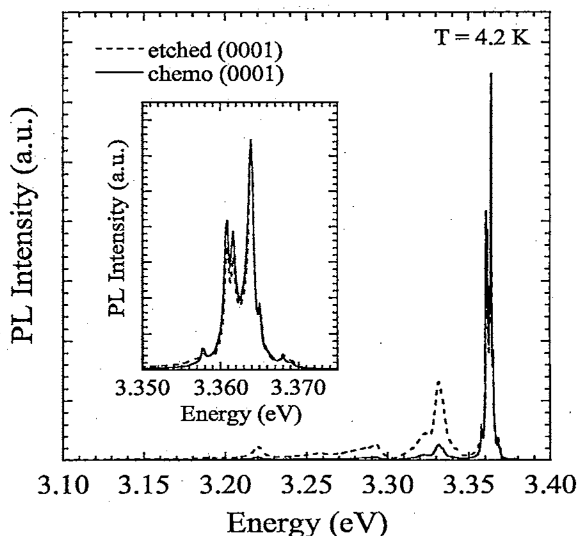


Figure 4.10: Comparison of the 4.2 K PL spectra for (0001) chemomechanically polished and (0001) etched ZnO. Inset shows detail of exciton emission.

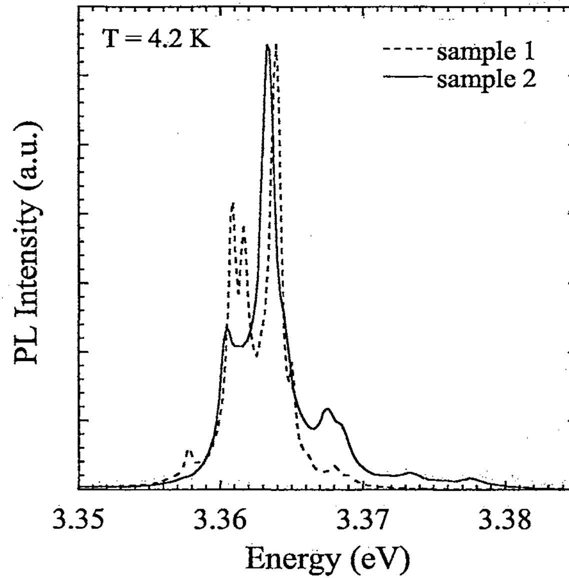


Figure 4.11: Comparison of the 4.2 K PL from two different (0001) ZnO samples prepared by chemomechanical polishing.

the 4.2 K PL from samples cut from the same wafer. These results point to the need for individual sample characterization prior to any subsequent finishing processes when using PL as the relative measure of near surface damage.

### 4.2.2 Aging Effects

Initial PL results suggest that long-term storage of ZnO in atmospheric conditions leads to observable differences in the bound-exciton emission, as seen in Fig. 4.12. Shown are two 4.2 K PL curves collected from the same sample (and same location) for two different dates separated by about seven months. The spectra are normalized using the 3.364 eV peak. As discussed previously, atmospheric aging effects on low temperature PL have been observed for other materials, such as CdTe:In [55]. In that study, point defects were implicated as the likely cause for changes in the low temperature PL over extended periods of time. Further study is required to determine the cause for the observed aging effect in ZnO, however, it appears that special care (e.g., vacuum sealed containers, desiccator, and no UV exposure) may be necessary for long-term storage.

### 4.2.3 Temperature-dependent Exciton Luminescence

Results from this temperature-dependent exciton luminescence study are also reported in Ref. [171]. A 20 K PL spectrum from a chemomechanically polished (0001) ZnO sample is shown in Fig. 4.13.

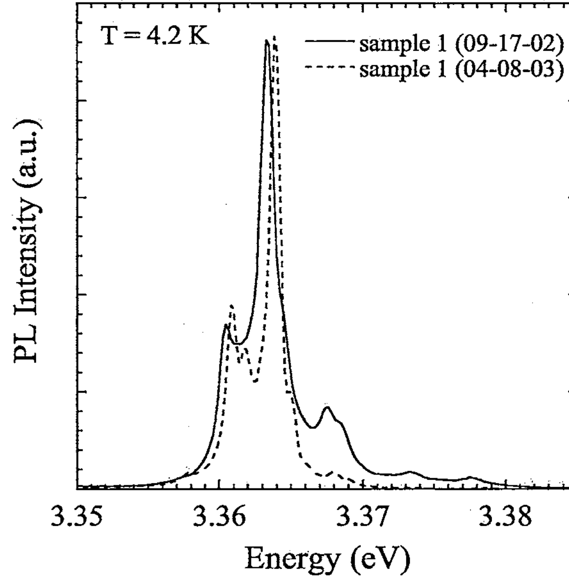


Figure 4.12: Comparison of an initial 4.2 K PL spectrum from a chemomechanically polished (0001) ZnO sample to one collected seven months after the initial characterization. Seven months aging in atmospheric conditions is seen to significantly affect the bound-exciton luminescence spectrum.

This spectrum is shown because it best illustrates both polariton and free-exciton emission. No measurable difference in exciton peak position was observed for the 4.2 K and 20 K spectra. The low temperature (20K) PL spectrum of chemomechanically polished (0001) ZnO exhibits six bound-exciton peaks from 3.358-3.368 eV. As discussed previously, Reynolds et al. [82], in a study of bulk ZnO also produced by Eagle-Picher, attributed this emission to excitons bound to defect-pair complexes that simulate neutral donors. In the present study, we observed narrow peaks, with the strongest peak at 3.364 eV exhibiting a width (FWHM) of about 1 meV, characteristic of neutral-donor-bound-exciton ($D^0X$) emission. The 3.364 eV $D^0X$ peak, the most intense of the six apparently similar bound-exciton peaks, was selected for further temperature dependence measurements and analysis. In addition to bound-exciton luminescence, two resolved peaks were observed at 3.374 and 3.378 eV, also seen in Fig. 4.13. The 3.374 eV peak has been identified in another study by Reynolds et al. [125] as emission from the "bottleneck" region of the lower polariton branch of the A valence band ($LPB_A$). We identify the 3.378 eV peak as the free A exciton, FX (A), based on the consistency of this value with those reported in the literature for vapor phase grown bulk ZnO shown in Table 4.2. Based on the energy positions of the 3.358 eV to 3.368 eV $D^0X$ and 3.378 eV FX (A) peaks, we conclude that the binding energy of the exciton to the defect-pair complexes ranges

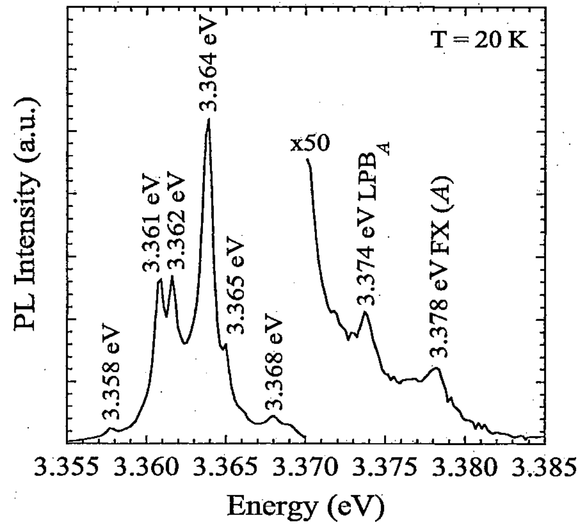


Figure 4.13: 20 K PL spectrum of (0001) ZnO. Six bound-exciton peaks are identified from 3.358-3.368 eV. $LPB_A$ (3.374 eV) and FX (A) (3.378 eV) peaks are also shown.

| Technique | Temperature (K) | FX (A) (eV) | Reference |
|---|---|---|---|
| PL | 4.2 | 3.378 | Present work |
| Reflection | 4.2 | 3.377 | [63] |
| Reflection | 2 | 3.3776 | [173] |
| PL | 2 | 3.3773 | [173] |
| PL | 2 | 3.377 | [82, 125] |

Table 4.2: Comparison of FX (A) values from the literature

from 10 meV to 20 meV. In addition to the peaks reported at 20 K, another peak emerges at 50 K with an energy of 3.385 eV. The observed energy spacing between this peak and the FX (A) is 9 meV. This leads us to attribute this emission to the free B exciton, FX (B), in light of Thomas' reported value [63] for the energy spacing between FX (A) and FX (B) of 7.5 meV.

Figure 4.14 shows the PL spectra for selected temperatures between 4.2 K and 300 K. These spectra illustrate that: 1) the exciton emission is shifted to lower energy with increasing temperature and 2) as the temperature is increased the FX and LO phonon-assisted FX peaks become stronger in intensity relative to the $D^0X$ peak. The bound-exciton emission appears to be thermally quenched above approximately 150 K. Significant FX (A) and LO-assisted FX (A) peaks are observed at 77 K and are labeled in Fig. 2 as FX (A), FX (A)-1LO and FX (A)-2LO for the zero, one and two phonon assisted peaks, respectively. Above 150 K convolution of the FX (A), FX (B) and LO-assisted FX peaks prevented adequate identification of FX (A) peak position.

The variation of exciton peak position with temperature can be seen in Fig. 4.15. Shown are the 3.364 eV $D^0X$, the FX (A) and the FX (B) peak positions for temperatures ranging from 4.2-150 K. A value of 3.31 eV for the 300 K FX (A) peak position based on the widely accepted room temper-

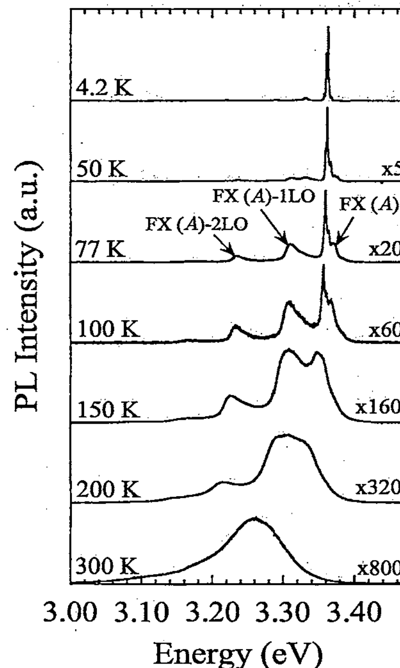


Figure 4.14: Photoluminescence spectra of (0001) ZnO at selected temperatures. Zero-, one-, and two-LO phonon-assisted FX (A) transitions are indicated by arrows for the 77 K spectrum and labeled as FX (A), FX (A)-1LO and FX (A)-2LO, respectively.

ature value for the band gap of ZnO (3.37 eV [17]) minus the presumably temperature-independent exciton binding energy of 60 meV [17] is represented in the figure with the symbol (■). A nonlinear peak-fitting routine [174] was used to deconvolve each experimental spectrum into individual Lorentzian peaks to determine peak position and width. FX (A) and FX (B) peak positions were corrected for the selected Lorentzian lineshape broadening using the approach reported in Bebb and Williams [102]. Typical correction values were less than 1 meV with the largest correction of about 3 meV for the position of the FX (A) peak occurring at 150 K. Included in Fig. 4.15 is the peak position of the LO phonon assisted FX (A) emission together with the predicted energy [102] for both FX (A)-1LO and FX (A)-2LO peaks based on the energy of the FX (A) peak ($E_{FX(A)}$) and the LO phonon energy ($h\omega_{LO}$ = 72 meV [175]). The convergence of the FX (A) and FX (A)-1LO peaks coupled with the line broadening of each of these peaks with increasing temperature significantly limits the analysis of peak position above 150 K. This is best illustrated in Fig. 4.14 from a comparison of the 150 K and 200 K spectra. At temperatures above 150 K, the $D^0X$ peak was not observed.

Using the room temperature value of free-exciton peak position of 3.31 eV from the literature together with our experimental data from 4.2-150 K, a fit of the temperature-dependent FX (A) peak energy can then be made in the range of 4.2-300 K. Using a least-squares routine, the temperature dependence of FX (A) peak position was fit according to a model by Manoogian and Woolley (MW) [119]:

$$E = E_o + UT^s + V\theta \left[\coth\left(\frac{\theta}{2T}\right) - 1\right] \tag{4.1}$$

This choice was motivated by previous applications for other II-VI semiconductors such as CdTe [123] and CdS [122] and the reported limitations [119] of the well-known Varshni equation [84] when applied to data in a temperature range much less than the Debye temperature ($\theta_D$). In this work, the maximum temperature investigated was 300 K, which is significantly less than the reported Debye temperature for ZnO ($\theta_D$ = 920 K [176]). Pässler [118] has also implicated "unwarranted applications" of Varshni's expression to restricted data sets (T $\leq$ 300 K) as the reason for excessively large scatter of fitting coefficients in the literature. The (MW) equation consists of three terms [119]: (i) T = 0 K intercept, $E_o$, (ii) lattice dilatation, $UT^s$ and (iii) electron-phonon interaction, $V\theta[\coth(\theta/2T) - 1]$. The coefficients obtained from fitting the (MW) equation to the FX (A) temperature-dependent peak position data are: $E_o$ = 3.379 eV, $U = -5.04 \times 10^{-5}$ eV/K$^{1.01}$, $s$ = 1.01, $V = -1.84 \times 10^{-4}$ eV/K and $\theta$ = 398.4 K. We can compare our fitted value of $U$ to a theoretical estimate of the coefficient of the lattice dilatation term for the special case of $s \approx 1$

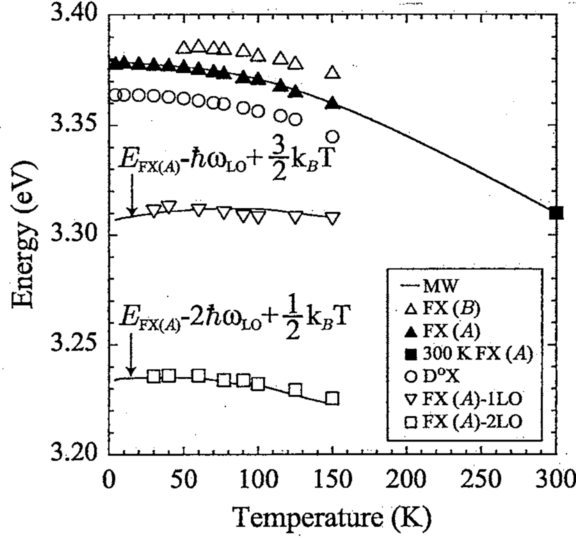


Figure 4.15: Temperature-dependent exciton peak position for (0001) ZnO. Individual FX (A) (▲) and FX (B) (△) peaks are not resolvable above 150 K. The 300 K FX (A) peak position (■) is based on the band gap energy of ZnO (3.37 eV (see Ref. [17])). The FX (A) data were fit using (MW). Also shown are the measured energy positions for the 1LO-(▽) and 2LO-(□) phonon assisted FX (A) transitions and the predicted temperature dependence for both peaks (see Ref. [102]). The 3.364 eV bound-exciton peak ($D^0X$) (∘) is not observed at temperatures above 150 K.

using the equation [123]: $U \approx -3B(\partial E_g/\partial P)\langle\alpha_L\rangle$, where $B$ is the bulk modulus, $\partial Eg/\partial P$ is the band gap pressure coefficient, and $\langle\alpha_L\rangle$ is the mean thermal expansion coefficient. From this expression $U$ is computed to be -5.5x10$^{-5}$ eV/K using $B$=157 GPa (determined from an elastic modulus $E$=124 GPa and a shear modulus of $G$=45.3 GPa [177]), $\partial Eg/\partial P = 2.7 \times 10^{-6}$ eV/bar [178] and a mean thermal expansion coefficient reported by Heiland et al. [179] of $\langle\alpha_L\rangle = 4.3 \times 10^{-6}$ 1/K. The fitted value of $s$=1.01 from the lattice dilatation term was found to be similar to previous reports for CdS (0.93) [122] and CdTe (1) [123] and within the accepted range (0.6 to 1.2) for this parameter [180]. $V$ is found to be within an order of magnitude of the reported temperature shift $dE_g/dT$ for ZnO of $-8 \times 10^{-4}$ eV/K determined from a temperature range of 200-800 K [181]. The coefficient $\theta$ is related to the Debye temperature by $\theta \approx (3/4)\theta_D$ [182]. From our fitted value of $\theta$, we compute an estimate of the Debye temperature to be $\theta_D \approx 531$ K, which is within a factor of 2 of the reported value of 920 K [176].

The temperature dependence of the 3.364 eV $D^0X$ peak intensity was investigated using the approach of Viswanath et al. [126] in their study of GaN. Figure 4.16 shows the natural logarithm

of the normalized total intensity for the 3.364 eV peak as a function of 1/T. From a fit of the linear portion (first six data points) of the data, a thermal activation energy ($E_A$) was estimated to be 14 meV. This is in agreement with the exciton-to-defect binding (localization) energy of 14 meV shown in Fig. 4.13. The ratio of FX (A) to $D^0X$ peak intensities shown as an inset in Fig. 4.16 is seen to increase with increasing temperature. Viswanath et al. [126] also observed an increase in this ratio and inferred that with increasing temperature the donor-bound exciton dissociated into a free exciton and a neutral donor. Based on this, and the work of Reynolds et al. [82], we similarly conclude that thermal dissociation of the 3.364 eV bound exciton results in the creation of a free exciton and a neutral-donor-like defect-pair complex. In support of this argument the $D^0X$ peak exhibited a decrease in intensity with increasing temperature whereas the intensity of the FX (A) peak actually increased from 4.2-60 K then decreased with increasing temperature.

### 4.2.4 Comparison of Low Temperature PL from Etched and Chemomechanically Polished Surfaces

Whereas very few differences are observed between the 4.2 K PL for chemomechanically polished and etched samples, significant differences can be seen as the temperature is increased to 77 K. Figure 4.17 shows the 77 K PL spectra for two (0001) ZnO samples, one prepared by chemomechanical

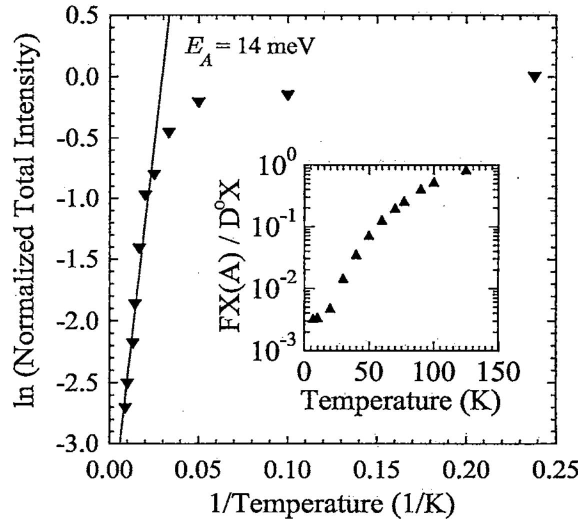


Figure 4.16: Natural logarithm of the normalized total intensity (peak intensity times FWHM) of the 3.364 eV $D^0X$ peak as a function of 1/T. The thermal activation energy ($E_A$) was determined to be approximately 14 meV. Inset: Temperature dependence of FX (A) to $D^0X$ intensity ratio.

polishing, curve (a), and the other by wet etching, curve (b). Both spectra are normalized using the $D^0X$ peak at 3.360 eV. The peaks at approximately 3.370, 3.310, and 3.235 eV have been previously identified for chemomechanically polished (0001) ZnO as FX, FX-1LO, and FX-2LO luminescence, respectively (see Fig. 4.14). From Fig. 4.17, it is seen that the etched sample exhibits much stronger relative luminescence for the 3.310 and 3.235 eV peaks when compared to PL at the same energies from the chemomechanically polished sample. Whereas each of the PL peaks observed at 77 K for etched ZnO is coincident in energy with those observed for the polished sample, we believe their identification is slightly different. The 3.235 eV peak from etched ZnO is believed to be FX-2LO emission just as reported for chemomechanically polished ZnO. It is proposed, however, that the 3.310 eV peak observed from the 77 K PL spectrum for etched ZnO is the result of a TO phonon-assisted transition of a bound exciton ($D^0X$-1TO) not a LO phonon-assisted transition of a free exciton (FX-1LO). This identification is based on the following observations. First, the relative intensity of the 3.310 eV peak for the etched sample is observed to be much stronger than that for the chemomechanically polished sample. Whereas the intensity of the 3.310 eV peak (labeled FX-1LO) for the polished sample is on the order of the FX peak, the intensity of the 3.310 eV peak (labeled $D^0X$-1TO) for the etched sample is seen to be on the order of the $D^0X$ peak. A larger relative FX-2LO peak for the etched sample, as compared to the chemomechanically polished sample, is expected considering Frölich intraband scattering theory [151] and observations reported by Verbin et al. [152] for their comparison of luminescence from "perfect" ZnO crystals and those

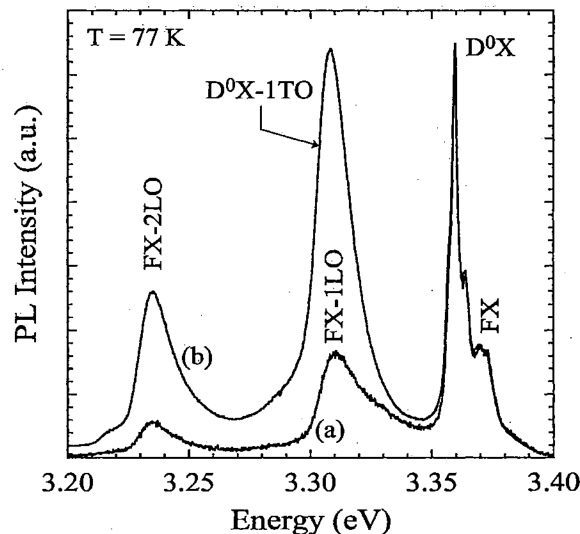


Figure 4.17: 77 K PL spectra for (a) chemomechanically polished and (b) wet etched (0001) ZnO samples. Spectra are normalized using the 3.360 $D^0X$ peak.

with defects. Second, the temperature-dependent data suggests that the peaks at 3.310 eV seen for both samples at 77 K are of different origin. From this point forward, we will refer to each peak according to our identification (i.e., for etched, the 3.310 eV peak is identified as $D^0X$-1TO and for chemomechanically polished, the 3.310 eV peak is identified as FX-1LO). Figure 4.18 shows the normalized PL from the same two samples as in Fig. 4.17 for an increased temperature of 100 K. Three general observations can be made. First, consistent with the shrinking band gap, each of the peaks is shifted slightly to lower energy. However, the $D^0X$-1TO peak appears to have redshifted more for the etched sample than the FX-1LO peak for the polished sample at 100 K. The difference is observed to be about 6.7 meV. In contrast, the FX-2LO peaks, observed for both samples at 77 K, seem to have shifted to lower energy by the same amount such that their energies at 100 K are equivalent (illustrated by vertical line). Second, the $D^0X$-1TO peak exhibits a significant decrease in relative intensity as compared to the FX-2LO peak for the etched sample. In fact, the intensity of the $D^0X$-1TO peak appears to scale with the $D^0X$ peak for increased temperature, whereas the FX-2LO peak is seen to scale with the FX peak. Third, the lineshape of the $D^0X$-1TO peak suggests that it is not related to free excitons. As discussed in Section 2.4, LO phonon-assisted FX emission is characterized by an asymmetric lineshape (i.e., high-energy tail) due to recombination of excitons with nonzero kinetic energy. The $D^0X$-1TO lineshape appears to be symmetric suggesting it is the result of interaction between phonons and bound excitons, not free excitons. If the peak at ~3.30 eV for etched ZnO is the convolution of FX-1LO and a $D^0X$-1TO peaks, the FX-1LO peak

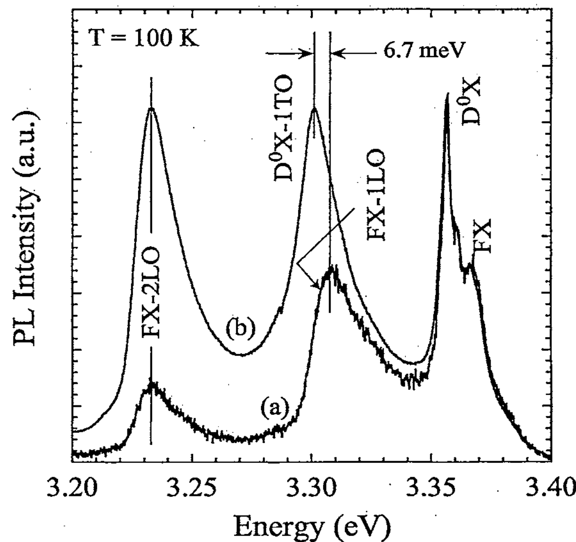


Figure 4.18: 100 K PL spectra from (a) chemomechanically polished and (b) wet etched (0001) ZnO. Spectra are normalized using the 3.360 $D^0X$ peak.

must necessarily be less intense than the FX-2LO which is consistent with the Frölich model. The identification of the $D^0X$-1TO peak is further supported by comparing the predicted energy and lineshape for LO phonon-assisted FX emission to the experimentally observed spectra at 100 K for both surfaces, shown in Figs. 4.19 and 4.20.

Shown in Fig. 4.19 is the 100 K spectrum for chemomechanically polished (0001) ZnO (solid line) with theoretical predictions for the FX-1LO (dashed line) and FX-2LO (dotted line) transitions using Eqns. (2.9) and (2.10), respectively. The intensities of the theoretical curves were scaled to the intensities of the respective experimental peaks. Good agreement is observed between the model and the experimental results confirming the identification of the FX-1LO and FX-2LO peaks in chemomechanically polished ZnO. Results for the wet-etched surface are seen to be significantly different. Figure 4.20 shows that whereas good agreement is observed for the FX-2LO identification, the peak at 3.30 eV is clearly not in agreement with the predicted energy for FX-1LO emission. We also note that the energy separation between the 3.30 eV ($D^0X$-1TO) peak and the bound-exciton peak at ~3.36 eV is observed to be approximately 55 meV which is close to the value for the TO phonon energy of ZnO (51.2 meV [110]).

From Fig. 4.21, the experimentally observed FX-1LO peak is seen to follow closely the predicted energy for this transition, curve (b) from Eqn. (2.12). It is possible, however, that the experimentally observed peak identified as FX-1LO is a convolution of FX-1LO and $D^0X$-1TO peaks. The

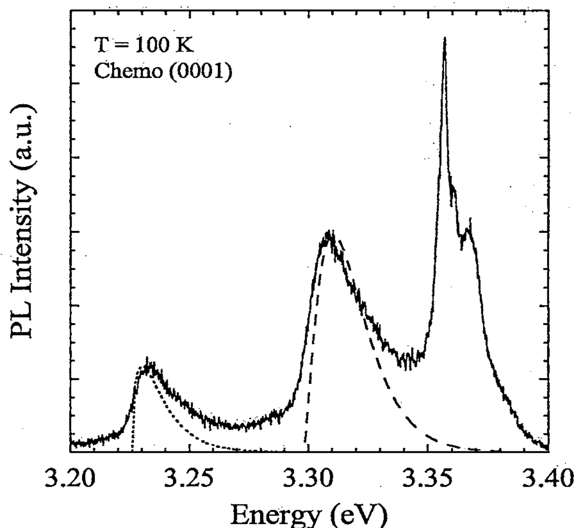


Figure 4.19: 100 K PL spectrum from chemomechanically polished (0001) ZnO (solid line). Shown are the predicted energies and lineshapes for both FX-1LO (dashed line) and FX-2LO (dotted line) transitions using Eqns. (2.9) and (2.10), respectively.

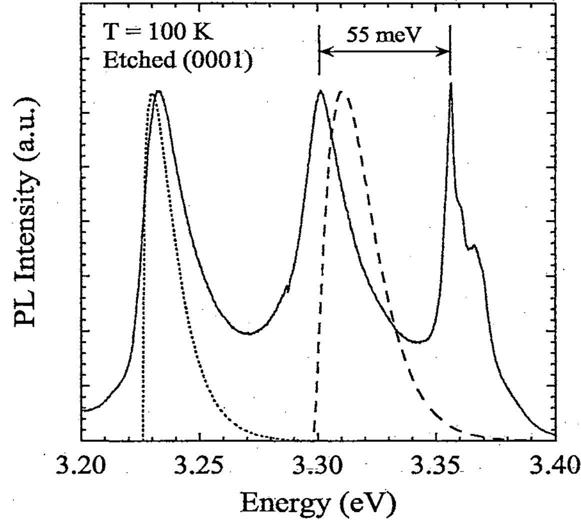


Figure 4.20: 100 K PL spectrum from etched (0001) ZnO (solid line). Shown are the predicted energies and lineshapes for both FX-1LO (dashed line) and FX-2LO (dotted line) transitions using Eqns. (2.9) and (2.10), respectively. Also shown is the measured energy difference (55 meV) between the $D^0X$ and $D^0X$-1TO peaks which is consistent with the reported TO phonon energy of 51.2 meV for ZnO [110]

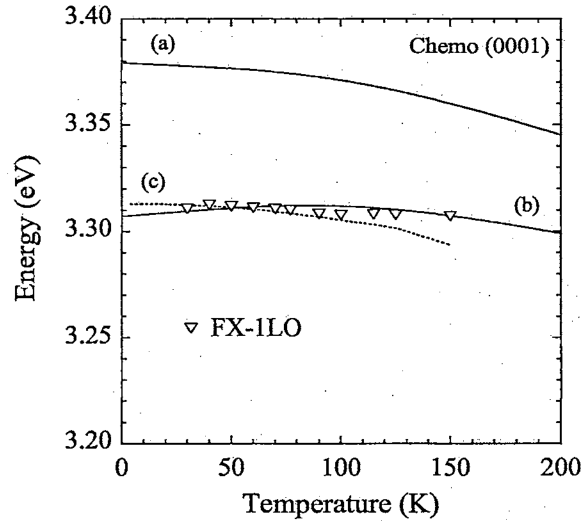


Figure 4.21: Temperature-dependent PL of experimentally observed FX-1LO peak for chemomechanically polished (0001) ZnO. Shown are theoretical predictions for (a) FX(E) from Ref. [171], (b) FX-1LO(E) using Eqn. (2.12), (c) $D^0X$-1TO(E) assuming a temperature independent TO phonon energy of 51 meV and the experimentally observed temperature dependence of the FX-1LO peak.

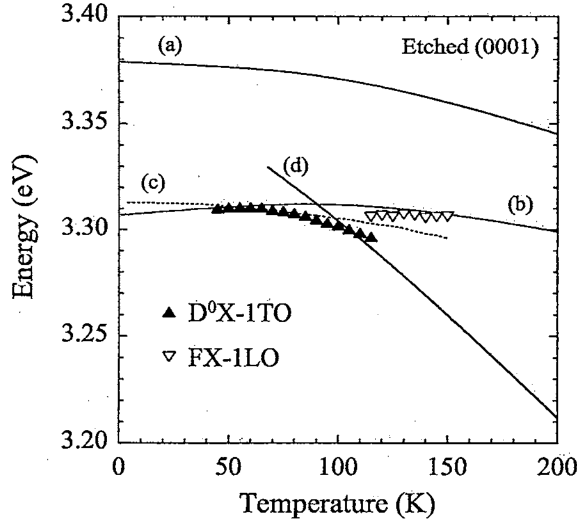


Figure 4.22: Temperature-dependent PL of experimentally observed $D^0X$-1TO peak for etched (0001) ZnO. Shown are theoretical predictions for (a) FX(E) from Ref. [171], (b) FX-1LO(E) using Eqn. (2.12), (c) $D^0X$-1TO(E) assuming a temperature independent TO phonon energy of 51 meV, (d) exciton-electron predicted energy from Eqn. (2.7) with $\gamma$=7.74. Also shown is the temperature dependence of the FX-1LO peak observed at temperatures between about 120-150 K.

temperature dependence of the PL from etched (0001) ZnO is shown in Fig. 4.22. Shown are (a) FX(E) from Ref. [171], (b) FX-1LO(E) using Eqn. (2.12), (c) $D^0X$-1TO(E) assuming a temperature independent TO phonon energy of 51 meV, (d) exciton-electron predicted energy from Eqn. (2.7) with $\gamma$=7.74, and the experimentally observed temperature dependence of the FX-1TO peak. A significant divergence between the theoretically predicted energy for FX-1LO transitions and the experimentally observed $D^0X$-1TO peaks is observed. The exciton-electron curve is added to illustrate the possibility that free carriers may affect the energy position of the $D^0X$-1TO peak. Above $\sim$115 K, a new peak is observed which we attribute to FX-1LO emission. The thermal evolution of this peak can be seen in Fig. 4.23 which shows a comparison of PL from etched (0001) ZnO for 115 K and 120 K. The proposed FX-1LO peak observed at temperatures above 120 K from etched ZnO is observed to be less intense than the FX-2LO peak from the same spectrum which is consistent with the Frölich model discussed previously.

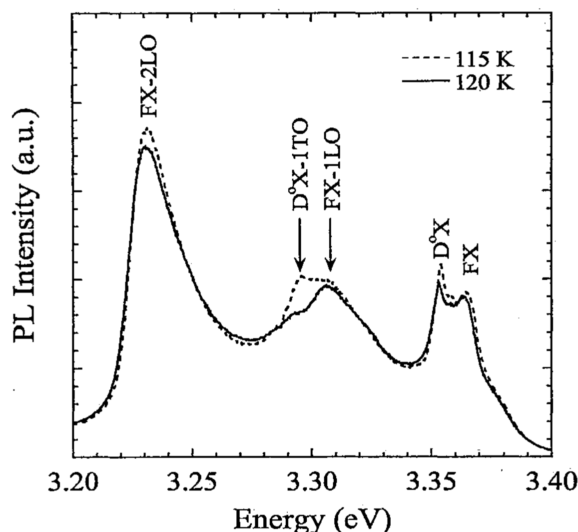


Figure 4.23: Comparison of 115 K and 120 K PL spectra for etched (0001) ZnO.

### 4.2.5 Comparison of RT PL from Etched and Chemomechanically Polished Surfaces

Figure 4.24 compares the RT PL from etched and chemomechanically polished surfaces for both polar faces of ZnO. PL from etched (0001) and $(000\bar{1})$ ZnO, curves (a) and (b), have been shown previously (see Fig. 4.8), but are repeated here for comparison to the RT PL from chemomechanically polished (0001) and $(000\bar{1})$, curves (c) and (d). The ratio of the FX-to-DL for the chemomechanically polished surfaces is seen to increase to 105 $\pm$ 15% from the value of 25 for the etched surfaces. For the spectra obtained for the chemomechanically polished surfaces, Fig. 4.24 curves (c) an (d), the individual FX and S emission peaks were found to be convolved into one broad peak. The S peak was initially attributed to optical-phonon-assisted free-exciton emission [172] based on the consistency of the observed energy difference between it and the presumed FX peak with twice the LO phonon energy of ZnO. Further investigation leads us to conclude that this peak is the result of exciton-electron (Ex-El) interaction as described by Klingshirn [65]. One plausible explanation for the reduced intensity of the Ex-El peak for the chemomechanically polished surfaces, as compared to the etched surfaces, is the presence of near-surface damage introduced by polishing. The minimal damage, acting as free-carrier traps, could effectively reduce the free-carrier concentration in the near surface. With fewer free electrons, the interaction of free excitons and free carriers would be reduced. The net result would then be a reduction in the luminescence intensity of the exciton-electron peak.

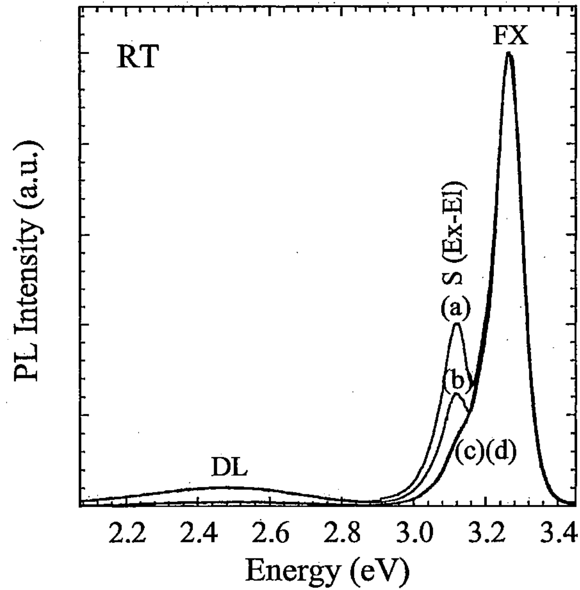


Figure 4.24: Normalized RT PL intensities for (a) etched $(000\bar{1})$, (b) etched (0001), (c) polished $(000\bar{1})$ and (d) polished (0001) ZnO surfaces. All spectra have been normalized by their FX peak intensity.

## 4.3 Mechanically Polished ZnO

For the mechanically polished ZnO studies, 1/4 $\mu$m and 1 $\mu$m diamond abrasive slurries were used to prepare the surfaces. PL results from these studies are compared to PL from chemomechanically polished surfaces.

### 4.3.1 Hot-exciton Luminescence

Whereas no clearly resolved free excitons were observed from the surfaces prepared by mechanical polishing, the 4.2 K PL did exhibit three small, equally spaced hot-exciton (HX) peaks, separated from the energy of the excitation source by the energy of an integer multiple of a LO phonon. HX luminescence, attributed to very short exciton lifetime [143], has been reported for several compound semiconductors including SiC [137], CdS [138, 139], CdSe [136], ZnTe [140] and GaSe [141], but to our knowledge this is the first observation for bulk ZnO.

Figure 4.25 shows the 4.2 K PL emission obtained for ZnO prepared with the 1 $\mu$m diamond abrasive slurry. Shown are the spectra for (a) (0001) and (b) $(000\bar{1})$ surfaces. Five resolved peaks at 3.312, 3.332, 3.364, 3.385, and 3.458 eV and one low-energy shoulder of the 3.332 eV peak can be seen. Consistent with previous results, we believe the peak at 3.364 eV to be defect-donor-bound

exciton luminescence ($D^0X$) and the peak at 3.332 eV and the slight shoulder on the low energy side to be a two-electron transition ($D^0X_{n=2}$) of the $D^0X$ peak.

In addition to bound-exciton (3.364 eV) and two-electron (3.332 eV) emission, three distinct peaks were observed at 3.458 (HX-1LO), 3.385 (HX-2LO) and 3.312 (HX-3LO) eV, which we attribute to hot-exciton emission. Because the exciton lifetime is short and emission occurs in the fundamental absorption region leading to strong absorption, the HX-$n$LO ($n$ = 1,2,3) peak intensity is very weak [143]. The HX-$n$LO peak separation from the excitation energy (3.532 eV) is consistent with an integer multiple of the reported value of 72 meV for the LO phonon energy of ZnO [175], and that of 75 meV experimentally observed on similar material produced by Eagle-Picher [57]. The width (FWHM) of the HX-2LO peak was measured to be approximately 3 meV. As reported by Permogorov [143], the individual HX-$n$LO peaks are narrow because the interaction of hot excitons with acoustic phonons, during the hot-exciton lifetime, does not significantly change the "quasi-discrete" energy distribution. Our results are consistent with those reported for CdS [139] as we observe a HX-1LO peak that is significantly less intense than the HX-2LO and HX-3LO emission. HX-1LO emission has also been reported for mechanically polished CdSe [136]. The HX-1LO peak arises, as reported by Gross et al. [136], from a breakdown in the momentum conservation resultant from

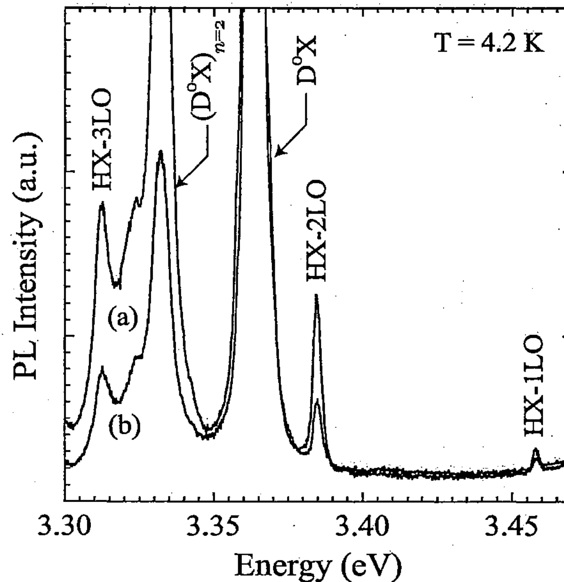


Figure 4.25: 4.2 K PL of 1 $\mu$m mechanically polished (a) (0001) and (b) (000$\bar{1}$) ZnO. In addition to donor-bound exciton ($D^0X$) and two-electron satellite ($D^0X_{n=2}$) emission, three hot-exciton peaks are observed at 3.458 (HX-1LO), 3.385 (HX-2LO) and 3.312 (HX-3LO) eV. The laser excitation energy is 3.532 eV.

disorder in the near surface of the polished crystal.

To further investigate the peaks as hot-exciton emission, the intensity of the HX-$n$LO lines for the (0001) surface was examined as a function of temperature. The HX-$n$LO peaks were thermally quenched as the temperature was increased from 4.2 to 300 K, while the energy of each of the peaks remained constant, as shown in Fig. 4.26. The inset to Fig. 4.26 shows the normalized HX-2LO emission for both (0001) and (000$\bar{1}$) polished surfaces as a function of temperature. The thermal quenching of the HX-2LO hot-exciton peak is consistent with results reported by Gross et al. [136] in their studies of CdSe. Results presented here are also consistent with those of Permogorov [143] who reported that thermal quenching of hot-exciton luminescence intensity with increasing temperature is a consequence of decreasing exciton lifetime due to the increased nonradiative decay probability. Also reported by Permogorov [143], thermal quenching of Raman peaks occurs only as a result of increased absorption of exciting or scattered light. For single crystal ZnO, the absorption coefficient for the exciting and scattered photon energy remains nearly constant from 77 to 300 K [25].

One plausible explanation for the reduced exciton lifetime leading to the observation of hot-exciton luminescence is near-surface damage introduced by the polishing process. Goncharov et al. [183] have reported that higher dislocation density results in shorter free-exciton lifetime in germanium. To examine the dependence of hot-exciton emission on near-surface disorder introduced

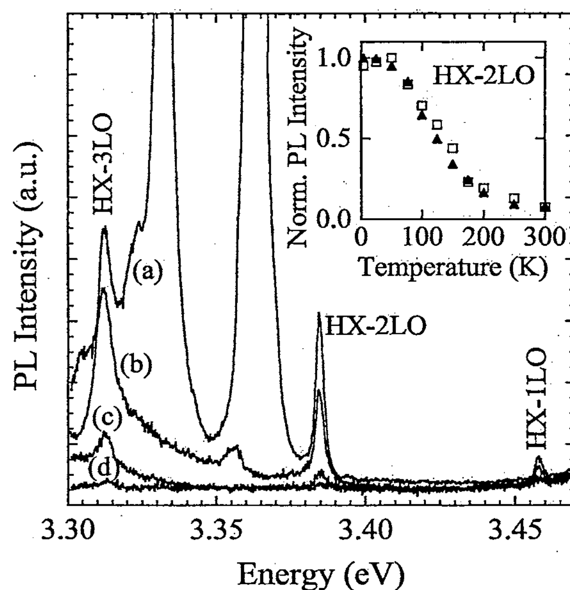


Figure 4.26: PL of 1 $\mu$m mechanically polished (0001) ZnO for the following temperature: (a) 4.2 K, (b) 100 K, (c) 200 K and (d) 300 K. Inset: Normalized PL intensity of HX-2LO emission for (□) (0001) and (▲) (000$\bar{1}$) as a function of temperature.

by polishing, PL from the mechanically polished sample was compared to that of a sample prepared by chemomechanical polishing.

Figures 4.27 and 4.28 show the 4.2 K PL from mechanically and chemomechanically polished surfaces for both (0001) and (000$\bar{1}$) sample orientation, respectively. Each PL signal is normalized by the $D^0X$ peak at 3.364 eV (not shown). For the chemomechanically polished samples, the observed FX (A) peak at 3.378 eV suggests the exciton lifetime is sufficiently long to allow complete thermalization. The energy of the FX (A) peak and the observation of higher intensity free-exciton emission from the (000$\bar{1}$) sample versus the (0001) surface are consistent with those results recently reported by Sherriff et al. [57] in their PL studies of chemomechanically polished bulk ZnO also produced by Eagle-Picher. In Figs. 4.27 and 4.28, the HX-2LO hot-exciton peak is clearly observed for both orientations of the mechanically polished samples, whereas no measurable hot-exciton emission was observed for either of the chemomechanically polished surfaces. The observed hot-exciton peaks could be the result of reduced exciton lifetime resultant from the near-surface disorder introduced from the mechanical polishing process.

## 4.3.2 Mechanical Damage Induced Luminescence

PL has been used extensively to study the effect of the polishing process on the luminescence of semiconductors [50–52, 54, 184]. Most often the near surface disorder introduced by polishing

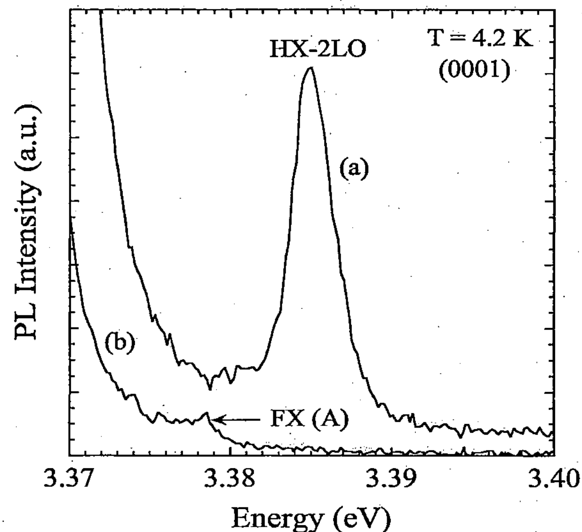


Figure 4.27: 4.2 K PL for (0001) ZnO. Shown are spectra for samples prepared by (a) 1 $\mu$m diamond abrasive mechanical polishing and (b) chemomechanical polishing. Each spectrum is normalized by the bound-donor exciton ($D^0X$) peak at 3.364 eV (not shown).

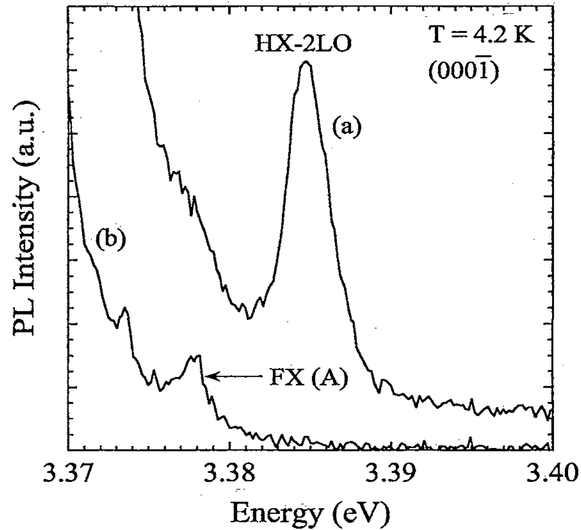


Figure 4.28: 4.2 K PL for (000$\bar{1}$) ZnO. Shown are spectra for samples prepared by (a) 1 $\mu$m diamond abrasive mechanical polishing and (b) chemomechanical polishing. Each spectrum is normalized by the bound-donor exciton ($D^0X$) peak at 3.364 eV (not shown).

leads to decreased luminescence, however there are examples in the literature of mechanical damage resulting in new radiative recombination paths for the nonequilibrium electrons and holes. These include PL studies of mechanically polished GaAs [50] and InP [51, 52]. In each case point defects resultant from dislocation motion were implicated as the source of luminescence. To date, very little information is available regarding the PL of various surface treatments for ZnO, though there have been some damage-related studies performed for this material, as discussed previously. Studies of subsurface damage for mechanically polished bulk ZnO have been performed using axial ion channeling in conjunction with room temperature PL [109], however low temperature PL of these surfaces has not been addressed. Below we show the 4.2 K PL of both (0001) Zn-terminated and (000$\bar{1}$) O-terminated mechanically polished bulk ZnO and report the observation of a luminescence peak at 3.211 eV believed to be the result of damage introduced during the polishing process.

Figure 4.29(a) shows the 4.2 K PL spectra obtained for (0001)- and (000$\bar{1}$)-oriented ZnO prepared by polishing with a 1 $\mu$m diamond abrasive slurry. Each spectrum is normalized by the peak at 3.364 eV, labeled $D^0X$. When the PL from the 1 $\mu$m mechanically polished ZnO is compared to the PL from a (0001)-oriented sample prepared by chemomechanical polishing, shown in Fig. 4.29(b), differences in emission in the range of 2.95-3.30 eV are observed. In this energy range there are four peaks (3.211, 3.138, 3.065 and 2.991 eV) observed from the 4.2 K PL of the mechanically polished sample that are not observed for the chemomechanically polished sample. Only the PL from the

(0001) chemomechanically polished sample is shown because the (000$\bar{1}$) spectrum is nearly identical. The peak at 3.257 eV is observed for both surface preparations, but it is much less intense for the chemomechanically polished samples. Comparing the linewidth of the 3.364 eV bound-exciton peak for the mechanically polished sample to that for the chemomechanically polished (0001)-oriented sample, shown as insets for both Figs. 4.29 (a) and (b), respectively, the 3.364 eV $D^0X$ peak is observed to be much broader for the mechanically polished sample. From a Lorentzian lineshape fitting routine [174] used to determine peak position and intensity for each of the bound-exciton peaks, the FWHM of the 3.364 eV $D^0X$ peak for the 1 $\mu$m diamond abrasive mechanically polished sample measures 2.3 meV, whereas for the chemomechanically polished sample the FWHM is about 1 meV. While no free-exciton emission was observed at 4.2 K for the mechanically polished samples, two hot-exciton (HX) peaks can be seen at 3.385 and 3.312 eV. This emission, as discussed in the previous section, is attributed to reduced exciton lifetime resultant from disorder introduced by the polishing process [185]. Whereas some of these low temperature PL results have been previously reported in the literature, the emission observed at 3.211, 3.138, 3.065 and 2.991 eV is to the best of our knowledge the first reported for mechanically polished bulk ZnO. These four peaks, observed only for the mechanically polished samples, and the peak at 3.257 eV were selected for further analysis.

Figure 4.30 shows PL spectra recorded at 4.2, 10, 25, 50 and 77 K for the 1 $\mu$m mechanically polished (0001) ZnO sample. All peaks presented here are labeled according to their observed energy at 4.2 K. Consistent with previous PL results reported in the literature for chemomechanically polished ZnO [57] also produced by Eagle-Picher, no longitudinal optical (LO) phonon replicas of the $D^0X$ peak were observed, however we believe the peak at 3.257 eV, labeled $(D^0X_{n=2})_{1LO}$, to be a LO phonon replica of the two-electron satellite peak at 3.332 eV ($D^0X_{n=2}$). This identification is based on the following observations: 1) the two peaks are separated by about 75 meV ($E_{LO}$ = 72 meV [175]) and 2) both peaks exhibit a simultaneous and proportional decrease in intensity with increased temperature. Both peaks are thermally quenched prior to the $D^0X$ peak. This is consistent with Martinez-Criado et al. [131] who reported that the $D^0X_{n=2}$ peak quenches faster with temperature than the principal $D^0X$ peak in their PL study of GaN. Figure 4.30 also illustrates that each of the four peaks in the range of 2.95-3.30 eV is equivalently spaced at an interval of about 73 meV. The four peaks at 3.211, 3.138, 3.065 and 2.991 eV exhibit a shift to higher energy with an increase in temperature whereas the $D^0X$, $D^0X_{n=2}$ and $(D^0X_{n=2})_{1LO}$ peaks are slightly red-shifted as shown in Fig. 4.30. Additionally, each of the four peaks is observed with strong emission after much of the bound-exciton emission has been thermally quenched at 77 K, suggesting that the peaks

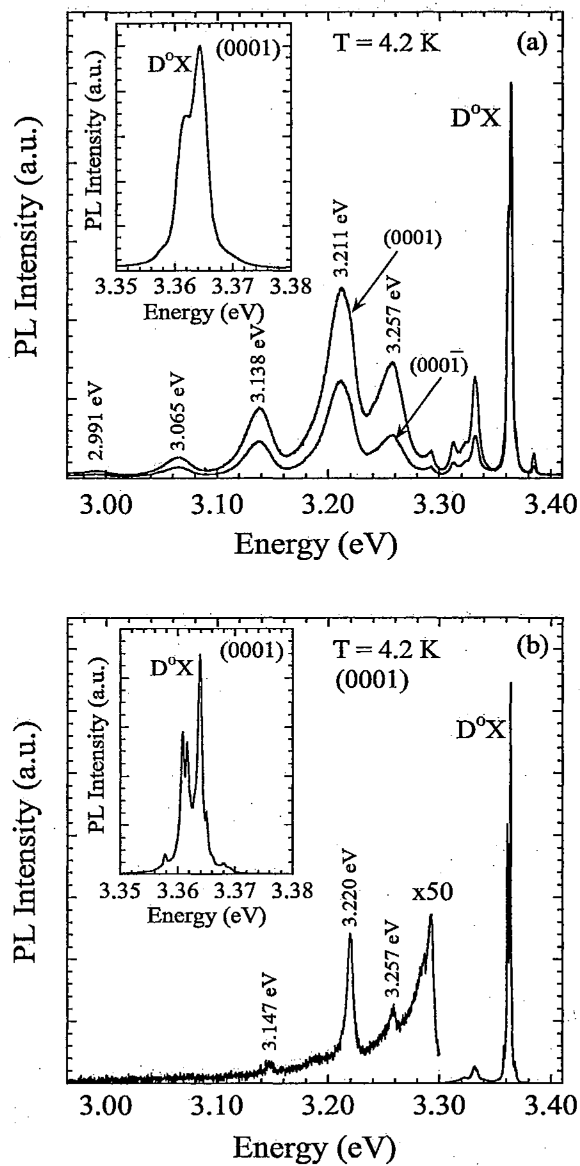


Figure 4.29: 4.2 K PL spectra of (a) mechanically polished (0001) and $(000\bar{1})$ ZnO and (b) chemomechanically polished (0001) ZnO. Spectra in (a) are normalized using the 3.364 eV $D^0X$ peak. Insets for both (a) and (b) show detail of (0001) exciton emission.

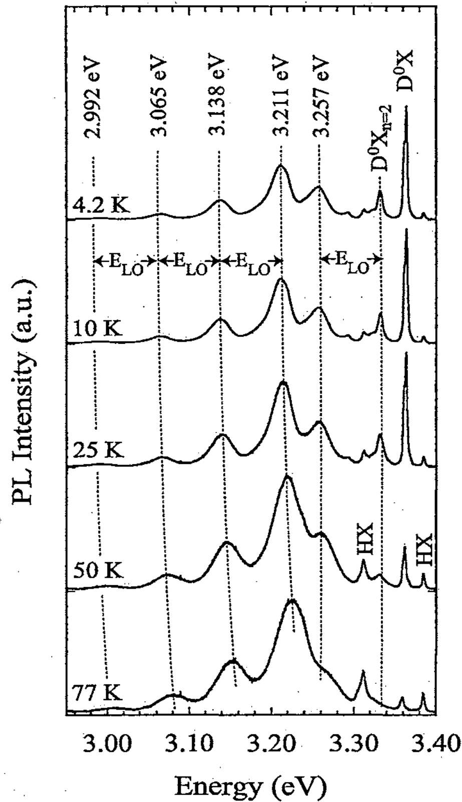


Figure 4.30: Temperature-dependent PL spectra of (0001) ZnO prepared by 1 $\mu$m diamond abrasive mechanical polishing. Shown are spectra recorded at 4.2, 10, 25, 50 and 77 K. Each spectrum is normalized by its maximum intensity.

are unrelated to exciton emission. This leads us to believe that the peak at 3.211 eV is a zero-LO phonon peak with three LO phonon replicas at 3.138 (1LO), 3.065 (2LO) and 2.991 (3LO) eV. Also shown in Fig. 4.30 for the 50 K spectrum is the HX emission observed at 3.385 and 3.312 eV.

Figure 4.31 further illustrates the thermal blue shift of the 3.211 eV peak for both polar faces as the temperature is increased from 4.2 to 125 K followed by a red shift as the temperature is further increased. This peak is not observed at temperatures above approximately 200 K. To approximate the shrinking bandgap with increasing temperature, the temperature-dependent peak position of the 3.364 eV $D^0X$ peak for both polar faces and a fit of the FX (A) temperature-dependent peak position [171] from a chemomechanically polished (0001) ZnO sample based on a model by Manoogian and Wooley (MW) are also shown in Fig. 4.31. The observed thermal blue shift of the 3.211 eV peak is consistent with results reported in the literature for donor-acceptor-pair (DAP) emission from GaN [156, 157] and GaS [161]. Our observation of multiple (3) LO phonon replicas of the proposed DAP peak is consistent with Zhu et al. [159] in their PL study of N-doped ZnSe. To further investi-

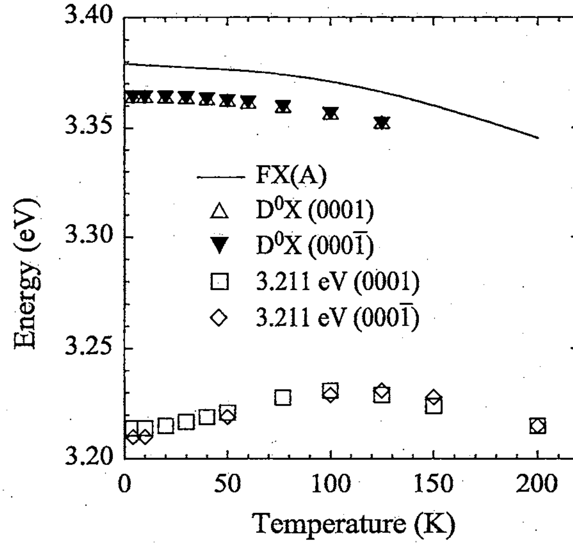


Figure 4.31: Temperature dependence of the 3.211 eV peak position for both (0001) (□) and (000$\bar{1}$) (◇) surfaces prepared by 1 $\mu$m diamond abrasive mechanical polishing. Also shown is the temperature dependence of the 3.364 eV $D^0X$ peak for the (0001) (△) and (000$\bar{1}$) (▼) mechanically polished samples and the MW fit of the free A exciton (FX (A)) temperature-dependent peak position [171] for a chemomechanically polished (0001) ZnO sample.

gate this peak as donor-acceptor-pair recombination, the 4.2 K PL spectra from a 1 $\mu$m mechanically polished (0001)-oriented ZnO sample was compared using two different excitation intensities. The 3.211 eV peak exhibited a blue shift of approximately 5 meV for an increase in excitation intensity from 8 mW to 80 mW. This type of blue shift is also consistent with observations reported in the literature for DAP emission from ZnSe [159] and GaN [162]. Reshchikov et al. [162] reported that a small blue shift with increased excitation intensity was indicative of DAP emission involving shallow donors and the shift to higher energy was the result of saturation of PL from distant pairs. Based on this, we conclude the 3.211 eV peak to be the result of zero-phonon-assisted recombination of distant donor-acceptor pairs, $(DAP)_{0LO}$.

Arrhenius plots of the 3.211 eV peak for both polar faces indicate thermal activation energies ($E_A$) of 52 meV for the (0001) Zn-terminated face and 54 meV for the (000$\bar{1}$) O-terminated face as shown in Fig. 4.32. These values are consistent with the range of reported values for donor binding energies of 56-61 meV [82, 165] for bulk ZnO. However, they do not agree with the ionization energy of the principal donor as computed from the TES peak. This value, as reported in Section 4.1, was determined to be 42.6 meV. The discrepancy between this energy and the ionization energy as

determined from Arrhenius plots (52-54 meV) suggests that both donors and acceptors may be created during the polishing process. The creation of donor and acceptor levels resultant from damage introduced to the crystal has been reported for bulk ZnO by Look et al. [62]. They showed that high-energy (E > 1.6 MeV) electron irradiation results in the creation of significant concentrations of donors and acceptors. The donors produced by irradiation were shallow ($E_c$-30 meV) and identified as Zn sub-lattice defects. The thermal activation energies presented in our study (52-54 meV) seem to rule out the possibility that this particular defect donor participates in our proposed DAP recombination.

One observation from the present study that points to the possibility that the 3.211 eV peak is the result of near surface damage introduced by polishing is the sample-to-sample variation of the intensity of this peak relative to the 3.364 eV $D^0X$ peak as shown in Fig. 4.33. Shown are the spectra collected from three different (0001)-oriented samples prepared by 1 $\mu$m diamond abrasive mechanical polishing. The three spectra are normalized by their respective 3.364 eV $D^0X$ peak. The most intense 3.211 eV peak, curve (a), is from a sample that was polished twice prior to the PL measurement. The sample-to-sample variation of intensity relative to the $D^0X$ peak suggests that

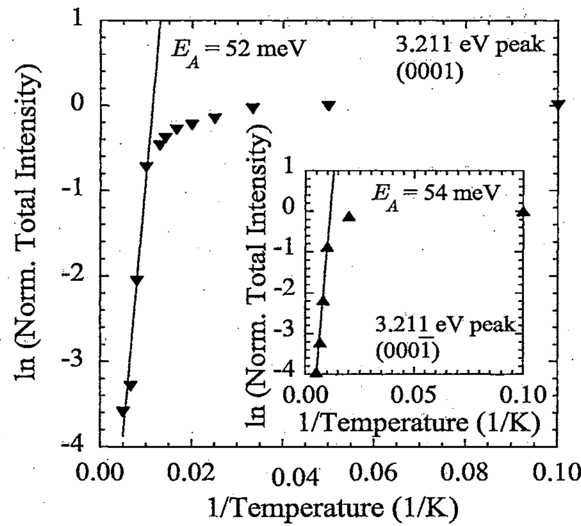


Figure 4.32: Natural logarithm of the normalized total intensity (peak intensity times FWHM) of the 3.211 eV peak as a function of 1/T for the (0001) Zn-terminated 1 $\mu$m mechanically polished surface. The inset shows the same analysis for the (000$\bar{1}$) O-terminated 1 $\mu$m mechanically polished surface. A fit of the linear portion of the data (first four data points) yields thermal activation energies for the (0001) and (000$\bar{1}$) surfaces of 52 and 54 meV, respectively.

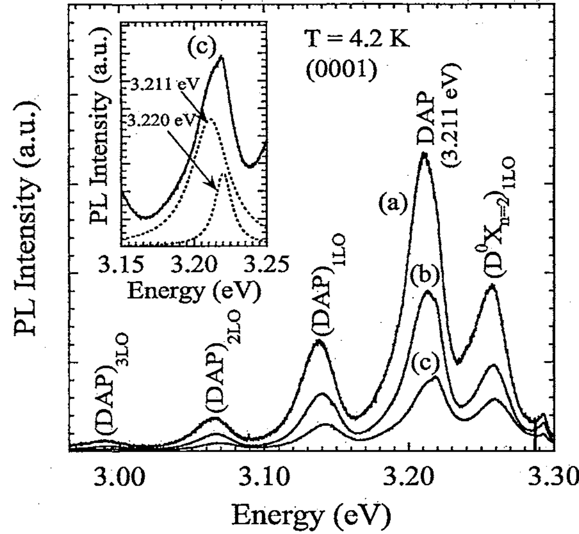


Figure 4.33: 4.2 K PL of three different (0001) 1 $\mu$m mechanically polished samples normalized by the $D^0X$ peak at 3.364 eV (not shown). Variation in 3.211 eV peak intensity relative to its $D^0X$ intensity suggests that it may be related to damage present in the crystal. Curve (a) is from a sample that had been polished twice prior to the PL measurement. Inset: Enlarged view of (c). Dotted lines are from the deconvolution of (b) using Lorentzian lineshapes and illustrate the possibility that both the 3.211 and 3.22 eV peaks are present in the PL of 1 $\mu$m mechanically polished (0001) ZnO.

the 3.211 eV emission may be related to the amount of damage introduced in the crystal by the mechanical polishing process as all three samples are from the same boule. For the smallest intensity DAP peak, shown as curve (c), an irregular lineshape is observed suggesting the convolution of the 3.211 eV peak with a second peak of similar energy. To further investigate the asymmetry of the 3.211 eV peak, a nonlinear peak-fitting routine using Lorentzian lineshapes was again used. The inset of Fig. 4.33 shows the deconvolution of spectrum (c) using Lorentzian lineshapes. Deconvolution indicates the possibility of a second peak occurring with an energy of 3.22 eV. This 3.22 eV peak is also observed for the chemomechanically polished samples and is consistent with Thonke et al. [87] who attributed it to DAP emission. We believe the 3.211 eV peak observed in our study to be different from the 3.22 eV peak reported in Thonke's PL investigation. The intensity variation of the 3.257 eV peak is in accordance with the variation observed for the $D^0X_{n=2}$ peak at 3.332 eV.

To further examine the dependence of the 3.211 eV peak on damage introduced by the polishing process we compared the 4.2 K PL from the 1 $\mu$m mechanically polished sample to the PL from 1/4 $\mu$m mechanically polished and chemomechanically polished samples for both (0001)- and

$(000\bar{1})$-oriented ZnO. Figure 4.34 shows the 4.2 K PL from each of the three surface preparations for the (0001)- oriented samples. Each spectrum is normalized by its 3.364 eV $D^0X$ peak (not shown). The 3.211 eV peak (and its LO phonon replicas) is dominant for the 1 $\mu$m mechanically polished sample, but it is also observed for the 1/4 $\mu$m mechanically polished crystal although with much less intensity. For the chemomechanically polished sample no peak at 3.211 eV is observed, however there is a small peak at 3.22 eV, mentioned previously [87]. The ordering of intensity for the 3.211 eV peak from highest for those samples prepared by 1 $\mu$m diamond abrasive mechanical polishing to lowest for those samples prepared by chemomechanically polished further suggests this peak may be due to damage introduced by the polishing process. The amount of subsurface damage resultant from polishing is confirmed by axial ion channeling results recently reported for ZnO using the same surface preparations [109].

Figure 4.35 shows the 4.2 K PL spectra for each of the three polished surfaces for $(000\bar{1})$-oriented samples. PL from the 1 $\mu$m diamond abrasive mechanically polished O-terminated surface exhibits a strong peak at 3.211 eV, but no peak is observed at this energy for the PL from either the 1/4

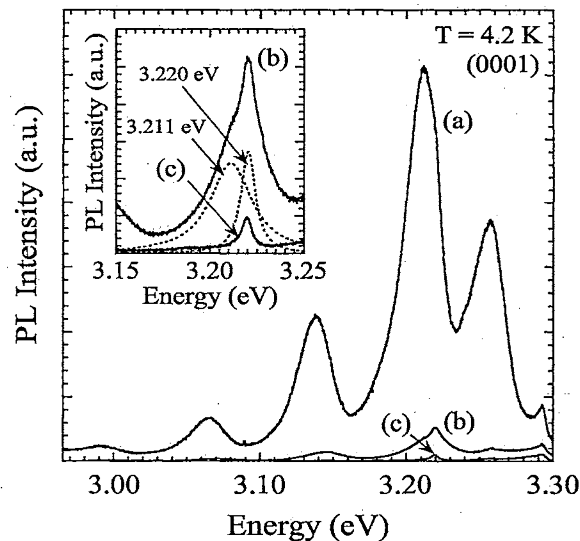


Figure 4.34: 4.2 K PL of (0001) ZnO. Shown are PL from samples prepared by (a) 1 $\mu$m diamond abrasive mechanical polishing, (b) 1/4 $\mu$m diamond abrasive mechanical polishing, and (c) chemomechanical polishing. Each spectrum is normalized by the $D^0X$ peak at 3.364 eV (not shown). Inset: Enlarged view of (b) and (c). Dotted lines are from the deconvolution of (b) using Lorentzian lineshapes and illustrate the possibility that both the 3.211 and 3.22 eV peaks are present in the PL of 1/4 $\mu$m mechanically polished (0001) ZnO.

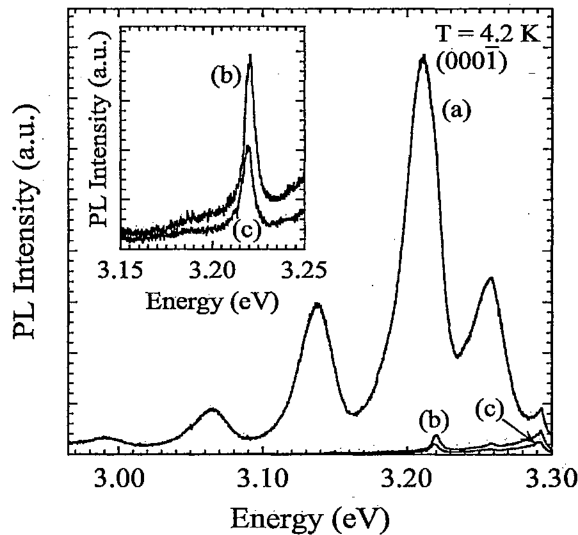


Figure 4.35: 4.2 K PL of (000$\bar{1}$) ZnO. Shown are PL from samples prepared by (a) 1 $\mu$m diamond abrasive mechanical polishing, (b) 1/4 $\mu$m diamond abrasive mechanical polishing, and (c) chemomechanical polishing. Each spectrum is normalized by the $D^0X$ peak at 3.364 eV (not shown). Inset: Enlarged view of (b) and (c). No peak was observed at 3.211 eV for (b) or (c).

$\mu$m mechanically polished or chemomechanically polished surfaces. For these two samples the DAP peak at 3.22 eV is observed. If the 3.211 eV peak is indicative of the amount of damage present in the crystal then the PL from the 1/4 $\mu$m mechanically polished samples (Figs. 4.34 and 4.35) suggest the Zn-terminated surface is damaged more than the O-terminated surface for the mechanical polishing process. This conclusion is consistent with axial ion channeling results [37] which showed larger amounts of damage for the Zn face compared to the O face for mechanically polished surfaces. The results presented here are also consistent with Look et al. [20, 62] who reported a higher defect production rate for the Zn-terminated (0001) surface than the O-terminated (000$\bar{1}$) surface using electron irradiation. Look et al. [20, 62] explained that for the (0001) surface, Zn is easily displaced into an interstitial region, however, for the (000$\bar{1}$) surface, the displacement of Zn atoms is much more difficult due to short-bonded O atoms beneath them.

### 4.3.3 Comparison of RT PL from Mechanically Polished and Chemomechanically Polished Surfaces

The PL spectra for (a) chemomechanically polished (000$\bar{1}$)-O face, (b) chemomechanically polished (0001)-Zn face, and for comparison (c) the relative intensities for the mechanically polished

surfaces are shown in Fig. 4.36. In all cases it was found that the O face resulted in higher PL emission when compared to the Zn face. This difference in PL emission from two polar faces is consistent with that reported by Kirilyuk et al. [186] for GaN. The PL response of the mechanically polished surfaces show a dramatic reduction in intensity when compared to the chemomechanically polished surfaces, and are barely visible in Fig. 4.36. These spectra are shown in Fig. 4.37 and include (a) 1/4 $\mu$m diamond abrasive-O face, (b) 1/4 $\mu$m diamond abrasive-Zn face, (c) 1 $\mu$m diamond abrasive-O face, and (d) 1 $\mu$m diamond abrasive-Zn face. The spectra for a given face (Zn or O) are normalized with respect to the chemomechanically polished results for that face, such that the normalized PL intensity plotted in Fig. 4.37 represents the relative change in intensity from a chemomechanically polished to mechanically polished surface. Similar to the chemomechanical polished surfaces, the O face for each of the mechanically polished conditions exhibited higher near-band-edge (NBE) PL intensity. The results indicate a two order of magnitude decrease in PL intensity for the mechanically polished surfaces. In addition, the difference in PL intensity for the 1/4 $\mu$m abrasive and 1 $\mu$m abrasive mechanically polished surfaces is a factor of 4 (for the O face) and a factor of 8 (for the Zn face).

For comparison to the PL results, axial ion channeling was used to obtain a measure of the damage depths and the amount of lattice disorder produced by polishing. To examine the average

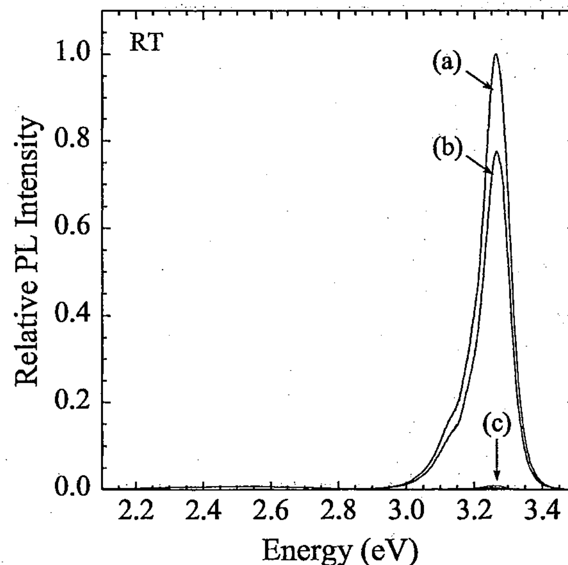


Figure 4.36: Relative PL intensities for polished surfaces, (a) chemomechanically polished-O face, (b) chemomechanically polished-Zn face, (c) mechanically polished surfaces for comparison.

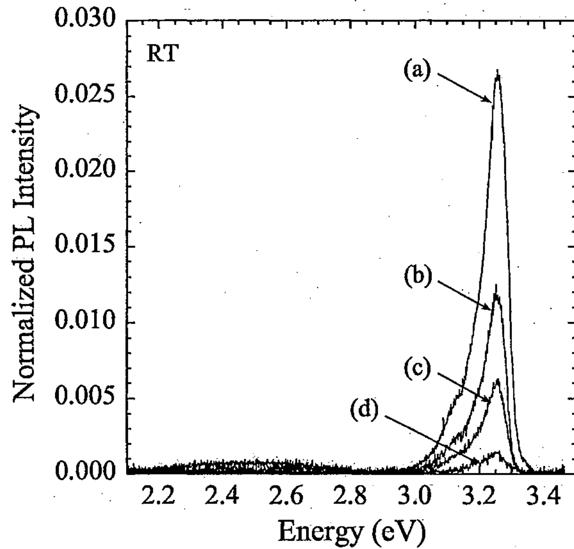


Figure 4.37: Normalized PL intensities for mechanically polished surfaces, (a) 1/4 $\mu$m-O face, (b) 1/4 $\mu$m-Zn face,(c) 1 $\mu$m-O face, (d) 1 $\mu$m-Zn face.

amount of lattice disorder, as measured by channeling in the near surface region which was probed by the PL measurements, an integration under each peak from the surface to 60 nm below the surface was made. These values can be normalized by the number of displaced Zn atoms/cm$^2$ for a totally amorphous layer (the area under the random spectrum), resulting in a relative disorder scale where 1 = totally amorphous and 0 = virgin material. Integration of the relative lattice disorder averaged over a depth of 60 nm resulted in 0.78 and 0.67 for the Zn and O faces respectively for the 1 $\mu$m abrasive, and 0.41 and 0.39 for the Zn and O faces respectively for the 1/4 $\mu$m abrasive. When compared to the PL results in Fig. 4.37, the overall trend of decreased PL intensity with increased lattice disorder is observed. This work is further reported in Ref. [109].

Each of the ZnO surface preparations presented in this study (i.e., chemomechanically polished and mechanically polished) exhibits unique PL features ranging from the observation of new peaks to diminished luminescence efficiency of pre-existing peaks when compared to PL from etched surfaces. These features, together with previous PL studies reported in the literature, an understanding of the underlying physics and results from axial ion channeling experiments on similarly prepared surfaces, allow for the identification of near-surface damage effects on the measured PL spectra.

PL has also been shown to be a very effective tool for the identification of impurities in semiconductors. It has been used in conjunction with ion implantation [93, 187], secondary ion mass spectroscopy [97, 188], muon spin rotation [90], and plasma-treatment [94, 189, 190] to verify the participation of hydrogen as a shallow donor in the luminescence spectrum of ZnO. In the following

section, we present PL results of H-treated (either ion implanted or plasma treated with 5% $H_2$/ 95% Ar) ZnO to implicate hydrogen as a likely shallow donor leading to the observed 3.361 eV emission at 4.2 K.

## 4.4 Hydrogen-treated ZnO

Recent studies of the low temperature PL of bulk ZnO have reported the observation of several neutral-donor-bound-exciton peaks [57,82,83], however, the identity of specific shallow donors resulting in the bound-exciton luminescence has remained unclear. Very recently, attention has focused on hydrogen as a shallow donor in ZnO [88, 90–97, 189]. Observations of two-electron satellites for specific bound-exciton transitions have implicated H as a likely shallow donor in recent PL studies of as-grown, bulk ZnO [87,191]. Luminescence techniques have also been used to investigate H-treated ZnO [78,93,94,188,189], however insufficient sample cooling or limited spectral resolution have precluded the observation of any resolved H-related bound-exciton peaks. In this section, the results from 4.2 K PL experiments performed for both H-implanted and 95% Ar/5% $H_2$ plasma-exposed ZnO samples are reported. Whereas the 3.364 eV emission is observed to be the dominant PL peak for untreated ZnO, the 3.361 eV peak is seen to be the strongest following hydrogen treatment by implantation or plasma exposure. For this particular study, two wurtzite structure ZnO samples were used. The samples were processed on both sides by first lapping and then chemomechanical polishing. Details of the polishing process are provided in Section 3.2. The samples were characterized by 4.2 K PL prior to H treatment. The (0001) face of one sample was implanted with 0.3 x $10^{15}$ H/cm$^2$ at 12 keV. The (0001) face of the other sample was exposed to a 200 W rf 95% Ar/5% $H_2$ plasma for 1 minute at 167 mTorr using a commercial plasma-cleaning instrument. Information about the measured hydrogen concentration for the two treated samples is reported in Section 3.2.

### 4.4.1 Hydrogen-Implanted ZnO

Figure 4.38 shows the 4.2 K PL spectra obtained for: (a) unimplanted and (b) H-implanted (0001) ZnO. The PL spectrum prior to implantation exhibits at least six narrow peaks at 3.358, 3.361, 3.362, 3.364, 3.365, and 3.368 eV with the strongest peak at 3.364 eV measuring about 1 meV full width at half maximum. As previously discussed, similar narrow peaks in this energy range have been reported by Reynolds et al. [82] in a study of ZnO also produced by Eagle-Picher and identified as the radiative recombination of excitons bound to defect-pair complexes which simulate neutral donors. Subsequent PL studies [87,191] have attributed the dominant luminescence peak in

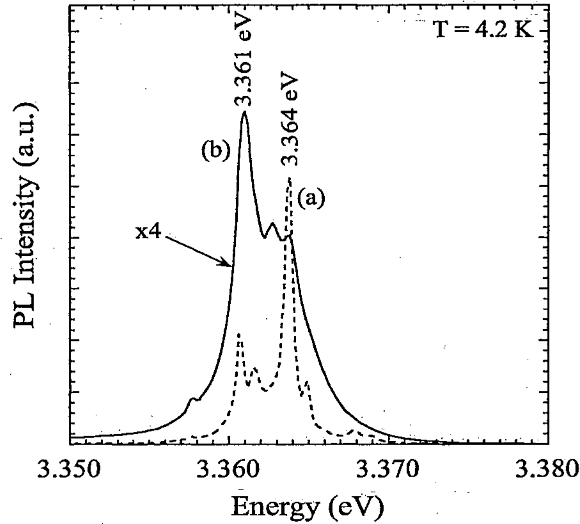


Figure 4.38: 4.2 K PL spectra for: (a) unimplanted and (b) H-implanted (0001) ZnO.

bulk ZnO (observed here at 3.364 eV) to the radiative recombination of excitons bound to shallow H-related donors. After implantation, differences in the 4.2 K exciton PL are observed. First, there is a significant change in the relative intensity for two of the bound-exciton peaks (3.361 eV and 3.364 eV). Whereas the 3.364 eV emission is observed to be strongest peak prior to implantation, the 3.361 eV peak is seen as the most intense of the four resolved peaks after implantation. Second, a new peak at approximately 3.363 eV is observed which was not observed prior to implantation. Third, there is a decrease in the overall exciton luminescence intensity (the ion-implanted spectrum is scaled by a factor of 4) and significant line broadening for each of the bound-exciton peaks. Line broadening may account in part for the reduction in number of resolved peaks from six, for the unimplanted sample, to four for the implanted case. We attribute the reduced overall luminescence intensity and line broadening to near surface damage introduced during the implantation process. This is consistent with Ip et al. [93] who reported severe degradation of optical properties following H-implantation of ZnO as measured by room temperature PL.

### 4.4.2 Hydrogen/Argon Plasma-treated ZnO

Figure 4.39 shows the 4.2 K PL spectra obtained for the sample: (a) before and (b) after plasma exposure. The PL prior to plasma treatment again exhibits at least six neutral-donor-bound-exciton peaks. After plasma exposure, a change in the relative intensities of the 3.361 eV and 3.364 eV peaks is observed again. We also observe a peak at 3.363 eV which was not observed from the sample prior to plasma treatment. These results are similar to those observed for the PL from the H-implanted

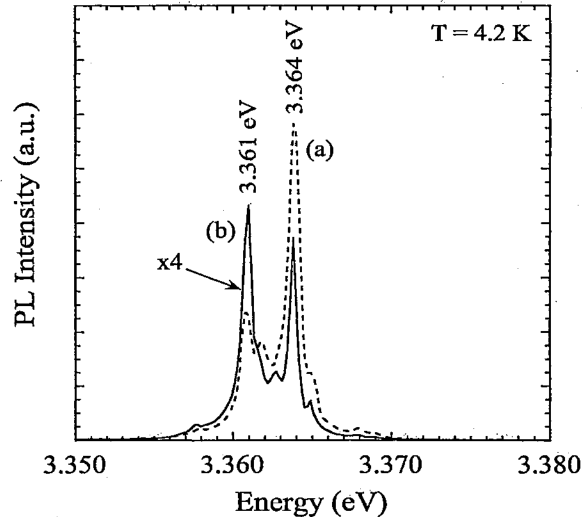


Figure 4.39: 4.2 K PL spectra for the sample: (a) before and (b) after plasma exposure.

ZnO however there does not appear to be any significant line broadening for the plasma-treated sample. The minimal line broadening for the plasma-exposed sample allows for better resolution of the individual peaks in the PL spectrum. From Fig. 4.39 (b), six clearly resolved peaks can be seen. There is a shoulder on the high-energy side of the 3.361 eV peak suggesting the presence of a seventh peak at 3.362 eV. Using Haynes' rule [192] with a coefficient of 0.3 reported in Alves [191] and the experimentally observed exciton-to-donor binding energy of 17 meV (using a free exciton energy of 3.378 eV [171]), a donor ionization energy of 57 meV is computed. This value is consistent with previously reported donor energies for H in ZnO. Cox et al. [90] in their investigation of H donors in ZnO using muon spin rotation, experimentally observed a donor energy for isolated muons in ZnO to be 60 $\pm$ 10 meV. In another recent report, Shimomura et al. [193] measured a donor energy of 50 meV for implanted muonium centers in bulk ZnO. Based on the consistency of these values, we conclude that the 3.361 eV peak is due to the collapse of excitons bound to hydrogen-related impurities (donors). These results also suggest that the 3.361 eV peak observed in the untreated samples may be due to hydrogen introduced during the growth process. The peak observed at 3.363 eV for the treated samples may also be related to hydrogen in the material, however this point requires further study.

### 4.4.3 He-implanted ZnO

To verify that the increased relative intensity of the 3.361 eV peak is not related to damage introduced during implantation, we compared the 4.2 K PL from H-implanted ZnO to that from

a He-implanted sample. For this study, one chemomechanically polished (0001) sample was used. One half of the surface was implanted with H and the other half implanted with He. Figure 4.40 shows a comparison of PL from the H-implanted region to that from the He-implanted region. For reference, PL from the sample prior to implantation is also shown. The spectra are normalized using the 3.364 eV peak. Whereas the PL from the H-implanted region is consistent with previous results (increased 3.361 eV peak intensity relative to the 3.364 eV peak), PL from the He-implanted region is similar to that from untreated ZnO. PL from the He-implanted region shows no measurable increase for the 3.361 eV or 3.363 eV peaks, relative to the untreated sample, further suggesting that these peaks (clearly observed for the H-implanted region) are from the recombination of excitons bound to H-related donors and not from damage introduced during the implantation process.

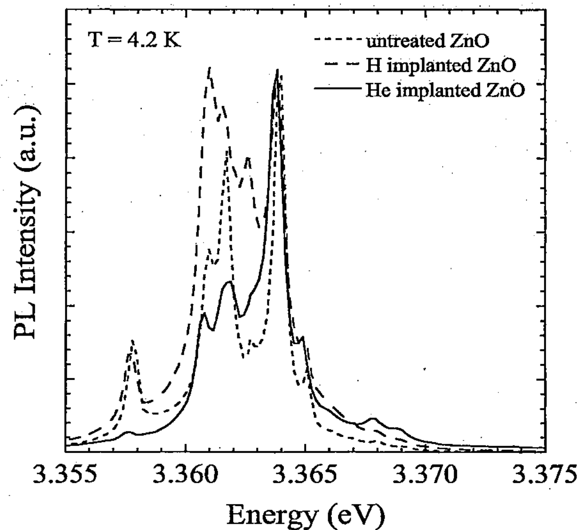


Figure 4.40: Comparison of 4.2 K PL spectra for H-implanted, He-implanted, and untreated ZnO. The spectra are normalized using the 3.364 eV peak.

# Chapter 5

# Conclusions and Possible Future Work

A study of the effects of subsurface damage on the PL of wurtzite, (0001)-oriented, bulk ZnO has been performed. Subsurface damage, resulting from ultrafine finishing processes such as polishing, is shown to have a significant effect on the PL of ZnO substrates. In addition to introducing nonradiative paths for the recombination of free carriers, effectively lowering the PL efficiency, near-surface disorder is shown to introduce new transitions for radiative recombination. PL is shown to be sensitive to small lattice disorder such as that found in chemomechanically polished substrates. It is also shown to be a good technique for characterizing the large range of lattice disorder found in this study (e.g., chemomechanically polished versus mechanically polished substrates).

## 5.1 Conclusions

1. Significant differences were observed between the RT PL from surfaces prepared by mechanical polishing as compared to those prepared by chemomechanical polishing. These include relative changes in both the spectral content and overall PL intensities. Mechanical polishing resulted in a two order of magnitude reduction in PL intensity over that for chemomechanically polished surfaces. Significant differences in PL intensity for the 1/4 $\mu$m abrasive and 1 $\mu$m abrasive mechanical polish were also observed. The PL results were compared to the amount of lattice disorder obtained by ion channeling, and the overall trend of decreased PL intensity with increased lattice disorder was observed.

2. Both free- and bound-exciton emission from the 20 K PL spectrum of (0001) ZnO were observed and are consistent with results published in the literature for similar material. The temperature-dependent free-exciton energy was fit using an equation developed by Manoogian and Woolley (MW). The coefficients of the MW equation $E = 3.379 - 5.04 \times 10^{-5}(T)^{1.01} - (1.84 \times 10^{-4})(398.4)(\coth(398.4/2T) - 1)$ obtained by curve fitting in the present study are in good agreement both with first-principle theoretical calculations and empirical values for other II-VI semiconductors. The strongest of the bound-exciton peaks exhibited a thermal activation energy of 14 meV, which is in agreement with the binding energy of the exciton to the defect (donor). Further analysis of the 3.364 eV bound-exciton peak observed at 4.2 K suggests a dissociation into a free exciton and a neutral-donor-like defect-pair complex occurs with increasing temperature.

3. We have observed three distinct peaks at 3.458 (HX-1LO), 3.385 (HX-2LO) and 3.312 (HX-3LO) eV from the 4.2 K PL spectra of bulk ZnO for both (0001) and $(000\bar{1})$ surfaces prepared by mechanical polishing with a 1 $\mu$m diamond abrasive slurry, which we associate with hot-exciton emission. The three peaks are thermally quenched as the temperature is increased from 4.2 to 300 K while the energy remains constant. No hot-exciton peaks were observed for surfaces prepared by chemomechanical polishing. The hot-exciton emission from the mechanically polished crystals is attributed to reduced exciton lifetime resultant from disorder introduced by the mechanical polishing process.

4. PL spectra from both polar faces, prepared by mechanical polishing with a 1 $\mu$m diamond abrasive slurry, exhibit a new 4.2 K luminescence peak at 3.211 eV believed to be DAP recombination. Sample-to-sample intensity variation of this DAP peak coupled with the absence or significantly reduced intensity of this peak from 1/4 $\mu$m mechanically polished and chemomechanically polished samples suggest it is related to the amount of subsurface damage present in the sample. From comparison of the 4.2 K PL to ion channeling results obtained from a previous study for each of the polished surfaces, an overall trend of increased PL intensity of the 3.211 eV DAP peak with increased lattice disorder is observed. We believe this peak to be resultant from defects introduced during the polishing process.

5. We have observed a distinct peak (S peak) from the RT PL of etched (0001) and $(000\bar{1})$ at ~3.12 eV which we attribute to inelastic exciton-electron interaction. The $(000\bar{1})$ etched surface is seen to exhibit a stronger S emission when compared to the (0001) etched surface. Chemomechanical polishing results in reduction of the intensity of the S peak. We attribute

this to disorder introduced by the polishing process.

6. We observe significant sample-to-sample differences in the bound-exciton emission of the 4.2 K PL spectra for chemomechanically polished samples. It is unknown whether these differences can be attributed to the growth process or the final finishing processes.

7. Aging is also seen to introduce measurable differences in the bound-exciton PL spectrum at 4.2 K. From our results, storing the samples in a desiccator for seven months resulted in changes in the relative intensities of each of the six identified $D^0X$ peaks.

8. The bound-exciton peaks were observed to be significantly broadened when compared to the same peaks for chemomechanically polished samples. This broadening is believed to be due to the introduction of defects during the mechanical polishing process.

9. Whereas the 1LO phonon-assisted-free-exciton (FX-1LO) luminescence is easily identified for the chemomechanically polished samples in the temperature range of 50-150 K, the wet-etched samples exhibit a 1TO phonon-assisted-bound-exciton luminescence that precludes the observation of an FX-1LO peak in the same temperature range. This difference in PL for these two surfaces may be caused in part by the presence of near-surface damage in the polished material.

10. The 4.2 K PL of ion-implanted H in ZnO exhibits an increased importance of the 3.361 eV peak relative to the 3.364 eV peak. Similar behavior is observed for the PL from a sample exposed to a plasma containing 5% $H_2$. To a first approximation, Haynes rule provides a donor energy of 57 meV for the observed 3.361 eV peak. This value is consistent with values for donor energies of H in ZnO reported in the literature. We conclude the peak observed at 3.361 eV is from the collapse of excitons bound to hydrogen-related donors for both the H-implanted and plasma-exposed samples. These results point to the possibility that the 3.361 eV peak observed in the PL from as-grown and polished ZnO may also be specifically related to the presence of hydrogen.

## 5.2 Possible Future Work

1. Estimate the DAP spacing for PL from mechanically polished substrates using experimentally observed Huang-Rhys factor and theoretical models from the literature.

2. Using taper polishing techniques or photoelectrochemical (PEC) etching, investigate the depth-resolved PL from polished ZnO substrates.

3. Determine the absorption coefficient for each of the prepared surfaces to better estimate the volume of investigation using PL.

4. Perform PL excitation (PLE) spectroscopy for each of the prepared surfaces. Because the PLE spectrum approximates the absorption spectrum [101], these experiments could serve as an alternative to the absorption measurements suggested above.

5. Investigate the effects of annealing on the H-related exciton luminescence from as-grown ZnO.

6. Optimize the chemomechanical polishing process parameters (e.g., slurry chemistry, pad speed, etc.) for ZnO using PL as characterization technique for the near-surface integrity of the substrates.

# Bibliography

[1] R. Koselka. Into the blue. *www.forbes.com/forbes/99/0614/6312196a.htm*, Sept. 23 1999.

[2] D. Green and M. Milanovic. Solid-state lighting offers 'vices' as well as 'virtues'. *Laser Focus World*, 39:99–103, 2003.

[3] Blue lasers for next-generation DVD. *Compound Semiconductor*, 6:11, 2000.

[4] J. Newey. Wide-bandgap materials and devices: Perfect substrate within reach for wide-bandgap materials. *Compound Semiconductor*, 8:45–48, 2002.

[5] D. C. Look, D. C. Reynolds, C. W. Litton, R. L. Jones, D. B. Eason, and G. Cantwell. Characterization of homoepitaxial p-type ZnO grown by molecular beam epitaxy. *Applied Physics Letters*, 81:1830–1832, 2002.

[6] D. M. Bagnall, Y. F. Chen, Z. Zhu, T. Yao, S. Koyama, M. Y. Shen, and T. Goto. Optically pumped lasing of ZnO at room temperature. *Applied Physics Letters*, 70:2230–2232, 1997.

[7] Z. K. Tang, G. K. L. Wong, P. Yu, M. Kawasaki, A. Ohtomo, H. Koinuma, and Y. Segawa. Room-temperature ultraviolet laser emission from self-assembled ZnO microcrystallite thin films. *Applied Physics Letters*, 72:3270–3272, 1998.

[8] A. Ohtomo, K. Tamura, M. Kawasaki, T. Makino, Y. Segawa, Z. K. Tang, G. K. L. Wong, Y. Matsumoto, and H. Koinuma. Room-temperature stimulated emission of excitons in ZnO/(Mg, Zn)O superlattices. *Applied Physics Letters*, 77(14):2204–2206, 2000.

[9] Y. Chen, N. T. Tuan, Y. Segawa, H-J. Ko, S-K. Hong, and T. Yao. Stimulated emission and optical gain in ZnO epilayers grown by plasma-assisted molecular-beam epitaxy with buffers. *Applied Physics Letters*, 78:1469–1471, 2001.

[10] P. Zu, Z. K. Tang, G. K. L. Wong, M. Kawasaki, A. Ohtomo, H. Koinuma, and Y. Segawa. Ultraviolet spontaneous and stimulated emissions from ZnO microcrystallite thin films at room temperature. *Solid State Communications*, 103:459–463, 1997.

[11] M. Zamfirescu, A. Kavokin, B. Gil, G. Malpuech, and M. Kaliteevski. ZnO as a material mostly adapted for the realization of room-temperature polariton lasers. *Physical Review B*, 65:1–4, 2002.

[12] C. R. Miskys, M. K. Kelly, O. Ambacher, G. Martinez-Criado, and M. Stutzmann. GaN homoepitaxy by metalorganic chemical-vapor deposition on free-ostanding GaN substrates. *Applied Physics Letters*, 77:1858–1860, 2000.

[13] M. Kamp, C. Kirchner, V. Schwegler, A. Pelzmann, K. J. Ebeling, M. Leszczynski, I. Grzegory, T. Suski, and S. Porowski. GaN homoepitaxy for device applications. *MRS Internet Journal of Nitride Semiconductor Research 4S1*, G10.2:1–12, 1999.

[14] S. Choopun, R. D. Vispute, W. Noch, A. Balsamo, R. P. Sharma, T. Venkatesan, A. Iliadis, and D. C. Look. Oxygen pressure-tuned epitaxy and optoelectronic properties of laser-deposited ZnO films on sapphire. *Applied Physics Letters*, 75:3947–3949, 1999.

[15] D. M. Bagnall, Y. F. Chen, Z. Zhu, T. Yao, M. Y. Shen, and T. Goto. High temperature excitonic stimulated emission from ZnO epitaxial layers. *Applied Physics Letters*, 73(8):1038–1040, 1998.

[16] S. Chang, N. B. Rex, R. K. Chang, G. Chong, and L. J. Guido. Stimulated emission and lasing in whispering-gallery modes of GaN microdisk cavities. *Applied Physics Letters*, 75:166–168, 1999.

[17] Y. Chen, D. M. Bagnall, H. Koh, K. Park, K. Hiraga, Z. Zhu, and T. Yao. Plasma assisted molecular beam epitaxy of ZnO on c-plane sapphire: growth and characterization. *Journal of Applied Physics*, 84(7):3912–3918, 1998.

[18] A. Yamamoto, T. Kido, T. Goto, Y. Chen, T. Yao, and A. Kasuya. Dynamics of photoexcited carriers in ZnO epitaxial thin films. *Applied Physics Letters*, 75(4):469–471, 1999.

[19] X. W. Sun and H. S. Kwok. Optical properties of epitaxially grown zinc oxide films on sapphire by pulsed laser deposition. *Journal of Applied Physics*, 86(1):408–411, 1999.

[20] D. C. Look, D. C. Reynolds, J. W. Hemsky, R. L. Jones, and J. R. Sizelove. Production and annealing of electron irradiation damage in ZnO. *Applied Physics Letters*, 75(6):811–813, 1999.

[21] D. C. Look. Recent advances in ZnO materials and devices. *Materials Science and Engineering B*, 80:383–387, 2001.

[22] Z. Laczik, G. R. Booker, and A. Mowbray. Residual polishing damage and surface quality of commercial InP wafers: A scaning PL study. *Materials Science and Engineering B*, 42:217–224, 1996.

[23] B. Molinas, M. Favaretto, L. Meregalli, A. Passaseo, L. Mirenghi, G. Rossetto, M. Natali, and G. Torzo. Preparation and test of special surfaces for epi-ready InP wafers. *Materials Science and Engineering B*, 44:213–216, 1997.

[24] S. Hong, E. Kurtz, J. Chang, T. Hanada, M. Oku, and T. Yao. Low stacking-fault density in ZnSe epilayers directly grown on epi-ready GaAs substrates without GaAs buffer layers. *Applied Physics Letters*, 78:165–167, 2001.

[25] J. F. Muth, R. M. Kolbas, A. K. Sharma, S. Oktyabrysky, and J. Narayan. Excitonic structure and absorption coefficient measurements of ZnO single crystal epitaxial films deposited by pulsed laser deposition. *Journal of Applied Physics*, 85(11):7884–7887, 1999.

[26] F. Hamdani, A. Botchkarev, W. Kim, H. Morkoc, M. Yeadon, J. M. Gibson, S.-C. Y. Tsen, David J. Smith, D. C. Reynolds, D. C. Look, K. Evans, C. W. Litton, W. C. Mitchel, and P. Hemenger. Optical properties of GaN grown on ZnO by reactive molecular beam epitaxy. *Applied Physics Letters*, 70:467–469, 1997.

[27] P. J. Caldwell, W. D. Laidig, Y. F. Lin, C. K. Peng, T. J. Magee, and C. Leung. Effects of substrate polishing on double-heterostructure AlyGa1-yAs-AlxGa1-xAs lasers grown by molecular beam expitaxy. *Journal of Applied Physics*, 57(3):984–986, 1985.

[28] F. A. Ponce, D. P. Bour, W. Gotz, N. M. Johnson, H. I. Helava, I. Grzegory, J. Jun, and S. Porowski. Homoepitaxy of GaN on polished bulk single crystals by metalorganic chemical vapor deposition. *Applied Physics Letters*, 68:917–919, 1996.

[29] E. Tournie, P. Brunet, J. P. Faurie, R. Triboulet, and J. O. Ndap. Molecular-beam epitaxy of high-quality ZnSe homo-epitaxial layers on solid-phase recrystallized substrates. *Applied Physics Letters*, 69:3221–3223, 1996.

[30] M. Schauler, F. Eberhard, C. Kirchner, V. Schwegler, A. Pelzmann, M. Kamp, K. J. Ebeling, F. Bertram, T. Riemann, J. Christen, P. Prystawko, M. Leszczynski, I. Grzegory, and S. Porowski. Dry etching of GaN substrates for high-quality homoepitaxy. *Applied Physics Letters*, 74:1123–1125, 1999.

[31] J. L. Weyher, A. R. A. Zauner, P. D. Brown, F. Karouta, A. Barcz, M. Wojdak, and S. Porowski. Growth of high quality, mocvd grown ga-polar GaN layers on GaN substrates after novel reactive ion etching. *Physica Status Solidi (A)*, 176:573–577, 1999.

[32] D. A. Lucca, M. J. Klopfstein, R. Ghisleni, and G. Cantwell. Investigation of polished single crystal ZnO by nanoindentation. *Annals of the CIRP*, 51(1):483–486, 2002.

[33] D. Black, L. Braun, H. Burdette, C. Evans, B. Hockey, R. Polvani, and G. White. Using advanced diagnostics to detect subsurface damage in sapphire. *SPIE*, 3134:272–283, 1997.

[34] T. George, Z. L. Weber, E. R. Weber, and F. H. Pollak. Polish-induced damage in <100> GaAs: A comparison of transmission electron microscopy and raman spectroscopy. *Journal of Applied Physics*, 67(9):4363–4365, 1990.

[35] I. Zarudi and L. Zhang. Subsurface damage in single-crystal silicon due to grinding and polishing. *Journal of Materials Science Letters*, 15:586–587, 1996.

[36] D. A. Lucca and C. J. Magiore. Subsurface lattice disorder in polished II-VI semiconductors. *Annals of the CIRP*, 46(1):485–488, 1997.

[37] D. A. Lucca, M. J. Klopfstein, G. Cantwell, C. J. Wetteland, J. R. Tesmer, and M. Nastasi. Ion channeling study of subsurface damage in polished ZnO. In *PRIME 2001*, pages 359–362, Genoa, Italy, 2001.

[38] G.-R. Yang, Y.-P. Zhao, Y. Z. Hu, T. P. Chow, and R. J. Gutmann. XPS and AFM study of chemical mechanical polishing of silicon nitride. *Thin Solid Films*, 333:219–223, 1998.

[39] M. P. Lisitsa, V. N. Malinko, E. V. Pidlisnyi, and G. G. Tsebulya. Edge absorption of semiconductors with mechanically polished surfaces. *Surface Science*, 11:411–418, 1968.

[40] R. T. Holm and E. D. Palik. Effects of mechanical polishing damage on the IR reflectance and attenuated total reflection spectra of n-type GaAs. *Journal of Vacuum Science and Technology*, 13:889–893, 1976.

[41] L. N. Borovich, A. V. Dudenkova, Yu. M. Popov, G. H. Talat, L. F. Komolova, G. V. Saparin, and G. V. Spivak. Influence of surface treatment on cathodoluminescence of CdS single crystals. *Sov. J. Quantum Electron*, 7:30–32, 1977.

[42] V. I. Kozlovskii and A. B. Krysa. Atomic hydrogen as a passivating agent for defects introduced by mechanical polishing into single-crystal CdS wafers. *Kratkie Soobshcheniya po Fizike*, 7:11–14, 1991.

[43] S. Myhajlenko, J. L. Batstone, H. J. Hutchinson, and J. W. Steeds. Luminescence studies of individual dislocations in II-VI (ZnSe) and III-V (InP) semiconductors. *Journal of Physics C: Solid State Physics*, 17:6477–6492, 1984.

[44] V. D. Negrii and Y. A. Osip'yan. Influence of dislocations on radiative recombination processes in cadmium sulfide. *Soviet Physics Solid State*, 20:432–436, 1978.

[45] V. D. Negrii and Y. A. Osipyan. Dislocation emission in CdS. *Physica Status Solidi*, 55:583–588, 1979.

[46] I. V. Akimova, L. N. Borovich, I. P. Vasilishcheva, A. V. Dudenkova, A. V. Egorov, A. S. Nasibov, O. N. Talenskii, Yu. M. Popov, and P. V. Shapkin. Determination of the depth of the disturbed layer in laser screens made of cadmium sulfide single crystals. *Sov. J. Quantum Electron*, 7:765–767, 1977.

[47] Z. Laczik, G. R. Booker, and A. Mowbray. Assessment of residual subsurface polishing damage in InP wafers by photoluminescence. *Journal of Crystal Growth*, 158:37–42, 1996.

[48] A. M. Huber and C. Grattepain. Crystal defect study in III-V compound technology. *Materials Science Forum*, 38-41:1345–1350, 1989.

[49] A. M. Huber and N. Briot. Material quality assessment of epitaxial layers of ZnSe and related compounds. *Materials Science and Engineering*, B28:61–64, 1994.

[50] V. Swaminathan, M. S. Young, and R. Caruso. Mechanical damage induced luminescence band in GaAs. *Journal of Applied Physics*, 57:1387–1390, 1985.

[51] R. A. Street and R. H. Williams. The luminescence of defects introduced by mechanical damage of InP. *Journal of Applied Physics*, 52:402–406, 1981.

[52] J. D. Oberstar and B. G. Streetman. Photoluminescence studies of surface damage states in InP. *Surface Science*, 108:L470–L475, 1981.

[53] K. Bohm and B. Fischer. Photoluminescence at dislocations in GaAs and InP. *Journal of Applied Physics*, 50:5453–5460, 1979.

[54] B. Tuck. Polishing damage and luminescence in p-type GaAs. *Physica Status Solidi*, 36:285–290, 1969.

[55] P.M. Amirtharaj and N.K. Dhar. Photoluminescence detection of native defects in the surface region of bulk CdTe. In Jr. F.J. Bartoli, H.F. Schaake, and J.F. Schetzina, editors, *Materials Research Society Symposium*, volume 161, pages 27–32, Boston, MA, 1990. Materials Research Society.

[56] K. Kornitzer, T. Ebner, K. Thonke, R. Sauer, C. Kirchner, V. Schwegler, M. Kamp, M. Leszczynski, I. Grzegory, and S. Porowski. Photoluminescence and reflectance spectroscopy of excitonic transitions in high-quality homoepitaxial GaN films. *Physical Review B*, 60:1471–1473, 1999.

[57] R. E. Sherriff, D. C. Reynolds, D. C. Look, B. Jogai, J. E. Hoelscher, T. C. Collins, G. Cantwell, and W. C. Harsch. Photoluminescence measurements from the two polar faces of ZnO. *Journal of Applied Physics*, 88:3454–3457, 2000.

[58] T. T. Lin and David Lichtman. A study of the optically produced hexagonal pattern on ZnO single crystals. *Journal of Applied Physics*, 48:2164–2168, 1977.

[59] B. Haskins (Eagle-Picher Technologies). private communication, 2000.

[60] V. Srikant and D. R. Clarke. On the optical band gap of zinc oxide. *Journal of Applied Physics*, 83(10):5447–5451, 1998.

[61] J. T. Czernuszka and N. Pratt. Cathodoluminescence-mode imaging of dislocations in zinc oxide. *Philosophical Magazine Letters*, 61:83–90, 1990.

[62] D. C. Look, J. W. Hemsky, and J. R. Sizelove. Residual native shallow donor in ZnO. *Physical Review Letters*, 82:2552–2555, 1999.

[63] D. G. Thomas. The exciton spectrum of zinc oxide. *Journal of Physics of Chemical Solids*, 15:86–96, 1960.

[64] Y. S. Park, C. W. Litton, T. C. Collins, and D. C. Reynolds. Exciton spectrum of ZnO. *Physical Review*, 143:512–519, 1966.

[65] C. Klingshirn. The luminescence of ZnO under high one- and two-quantum excitation. *physica status solidi (b)*, 71:547–556, 1975.

[66] C. F. Klingshirn. *Semiconductor optics.* Thomson Press, Karlsruhe, Germany, 1997.

[67] E. Tomzig and R. Helbig. Band-edge emission in ZnO. *Journal of Luminescence*, 14:403–415, 1976.

[68] J. M. Hvam. Exciton interaction in photoluminescence from ZnO. *physica status solidi (b)*, 63:511–517, 1974.

[69] S. A. Studenikin, M. Cocivera, W. Kellner, and H. Pascher. Band-edge photoluminescence in polycrystalline ZnO films at 1.7 K. *Journal of Luminescence*, 91:223–232, 2000.

[70] T. V. Butkhuzi, T. G. Chelidze, A. N. Georgobiani, D. L. Jashiashvili, T. G. Khulordava, and B. E. Tsekvava. Exciton photoluminescence of hexagonal ZnO. *Physical Review B*, 58(16):10692–10695, 1998.

[71] D. C. Look, D. C. Reynolds, Z.-Q. Fang, J. W. Hemsky, J. R. Sizelove, and R. L. Jones. Point defect characterization of GaN and ZnO. *Materials Science and Engineering*, B66:30–32, 1999.

[72] T. Monteiro, E. Pereira, M. R. Correia, C. Xavier, D. M. Hofmann, B. K. Meyer, S. Fischer, A. Cremades, and J. Piqueras. Broad emission band in GaN epitaxial layers grown on 6h-SiC and sapphire. *Journal of Luminescence*, 72-74:696–700, 1997.

[73] T. Suski, P. Perlin, H. Teisseyre, M. Leszczynski, I. Grzegory, J. Jun, M. Bockowski, S. Porowski, and T. D. Moustakas. Mechanism of yellow luminescence in GaN. *Applied Physics Letters*, 67:2188–2190, 1995.

[74] K. Vanheusden, C. H. Seager, W. L. Warren, D. R. Tallant, and J. A. Voigt. Correlation between photoluminescence and oxygen vacancies in ZnO phosphors. *Applied Physics Letters*, 68(3):403–405, 1996.

[75] K. Vanheusden, W. L. Warren, C. H. Seager, D. R. Tallant, J. A. Voigt, and B. E. Gnade. Mechanisms behind green photoluminescence in ZnO phosphor powders. *Journal of Applied Physics*, 79(10):7983–7990, 1996.

[76] D. C. Reynolds, D. C. Look, B. Jogai, and H. Morkoc. Similarities in the bandedge and deep-centre photoluminescence mechanisms of ZnO and GaN. *Solid State Communications*, 101(9):643–646, 1997.

[77] D. C . Reynolds, D. C. Look, B. Jogai, J. E. Van Nostrand, R. Jones, and J. Jenny. Source of the yellow luminescence band in GaN grown by gas-source molecular beam epitaxy and the green luminescence band in single crystal ZnO. *Solid State Communications*, 106(10):701–704, 1998.

[78] T. Sekiguchi, N. Ohashi, and Y. Terada. Effect of hydrogenation on ZnO luminescence. *Japanese Journal of Applied Physics*, 36:L289–L291, 1997.

[79] H. Kumano, A. A. Ashrafi, A. Ueta, A. Avramescu, and I. Suemune. Luminescence properties of ZnO films grown on GaAs substrates by molecular-beam epitaxy excited by electron-cyclotron resonance oxygen plasma. *Journal of Crystal Growth*, 214/215:280–283, 2000.

[80] N. Ohashi, T. Sekiguchi, K. Aoyama, T. Ohgaki, Y. Terada, I. Sakaguchi, T. Tsurumi, and H. Haneda. Band-edge emission of undoped and doped ZnO single crystals at room temperature. *Journal of Applied Physics*, 91:3658–3663, 2002.

[81] M. Suscavage, M. Harris, D. Bliss, P. Yip, S. Wang, D. Schwall, L. Bouthillette, J. Bailey, M. Callahan, D. C. Look, D. C. Reynolds, R. L. Jones, and C. W. Litton. High quality hydrothermal ZnO crystals. *MRS Internet Journal of Nitride Semiconductor Research*, 4S1:G3.40, 1999.

[82] D. C. Reynolds, D. C. Look, B. Jogai, C. W. Litton, T. C. Collins, W. Harsch, and G. Cantwell. Neutral-donor-bound-exciton complexes in ZnO crystals. *Physical Review B*, 57:12151–12155, 1998.

[83] C. Boemare, T. Monteiro, M. J. Soares, J. G. Guilherme, and E. Alves. Photoluminescence studies in ZnO samples. *Physica B*, 308-310:985–988, 2001.

[84] Y. P. Varshni. Temperature dependence of the energy gap in semiconductors. *Physica*, 34:149–154, 1967.

[85] M. Fernandez, P. Prete, N. Lovergine, A. M. Mancini, R. Cingolani, L. Vasanelli, and M. R. Perrone. Optical properties of MOVPE-grown ZnS epilayers on (100) GaAs. *Physical Review B*, 55:7660–7666, 1997. just abstract.

[86] R. Pässler, E. Griebl, H. Riepl, G. Lautner, S. Bauer, H. Preis, W. Gebhardt, B. Buda, D. J. As, D. Schikora, K. Lischka, K. Papagelis, and S. Ves. Temperature dependence of exciton peak energies in ZnS, ZnSe, and ZnTe epitaxial films. *Journal of Applied Physics*, 86:4403–4411, 1999.

[87] K. Thonke, Th. Gruber, N. Teofilov, R. Schönfelder, A. Waag, and R. Sauer. Donor-acceptor pair transitions in ZnO substrate material. *Physica B*, 308-310:945–948, 2001.

[88] C. G. Van de Walle. Hydrogen as a cause of doping in zinc oxide. *Physical Review Letters*, 85:1012–1015, 2000.

[89] A. F. Kohan, G. Ceder, Morgan D., and Chris G. Van de Walle. First-principles study of native point defects in ZnO. *Physical Review B*, 61:15 019–15 020, 2000.

[90] S. F. J. Cox, E. A. Davis, S. P. Cottrell, P. J. C. King, J. S. Lord, J. M. Gil, H. V. Alberto, R. C. Vilão, J. P. Duarte, N. Ayres de Campos, A. Weidinger, R. L. Lichti, and S. J. C. Irvine. Experimental confirmation of the predicted shallow donor hydrogen state in zinc oxide. *Physical Review Letters*, 86(12):2601–2604, 2001.

[91] D. M. Hofmann, A. Hofstaetter, F. Leiter, H. Zhou, F. Henecker, B. K. Meyer, S. B. Orlinskii, J. Schmidt, and P. G. Baranov. Hydrogen: A relevant shallow donor in zinc oxide. *Physical Review Letters*, 88:1–4, 2002.

[92] C. G. Van de Walle. Hydrogen as a shallow center in semiconductors and oxides. *physica status solidi (b)*, 235:89–95, 2003.

[93] K. Ip, E. Overberg, Y. W. Heo, D. P. Norton, S. J. Pearton, S. O. Kucheyev, C. Jagadish, J. S. Williams, R. G. Wilson, and J. M. Zavada. Thermal stability of ion-implanted hydrogen in ZnO. *Applied Physics Letters*, 81:3996–3998, 2002.

[94] N. Ohashi, T. Ishigaki, N. Okada, T. Sekiguchi, I. Sakaguchi, and H. Haneda. Effect of hydrogen doping on ultraviolet emission spectra of various types of ZnO. *Applied Physics Letters*, 80:2869–2871, 2002.

[95] C. G. Van de Walle. Defect analysis and engineering in ZnO. *Physica B*, 308-310:899–903, 2001.

[96] E. V. Lavrov, J. Weber, F. Börrnert, C. G. Van de Walle, and R. Helbig. Hydrogen-related defects in ZnO studied by infrared absorption spectroscopy. *Physical Review B*, 66:165205/1–7, 2002.

[97] K. Ip, E. Overberg, Y. W. Heo, D. P. Norton, S. J. Pearton, C. E. Stutz, B. Luo, F. Ren, D. C. Look, and J. M. Zavada. Hydrogen incorporation and diffusivity in plasma-exposed bulk ZnO. *Applied Physics Letters*, 82:385–387, 2003.

[98] C. G. Van de Walle. Strategies for controlling the conductivity of wide-band-gap semiconductors. *physica status solidi (b)*, 229:221–228, 2002.

[99] L. Pavesi and M. Guzzi. Photoluminescence of $Al_xGa_{1-x}As$ alloys. *Journal of Applied Physics*, 75:4779–4842, 1994.

[100] J. I. Pankove. *Optical Processes in Semiconductors.* Solid State Physical Electronics Series. Prentice-Hall, Inc., Englewood Cliffs, 1971.

[101] P. K. Yu and M. Cardona. *Fundamentals of Semiconductors: Physics and Materials Properties.* Springer, Berlin, second edition, 1999.

[102] H. B. Bebb and E. W. Williams. Photoluminescence I: Theory. In R. K. Willardson and A. C. Beer, editors, *Transport and Optical Phenomena*, volume 8 of *Semiconductors and Semimetals*, page 181. Academic Press, New York, 1972.

[103] P. K. Basu. *Theory of optical processes in semiconductors.* Clarendon Press, Oxford, 1997.

[104] G. F. Imbusch. Inorganic luminescence. In M. D. Lumb, editor, *Luminescence Spectroscopy*, pages 1–92. Academic Press, London, 1978.

[105] B. G. Streetman. *Solid State Electronic Devices.* Prentice Hall, Englewood Cliffs, fourth edition, 1995.

[106] H P. Myers. *Introductory Solid State Physics.* Taylor and Francis, London, second edition, 1997.

[107] D. A. Neamen. *Semiconductor Physics and Devices: Basic Principles.* Irwin, Burr Ridge, 1992.

[108] D. R. Vij and N. Singh. *Luminescence and Related Properties of II-VI Semiconductors.* Nova Science Publishers, New York, 1998.

[109] D. A. Lucca, D. W. Hamby, M. J. Klopfstein, G. Cantwell, C. J. Wetteland, J. R. Tesmer, and M. Nastasi. Effects of polishing on the photoluminescence of single crystal ZnO. *Annals of the CIRP*, 50(1):397–400, 2001.

[110] D. C. Reynolds and T. C. Collins. *Excitons: Their properties and uses.* Academic Press, New York, 1981.

[111] Y. Chen, H-J. Ko, S-K. Hong, and T. Yao. Layer-by-layer growth of ZnO epilayer on $Al_2O_3$ (0001) by using a MgO buffer layer. *Applied Physics Letters*, 76:559–561, 2000.

[112] Y. Toyozawa. Theory of line-shapes of the exciton absorption bands. *Progress of Theoretical Physics*, 20:53–81, 1958.

[113] Y. Toyozawa. Further contribution to the theory of the line-shape of the exciton absorption band. *Progress of Theoretical Physics*, 27:89–104, 1962.

[114] C. F. Li, Y. S. Huang, L. Malikova, and F. H. Pollak. Temperature dependence of the energies and broadening parameters of the interband excitonic transitions in wurtzite GaN. *Physical Review B*, 55(15):9251–9254, 1997.

[115] H. Herr, V. Alex, and J. Weber. Temperature dependence of the fundamental band gap in hexagonal GaN. *Materials Research Society Symposium Proceedings*, 482:719–724, 1998.

[116] B. Kim, I. Kuskovsky, I. P. Herman, D. Li, and G. F. Neumark. Reversible ultraviolet-induced photoluminescence degradation and enhancement in GaN films. *Journal of Applied Physics*, 86(4):2034–2037, 1999.

[117] L. Pavesi, F. Piazza, A. Rudra, J. F. Carlin, and M. Ilegems. Temperature dependence of the InP band gap from a photoluminescence study. *Physical Review B*, 44(16):9052–9055, 1991.

[118] R. Pässler. Dispersion-related assessments of temperature dependences for the fundamental band gap of hexagonal GaN. *Journal of Applied Physics*, 90:3956–3964, 2001.

[119] A. Manoogian and J. C. Woolley. Temperature dependence of the energy gap in semiconductors. *Canadian Journal of Physics*, 62:285–287, 1984.

[120] R. Pässler. Parameter sets due to fittings of the temperature dependencies of fundamental bandgaps in semiconductors. *physica status solidi (b)*, 216:975–1007, 1999.

[121] R. Pässler. Basic model relations for temperature dependencies of fundamental energy gaps in semiconductors. *physica status solidi (b)*, 200:155–172, 1997.

[122] A. Manoogian. Determination of the dilation and vibrational contributions to the temperature shift of excitons in CdS: melting of semiconductors. *Canadian Journal of Physics*, 60:1490–1495, 1982.

[123] G. Fonthal, L. Tirado-Mejia, J. I. Marin-Hurtado, H. Ariza-Calderon, and J. G. Mendoza-Alvarez. Temperature dependence of the band gap energy of crystalline CdTe. *Journal of Physics and Chemistry of Solids*, 61:579–583, 2000.

[124] J. Gutowski, N. Presser, and I. Broser. Acceptor-exciton complexes in ZnO: A comprehensive anaysis of their electronic states by high-resolution magnetooptics and excitation spectroscopy. *Physical Review B*, 38:9746–9758, 1988.

[125] D. C. Reynolds, D. C. Look, and B. Jogai. Fine structure on the green band in ZnO. *Journal of Applied Physics*, 89:6189–6191, 2001.

[126] A. K. Viswanath, J. I. Lee, S. Yu, D. Kim, Y. Choi, and C. Hong. Photoluminescence studies of excitonic transitions in GaN epitaxial layers. *Journal of Applied Physics*, 84(7):3848–3859, 1998.

[127] B. J. Skromme. Photoluminescence, magnetospectroscopy, and resonant electronic raman studies of heteroepitaxial gallium nitride. *MRS Internet Journal of Nitride Semiconductor Research*, 4 (15):1–12, 1999.

[128] J. A. Freitas, W. J. Moore, B. V. Shanabrook, G. C. B. Braga, S. K. Lee, S. S. Park, and J. Y. Han. Donor-related recombination processes in hydride-vapor-phase epitaxial GaN. *Physical Review B*, 66:233311/1–4, 2002.

[129] H. Venghaus and P. J. Dean. Shallow-acceptor, donor, free-exciton, and bound-exciton states in high-purity zinc telluride. *Physical Review B*, 21(4):1596–1609, 1980.

[130] M. A. Reshchikov, D. Huang, F. Yun, L. He, H. Morkoc, D. C. Reynolds, S. S. Park, and K. Y. Lee. Photoluminescence of GaN grown by molecular-beam epitaxy on a freestanding GaN template. *Applied Physics Letters*, 79:3779–3781, 2001.

[131] G. Martinez-Criado, C. R. Miskys, A. Cros, O. Ambacher, A. Cantarero, and M. Stutzmann. Photoluminescence study of excitons in homoepitaxial GaN. *Journal of Applied Physics*, 90:5627–5631, 2001.

[132] S. Iwai and S. Namba. Emission spectra in CdS under high excitation by electron beam. *Applied Physics Letters*, 19:41–43, 1971.

[133] T. Fischer and J. Billie. Recombination processes in highly excited CdS. *Journal of Applied Physics*, 45:3937–3942, 1974.

[134] J. M. Hvam. Temperature-induced wavelength shift of electron-beam-pumped lasers from CdSe, CdS, and ZnO. *Physical Review B*, 4:4459–4464, 1971.

[135] A. Z. Kolotov, I. G. Lang, and S. T. Pavlov. Scattering and dissociation of hot excitons in polar semiconductors. *Soviet Physics Solid State*, 17(11):2241–2242, 1976.

[136] E. Gross, S. Permogorov, Ya. Morozenko, and B. Kharlamov. Hot-exciton luminescence in CdSe crystals. *physica status solidi (b)*, 59:551–560, 1973.

[137] I. G. Ivanov, T. Egilsson, A. Henry, B. Monemar, and E. Janzen. Resonant sharp hot free-exciton luminescence in 6h- and 4h-SiC due to inhibited exciton-phonon interaction. *Physical Review B*, 64:1–7, 2001.

[138] E. Gross, S. Permogorov, V. Travnikov, and A. Selkin. Hot excitons and exciton excitation spectra. *Journal of Physics and Chemistry of Solids*, 31:2595–2606, 1970.

[139] S. Permogorov. Resonant scattering of exciton-polaritons in CdS crystals. *physica status solidi (b)*, 78:389–398, 1976.

[140] S. A. Permogorov and Y. V. Morozenko. Polarization of secondary radiation and relaxation of optical excitation in znte crystals. *Soviet Physics–Solid State*, 21:458–460, 1979.

[141] V. S. Bagaev, G. L. Belen'ki, V. V. Vaitsev, E. Y. Salaev, and V. B. Stopachinski. Hot luminescence in gallium selenide. *Soviet Physics*, 21:1275–1278, 1979.

[142] R. Riera, R. A. Rosas, J. L. Marin, and O. Sotolongo. Scattering and lifetime of hot excitons interacting with LO-phonons in InBr and InI polar semiconductors. *physica status solidi (b)*, 207:393–404, 1998.

[143] S. Permogorov. Hot excitons in semiconductors. *physica status solidi (b)*, 68:9–42, 1975.

[144] R. M. Martin and L. M. Falicov. Resonant raman scattering. In M. Cardona, editor, *Light Scattering in Solids I*, volume 8 of *Topics in Applied Physics*, pages 79–145. Springer-Verlag, Berlin, second edition, 1983.

[145] C. Weisbuch and R. G. Ulbrich. Resonant light scattering mediated by excitonic polaritons in semiconductors. In M. Cardona and G. Güntherodt, editors, *Light Scattering in Solids III*, volume 51 of *Topics in Applied Physics*, pages 207–263. Springer-Verlag, Berlin, 1982.

[146] E. F. Gross, S. A. Permogorov, V. V. Travnikov, and A. V. Sel'kin. Light excitons in CdS crystals. *Soviet Physics Solid State*, 13(3):578–585, 1971.

[147] S. A. Permogorov and V. V. Travnikov. Analysis of the inelastic scattering spectrum of polaritons in cadmium sulfide crystals. *Soviet Physics Solid State*, 13(3):586–590, 1971.

[148] S. Suga and T. Koda. Exciton-polariton luminescence in cuprous halides. *physica status solidi (b)*, 66:255–262, 1974.

[149] R. Planel, A. Bonnot, and C. Benoit a la Guillaume. Excitation spectra of luminescence in cadmium sulfide. *physica status solidi (b)*, 58:251–266, 1973.

[150] J. R. Packard, D. A. Campbell, and W. C. Tait. Evidence for indirect annihilation of free excitons in II-VI semiconductor lasers. *Journal of Applied Physics*, 38(13):5255–5257, 1967.

[151] S. Permogorov. Optical emission of excitons. In E. I. Rashba and M. D. Sturge, editors, *Optical emission due to exciton scattering by LO phonons in semiconductors*, pages 177–203. North-Holland Publishing Company, Leningrad, 1982.

[152] S. Y. Verbin, S. A. Permogorov, A. N. Reznitskii, and A. N. Starukhin. Change in the mechanism of the exciton-phonon interaction in ZnO crystals with defects. *Soviet Physics Solid State*, 19:2028–2029, 1977.

[153] B. Segall and G. D. Mahan. Phonon-assisted recombination of free excitons in compound semiconductors. *Physical Review*, 171:935–948, 1968.

[154] R. L. Weiher and W. C. Tait. Contribution of excitons to the edge luminescence in zinc oxide. *Physical Review*, 166:791–796, 1968.

[155] D. C. Reynolds and T. C. Collins. Donor-acceptor pair recombination in cadmium sulfide crystals. *Physical Review*, 188:1267–1271, 1969.

[156] P. W. Yu, C. S. Park, and S. T. Kim. Photoluminescence studies of GaN layers grown by hydride vapor phase epitaxy. *Journal of Applied Physics*, 89:1692–1695, 2001.

[157] G. B. Ren, D. J. Dewsnip, D. E. Lacklison, J. W. Orton, T. S. Cheng, and C. T. Foxson. Donor acceptor pair in molecular beam epitaxy grown GaN. *Materials Science and Engineering B*, 43:242–245, 1997.

[158] P. Bäume, J. Gutowski, D. Wiesmann, R. Heitz, A. Hoffmann, E. Kurtz, D. Hommel, and G. Landwehr. Intensity-dependent energy and line shape variation of donor-acceptor-pair bands in ZnSe:N at different compensation levels. *Applied Physics Letters*, 67:1914–1916, 1995.

[159] Z. M. Zhu, G. H. Li, N. Z. Liu, S. Z. Wang, H. X. Han, and Z. P. Wang. Quantitative analysis of excitonic photoluminescence in nitrogen-doped ZnSe epilayers. *Journal of Applied Physics*, 85(3):1775–1779, 1999.

[160] M. Moldovan, T. H. Myers, and N. C. Giles. Investigation of donor-accepted pair lumisecence from ZnSe:N epilayers. *Journal of Applied Physics*, 84(10):5743–5749, 1998.

[161] A. Aydinli, N. M. Gasanly, and Göksen. Donor-acceptor pair recombination in gallium sulfide. *Journal of Applied Physics*, 88:7144–7149, 2000.

[162] M. A. Reshchikov, F. Shahedipour, R. Y. Korotkov, B. W. Wessels, and M. P. Ulmer. Photoluminescence band near 2.9 ev in undoped GaN epitaxial layers. *Journal of Applied Physics*, 87:3351–3354, 2000.

[163] J. S. Colton, P. Y. Yu, K. L. Teo, P. Perlin, E. R. Weber, I. Grzegory, and K. Uchida. Selective excitation of the yellow luminescence of GaN. *Physica B*, 273-274:75–79, 1999.

[164] F. H. Leiter, H. R. Alves, A. Hofstaetter, D. M. Hofmann, and B. K. Meyer. The oxygen vacancy as the origin of a green emission in undoped ZnO. *physica status solidi (b)*, 226:R4–R5, 2001.

[165] D. C. Look, D. C. Reynolds, J.R. Sizelove, R. L. Jones, C. W. Litton, G. Cantwell, and W. C. Harsch. Electrical properties of bulk ZnO. *Solid State Communications*, 105(6):399–401, 1998.

[166] G. Cantwell (Eagle-Picher Technologies). private communication, 2002.

[167] M. J. Klopfstein, D. A. Lucca, and G. Cantwell. Effects of illumination on the response of (0001) ZnO to nanoindentation. *physica status solidi (a)*, 196:R1–R3, 2003.

[168] J. F. Ziegler, J. P. Biersack, and U. Littmark. *The Stopping and Range of Ions in Solids.* Pergamon Press, Inc., New York, 1985.

[169] G. E. Jellison and L. A. Boatner. Optical functions of uniaxial ZnO determined by generalized ellipsometry. *Physical Review B*, 58:3586–3589, 1998.

[170] L. Wang and N. C. Giles. Temperature dependence of the free-exciton transition energy in zinc oxide by photoluminescence excitation spectroscopy. *Journal of Applied Physics*, 94:973–978, 2003.

[171] D. W. Hamby, D. A. Lucca, M. J. Klopfstein, and G. Cantwell. Temperature dependent exciton photoluminescence of bulk ZnO. *Journal of Applied Physics*, 93:3214–3217, 2003.

[172] D. A. Lucca, D. W. Hamby, M. J. Klopfstein, and G. Cantwell. Chemomechanical polishing effects on the room temperature photoluminescence of bulk ZnO: exciton-LO phonon interaction. *physica status solidi (b)*, 229:845–848, 2002.

[173] D. C. Reynolds, D. C. Look, B. Jogai, C. W. Litton, G. Cantwell, and W. C. Harsch. Determination of defect pair orientation in ZnO. *Solid State Communications*, 109:419–422, 1999.

[174] D. W. Marquardt. An algorithm for least-squares estimation of nonlinear parameters. *J. Soc. Indust. Appl. Math.*, 11:431–441, 1963.

[175] D. C. Reynolds, D. C. Look, B. Jogai, R. L. Jones, C. W. Litton, W. Harsch, and G. Cantwell. Optical properties of ZnO crystals containing internal strains. *Journal of Luminescence*, 82:173–176, 1999.

[176] A. R. Hutson. Electronic properties of ZnO. *Physics and Chemistry of Solids*, 8:467–472, 1959.

[177] G. Simmons and H. Wang. *Single Crystal Elastic Constants and Calculated Aggregate Properties: A Handbook.* M.I.T. Press, Cambridge, 1971.

[178] R. L. Knell and D. W. Langer. Pressure coefficient of the ZnO band-to-band transition. *Physics Letters*, 21:370–371, 1966.

[179] G. Heiland and H. Ibach. Pyroelectricity of zinc oxide. *Solid State Communications*, 4:353–356, 1966.

[180] C. Lárez and C. Rincon. Alloy composition and temperature dependence of the direct energy gap in $Al_xGa_{1-x}As$. *Journal of Physics and Chemistry of Solids*, 58:1111–1114, 1997.

[181] H. Watanabe, M. Wada, and T. Takahashi. Optical and electrical properties of ZnO crystals. *Japanese Journal of Applied Physics*, 3:617–625, 1964.

[182] C. Rincon, S. M. Wasim, G. Marin, G. S. Perez, and G. Bacquet. Temperature dependence of the photoluminescence spectra of single crystals of $CuInTe_2$. *Journal of Applied Physics*, 82:4500–4503, 1997.

[183] L. G. Goncharov, L. V. Ryabykina, and K. I. Svistunova. Influence of dislocations on the lifetime of free excitons in germanium. *Soviet Physics Solid State*, 19:1659–1660, 1977.

[184] A. Karpol and B. Pratt. Dependence of photoluminescence of n-GaAs on surface treatment. *Solid State Communications*, 12:325–327, 1973.

[185] D. A. Lucca, D. W. Hamby, M. J. Klopfstein, and G. Cantwell. Hot-exciton luminescence from the two polar faces of mechanically polished bulk ZnO. *Solid State Communications*, to be submitted.

[186] V. Kirilyuk, A. R. A. Zauner, P. C. M. Christianen, J. L. Weyher, P. R. Hageman, and P. K. Larsen. Exciton-related photoluminescence in homoepitaxial GaN of Ga and N polarities. *Applied Physics Letters*, 76(17):2355–2357, 2000.

[187] D. J. Brink and H. W. Kunert. Optical properties of as-grown and proton irradiated ZnO. *physica status solidi (b)*, 229:859–862, 2002.

[188] N. Ohashi, T. Ishigaki, N. Okada, H. Taguchi, I. Sakaguchi, S. Hishita, T. Sekiguchi, and H. Haneda. Passivation of active recombination centers in ZnO by hydrogen doping. *Journal of Applied Physics*, 93:6386–6392, 2003.

[189] A. Y. Polyakov, N. B. Smirnov, A. V. Govorkov, K. Ip, M. E. Overberg, Y. W. Heo, D. P. Norton, S. J. Pearton, B. Luo, F. Ren, and J. M. Zavada. Hydrogen plasma treatment effects on electrical and optical properties of n-ZnO. *Journal of Applied Physics*, 94:400–406, 2003.

[190] Y. M. Strzhemechny, J. Nemergut, P. E. Smith, J. Bae, D. C. Look, and L. J. Brillson. Remote hydrogen plasma processing of ZnO single crystal surfaces. *Journal of Applied Physics*, 94:4256–4262, 2003.

[191] H. Alves, D. Pfisterer, A. Zeuner, T. Riemann, J. Christen, D. M. Hofmann, and B. K. Meyer. Optical investigations on excitons bound to impurities and dislocations in ZnO. *Optical Materials*, 23:33–37, 2003.

[192] J. R. Haynes. Experimental proof of the existence of a new electronic complex in silicon. *Physical Review Letters*, 4:361–363, 1960.

[193] K. Shimomura, K. Nishiyama, and R. Kadono. Electronic structure of the muonium center as a shallow donor in ZnO. *Physical Review Letters*, 89:255505, 2002.

[194] *Handbook of Chemistry and Physics*. CRC Press LLC, Boca Raton, 1999.

[195] J. Daleiden, R. Kiefer, S. KluSSmann, M. Kunzer, C. Manz, M. Waihler, J. Braunstein, and G. Weimann. Chemically-assisted ion-beam etching of (AlGa)As/GaAs: lattice damage and removal by in-situ $Cl_2$ treatment. *Microelectronic Engineering*, 45:9–14, 1999.

[196] R. Khare and E. L. Hu. Dopant selective photoelectrochemical etching of GaAs homostructures. *Journal of Electrochemical Society*, 138(5):1516–1519, 1991.

[197] H. Cho, K. H. Auh, J. Han, R. J. Shul, S. M. Donovan, C. R. Abernathy, E. S. Lambers, F. Ren, and S. J. Pearton. UV-photoassisted etching of GaN in KOH. *Journal of Electronic Materials*, 28(3):290–294, 1999.

[198] F. Ren, J. R. Lothian, S. J. Pearton, C. R. Abernahty, C. B. Vartuli, J. D. Mackenzie, R. G. Wilson, and R. F. Karlicek. Effect of dry etching on surface properties of III-nitrides. *Journal of Electronic Materials*, 26(11):1287–1291, 1997.

[199] R. Khare, E.L. Hu, D. Reynolds, and S.J. Allen. Photoelectrochemical etching of high aspect ratio submillimeter waveguide filters from n+ GaAs wafers. *Applied Physics Letters*, 61(24):2890–2892, 1992.

[200] D. A. Stocker, E. F. Schubert, K. S. Boutros, and J. M. Redwing. Fabrication of smooth GaN-based laser facets. *MRS Internet Journal of Nitride Semiconductor Research 4S1*, page G7.5, 1999.

[201] W. S. Lee, Y. H. Choi, K. W. Chung, D. C. Moon, and M. W. Shin. High temperature performance of recessed gate GaN MESFETs fabricated using photoelectrochemical etching process. *Electronics Letters*, 36(3):265–267, 2000.

[202] M. S. Minsky, M. White, and E. L. Hu. Room-temperature photoenhanced wet etching of GaN. *Applied Physics Letters*, 68(11):1531–1533, 1996.

[203] R. Khare, E. L. Hu, J. J. Brown, and M. A. Melendes. Micromachining in III-V semiconductors using wet photoelectrochemical etching. *Journal of Vacuum Science and Technology B*, 11(6):2497–2501, 1993.

[204] J. S. Shor and Jr. R. M. Osgood. Broad-area photoelectrochemical etching of n-type beta-SiC. *Journal of the Electrochemical Society*, 140(8):L123–L125, 1993.

[205] H. Lu, Z. Wu, and I. Bhat. Photoassisted anodic etching of gallium nitride. *Journal of Electrochemical Society*, 144(1):L8–L11, 1997.

[206] C. Youtsey, I. Adesida, and G. Bulman. Highly anisotropic photoenhanced wet etching of n-type GaN. *Applied Physics Letters*, 71(15):2151–2153, 1997.

[207] L.-H. Peng, C.-W. Chuang, J.-K. Ho, C.-N. Huang, and C.-Y. Chen. Deep ultraviolet enhanced wet chemical etching of gallium nitride. *Applied Physics Letters*, 72(8):939–941, 1998.

[208] J. L. Weyher, P. D. Brown, J. L. Rouviere, T. Wosinski, A. R. A. Zauner, and I. Grzegory. Recent advances in defect-selective etching of GaN. *Journal of Crystal Growth*, 210:151–156, 2000.

[209] C. Youtsey, L. T. Romano, and I. Adesida. Gallium nitride whiskers formed by selective photoenhanced wet etching of dislocations. *Applied Physics Letters*, 73(6):797–799, 1998.

[210] C. Youtsey, L. T. Romano, R. J. Molnar, and I. Adesida. Rapid evaluation of dislocation densities in n-type GaN films using photoenhanced wet etching. *Applied Physics Letters*, 74:3537–3539, 1999.

[211] C. Youtsey, I. Adesida, L. T. Romano, and G. Bulman. Smooth n-type GaN surfaces by photoenhanced wet etching. *Applied Physics Letters*, 72(5):560–562, 1998.

[212] D. A. Stocker and E. F. Schubert. Reduction of surface roughness in photoenhanced electrochemical wet-etched GaN. *Journal of the Electrochemical Society*, 146(7):2702–2704, 1999.

[213] B. S. Shelton, T. G. Zhu, M. M. Wong, H. K. Kwon, C. J. Eiting, D. J. H. Lambert, S. P. Turini, and R. D. Dupuis. Ultrasmooth GaN etched surfaces using photoeletrochemical wet etching and an ultrasonic treatment. *Electrochemical and Solid-State Letters*, 3(2):87–89, 2000.

[214] M. Futsuhara, K. Yoshioda, Y. Ishida, O. Takai, K. Hashimoto, and A. Fujishima. Micropattern formation on ZnO films using a photodissolution reaction. *Journal of the Electrochemical Society*, 143:3743–3746, 1996.

[215] W. L. Ng, M. A. Lourenco, R. M. Gwilliam, S. Ledain, G. Shao, and K. P. Homewood. An efficient room-temperature silicon-based light-emitting diode. *Nature (addendum)*, 414:470, 2001.

[216] D. Dimova-Malinovska, M. Sendova-Vassileva, M. Kamenova, N. Tzenov, and M. Tzolov. On the origin of the visible luminescence from porous silicon. *Vacuum*, 47:1133–1138, 1996.

[217] N. Yamamoto and H. Takai. Visible luminescence from photo-chemically etched silicon. *Thin Solid Films*, 359:184–187, 2000.

[218] W. L. Ng, M. A. Lourenco, R. M. Gwilliam, S. Ledain, G. Shao, and K. P. Homewood. An efficient room-temperature silicon-based light-emitting diode. *Nature*, 410:192–194, 2001.

[219] L. Pavesi, G. Giebel, R. Tonini, F. Corni, C. Nobili, and G. Ottaviani. Visible luminescence from silicon by hydrogen implantation and annealing treatments. *Applied Physics Letters*, 65:454–456, 1994.

[220] G. P. Karwasz, A. Misiuk, M. Ceschini, and L. Pavesi. Visible photoluminescence from pressure annealed intrinsic czochralski-grown silicon. *Applied Physics Letters*, 69:2900–2902, 1996.

[221] J. Xu, Z. He, K. Chen, X. Huang, D. Feng, H. Han, Z. Wang, and G. Li. Role of surface defect states in visible luminescence from oxidized hydrogenated amorphous Si/hydrogenated amorphous ge multilayers. *Applied Physics Letters*, 74:3773–3775, 1999.

[222] C. Wu, C. H. Crouch, L. Zhao, and E. Mazur. Visible luminescence from silicon surfaces microstructured in air. *Applied Physics Letters*, 81:1999–2001, 2002.

[223] P. M. Fauchet and J. V. Behren. The strong visible luminescence in porous silicon: Quantum confinement, not oxide-related defects. *physica status solidi (b)*, 204:R7–R8, 1997.

[224] T. Shimizu-Iwayama, T. Hama, D. E. Hole, and I. W. Boyd. Characteristic photoluminescence properties of Si nanocrystals in $SiO_2$ fabricated by ion implantation and annealing. *Solid State Electronics*, 45:1487–1494, 2001.

[225] S. Cheylan and R. G. Elliman. The effect of ion dose and annealing ambient on room temperature photoluminescence from Si nanocrystals in $SiO_2$. *Nuclear Instruments and Methods in Physics Research B*, 148:986–990, 1999.

[226] T. S. Iwayama, T. Hama, D. E. Hole, and I. W. Boyd. Optical and structural properties of encapsulated Si nanocrystals formed in $SiO_2$ by ion implantation. *Surface and Coatings Technology*, 158-159:712–716, 2002.

[227] K. S. Zhuravlev, A. M. Gilinsky, and A. Y. Kobitsky. Mechanism of photoluminescence of Si nanocrystals fabricated in a $SiO_2$ matrix. *Applied Physics Letters*, 73:3962–2964, 1998.

[228] J. Y. Jeong, S. Im, M. S. Oh, H. B. Kim, K. H. Chae, C. N. Whang, and J. H. Song. Defect versus nanocrystal luminescence emitted from room temperature and hot-implanted $SiO_2$ layers. *Journal of Luminescence*, 80:285–289, 1999.

[229] Y. Kanzawa, T. Kageyama, S. Takeoka, M. Fujii, S. Hayashi, and K. Yamamoto. Size-dependent near-infrared photoluminescence spectra of Si nanocrystals embedded in $SiO_2$ matrices. *Solid State Communications*, 102:533–537, 1997.

# Appendix A

# ZnO Properties

| Property | Symbol | Value | Reference |
|---|---|---|---|
| Symmetry | | hexagonal (wurtzite) | [110] |
| Lattice Parameters | $a$ | 3.249 Å | [17] |
| | $c$ | 5.207 Å | [17] |
| Room Temperature Band Gap Energy | $E_g$ | 3.37 eV | [17] |
| Exciton Binding Energy | $E_{ex}$ | 60 meV | [17] |
| Longitudinal Optical Phonon Energy | $\hbar\omega_{LO}$ | 72 meV | [175] |
| Exciton Effective Mass | $m^*_{ex}$ | $0.31m_0$ | [110] |
| Dielectric Constant | $\epsilon_s$ | 8.5 | [110] |
| | $\epsilon_\infty$ | 4.0 | [110] |
| Refractive Index | $n$ | 2.0 | [110] |
| Debye Temperature | $\theta_D$ | 920 K | [176] |
| Melting Temperature | $T_m$ | 2250 K | [194] |
| Modulus of Elasticity | $E$ | 124 GPa | [177] |
| Shear Modulus | $G$ | 45.3 GPa | [177] |
| Mean Thermal Expansion Coefficient | $\alpha_L$ | $4.3 \times 10^{-6}$ 1/K | [179] |
| Band Gap Pressure Coefficient | $\frac{\partial E_g}{\partial P}$ | $2.7 \times 10^{-6}$ eV/bar | [178] |
| Band Gap Temperature Coefficient | $\frac{\partial E_g}{\partial T}$ | $-8 \times 10^{-4}$ eV/K | [181] |

Table A.1: ZnO material properties

# Appendix B

# RT PL of As-grown ZnO

Figure B.1 shows the RT PL of as-grown (i.e., prior to sawing, lapping, dicing, and polishing) bulk ZnO. For comparison, the RT PL from a chemomechanically polished surface is included. A reduction in PL intensity is observed.

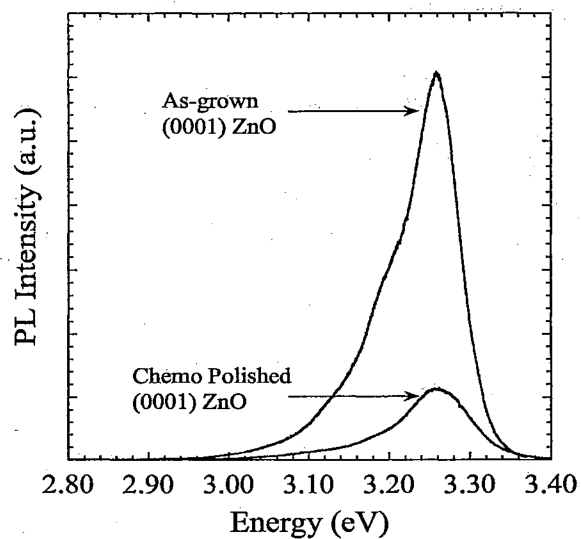


Figure B.1: Comparison of RT PL from as-grown (0001) and chemomechanically polished (0001) ZnO

# Appendix C

# PL of Ion Channeled ZnO

Axial ion channeling has been used to characterize each of the polished surfaces in this study. Ion channeling is known to introduce some lattice disorder during the channeling process. We have investigated the effect of this damage on the RT PL from (0001) ZnO and compared this luminescence to a spectrum from a chemomechanically polished (0001) sample. These results are shown in Fig. C.1. The net effect of damage resultant from ion channeling on the RT PL initially appears to be the introduction of nonradiative paths for the recombination of free carriers in the channeled region of the crystal resulting in significantly reduced luminescence intensity.

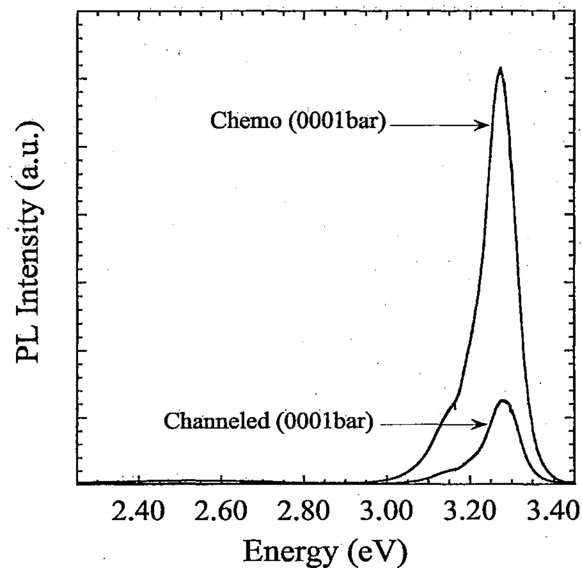


Figure C.1: Comparison of RT PL for channeled and chemomechanically polished $(000\bar{1})$ ZnO.

# Appendix D

# RT PL of Etched CdS

Figure D.1 is a comparison of the RT PL for etched (wurtzite) CdS and etched ZnO. The spectra have been normalized by their characteristic emission peak and plotted using two different energy scales so that a direct comparison of their lineshapes can be made. Only one characteristic peak is observed for CdS.

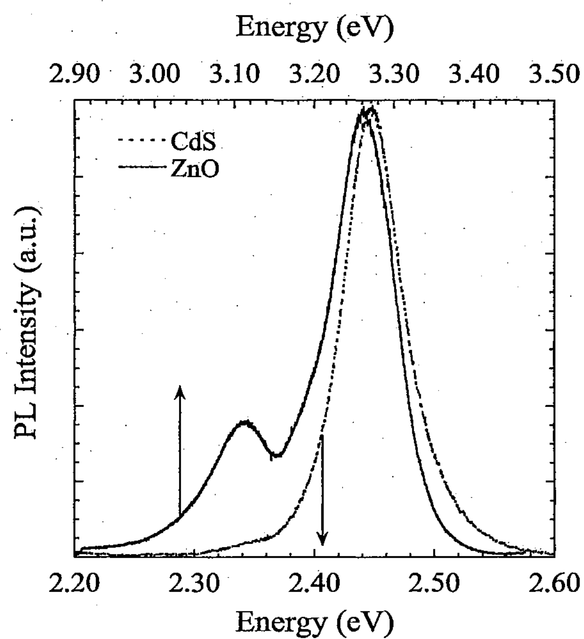


Figure D.1: RT PL comparison between etched (0001) ZnO and etched (0001)-oriented CdS.

# Appendix E

# Operation of PL System

## E.1 $Ar^+$ Laser

The following checklist is not intended as a replacement for proper safety practices. Rather, it is a way to ascertain that the laser is working properly and offers the user a series of steps to follow to ensure reliable operation. For each system, the user should rely on manuals (provided by the manufacturer) located in the laboratory for safe operation.

1. Lock all doors, put on safety spectacles and unlock switchbox.

2. Place the 10 W power meter sensor in front of the laser (at a slight angle) and turn on the power meter.

3. Turn on the heat exchanger (switch to "on" position)

4. Slowly open the valve labeled Lab Chilled Wtr Return.

5. Slowly open the valve labeled Lab Chilled Wtr Supply.

6. Make sure the chilled water is flowing and cold by looking at the flow meter and feeling the supply line. The flow meter should make a vibration noise at startup. The flow valve on the heat exchanger is open and so the flow through the heat exchanger is a maximum.

7. Turn on the main power at the switchbox.

8. Turn the key (for remote box) to the on position (90° cw). The current should rise at 1 A/s after a short delay (5-10 seconds).

9. Allow the laser 20-30 minutes to stabilize. When the laser has stabilized, the beamlock indicator should be centered. The current (power mode) or the power (current mode) should be stabilized.

10. The temperature of the water in the heat exchanger should stabilize at 20°C. The temperature of the supply water should be about 11°C. The flow rate should vary between 2-3.5 gpm. The pressure should vary accordingly between 26-30 psi. The valve on the heat exchanger should begin to close about 5 minutes after starting the heat exchanger and the vibration noise should dissipate. The DI LED should turn from red to green after a few minutes. (If LED stays red, cooling water and filter must be changed in the heat exchanger.)

11. For 125 mW output power with the UV prism, the current should be about 58 A.

12. Remember the following: Don't close the aperture while in power mode. Don't make vertical and/or horizontal adjustments (for the high reflector or the output coupler) while beamlok is on. (Always turn beamlok off when adjusting the beam.) Always close the shutter and turn beamlok off when cleaning or replacing optics in the laser. Refer to the Spectra-Physics manual for specific operation issues for the laser.

13. To shut down the laser, turn the key (remote box) to the off position (90° ccw). Turn off the main power at the switchbox and lock the padlock. Turn off the power meter.

14. Allow the heat exchanger to run at least 10 minutes. After 10 minutes, slowly close the valve labeled Lab Chilled Wtr Supply, then slowly close the valve labeled Lab Chilled Wtr Return. Turn the heat exchanger off (switch to "off").

## E.2 Monochromator

The following checklist is not intended as a replacement for proper safety practices. Rather, it is a way to ascertain that the laser is working properly and offers the user a series of steps to follow to ensure reliable operation. For each system, the user should rely on manuals (provided by the manufacturer) located in the laboratory for safe operation.

1. Monochromator and CCD controller should be left on at all times. If not, the CCD must be initialized prior to pouring liquid nitrogen into the CCD dewar.

2. Launch the Spectramax software. The correct version is loaded on the C drive of "Lumen".

Always launch the software using the shortcut on the desktop. Do not use the default layout. Select the layout (CCD or V1 for the InGaAs detector).

3. For the CCD, make certain controller is on and connected to the detector head before adding liquid nitrogen. Slowly add liquid nitrogen. Stop occasionally to allow the detector to cool. The monochromator must be moved to a new wavelength before the CCD controller will register a temperature.

4. For the InGaAs detector, make certain the head is disconnected from the controller before adding liquid nitrogen. Slowly add liquid nitrogen. Stop occasionally to allow the detector to cool.

5. Remove the entrance slit cap. Make certain the slit height adjustment is closed (pushed all the way in). Check (and set) entrance (and exit, if necessary) slit widths.

6. Occasionally check CCD temperature (if applicable) using visual setup on Spectramax. Allow the CCD to stabilize at 140-150 K (this can take up to an hour).

7. Move the monochromator to desired wavelength position.

8. Turn off all fluorescent lights. Turn on incandescent lights.

9. Open slit height to desired setting.

10. Using RTD, make necessary adjustments to maximize signal. Use incandescent lights for adjustments for RTD measurements. (Fluorescent light have a specific large spectral signal)

11. Switch to Experiment window in Spectramax, prepare data collection information and begin collecting data. Any software settings made in RTD DO NOT translate into the Experiment window. All settings must be made in Experiment window.

12. Remember to select dark offset and linearization (CCD) for data collection.

13. ONLY 8 characters are allowed for the file name in Spectramax.

14. To shut the system down, move grating in monochromator to 500 nm (monochromator wavelength meter should read 10,000 Å).

15. Close slit (using slit height adjustment). Replace cap over slit. Exit from Spectramax. Exit from Instrument Control Center window last. Do not save settings as default.

16. Remember to leave the monochromator controller and the CCD controller on at all times.

## E.3 Cryostat

The following checklist is not intended as a replacement for proper safety practices. Rather, it is a way to ascertain that the cryostat is working properly and offers the user a series of steps to follow to ensure reliable operation. For each system, the user should rely on manuals (provided by the manufacturer) located in the laboratory for safe operation.

1. The first step is to evacuate the two vacuum spaces for use with liquid cryogen. The two volumes are the transfer line and the cryostat. It is best to evacuate the transfer line first.

2. Connect the transfer line to the turbomolecular pump (Pico DRY) and open the valve (CCW) on the transfer line.

3. Once the pump is connected to the transfer line, open the valve on the pump (switch from "SHUT" to "OPEN").

4. Connect the Active Gauge Controller (AGC) to the Active Inverted Magnetron (AIM) pressure gage (red cylinder attached to pump) using the FCC68 (3 m) cable. Connect pressure gage to channel 1 on the AGC.

5. Turn on the AGC. After initializing, the display should read "1 OFF". Make sure units are Torr.

6. Turn on the pump. The green "RUNNING" LED should be lit. After about 3 minutes, the "NORMAL SPEED" green LED should light.

7. IMPORTANT: Once the pump is running, DO NOT move the pump. The rotor is turning at about 90,000 rpm. Any deflection could damage the pump.

8. Once the "NORMAL SPEED" light comes on, press the button on the AGC that has the circular shape next to it on the front panel. This will spark the pressure gage. Once the gage has ignited (should happen very quickly after pressing button), it will display a pressure (in Torr).

9. Allow the pump to run until the desired pressure ($< 2.0 \times 10^{-5}$ Torr) is achieved. For the transfer line this time can vary between 3-6 hours.

10. To achieve better vacuum, use a hair dryer to heat (vaporize) the adsorbed water in the annular space, so that the water vapor can be pumped out faster.

11. After the desired pressure is achieved, very carefully and slowly (without disturbing the hose or transfer line) close the valve on the transfer line (CW). Note: DO NOT disturb the pump during operation! After closing the valve (hand tight), the pressure display will begin to decrease further. This is a good indication that the valve has been closed.

12. Switch off the pump. Turn off the pressure gage (by pressing the same button with the circular shape next to it) before the pressure increases to $7.5 \times 10^{-3}$ Torr. The spin down times are: a.) After about 1.5 minutes, the "NORMAL SPEED" light turns off. b.) After about 3 minutes, the "FAIL" light turns on. c.) After about 3.5 minutes, the "FAIL" light turns off. d.) After about 6.5 minutes, the pump passes through a natural frequency and the pump makes a slight vibration noise.

13. Wait for at least 1 hour after shutting down the pump, before disconnecting or moving the pump to ensure it has stopped spinning.

14. After about 1 hour, close the valve on the pump (switch from "OPEN" to "SHUT"). Disconnect the transfer line from the pump.

15. Connect the pump to the cryostat and open the valve on the cryostat.

16. Once the pump is connected to the cryostat, open the valve on the pump (switch from "SHUT" to "OPEN").

17. Connect the Active Gauge Controller (AGC) to the Active Inverted Magnetron (AIM) pressure gage and turn on the AGC.

18. Turn on the pump. After the "NORMAL SPEED" light comes on, turn on the AIM pressure gage. Allow the pump to run until the desired pressure ($\sim 2.0 \times 10^{-5}$ Torr) is achieved. For the cryostat, this time can vary between 1-4 hours.

19. After the desired pressure is achieved, very carefully and slowly (without disturbing the hose or cryostat) close the valve (hand tight) on the cryostat.

20. Switch off the pump. Turn off the pressure gage (by pressing the same button with the circular shape next to it) before the pressure increases to $7.5 \times 10^{-3}$ Torr. The spin down times are: a.) After about 1.5 minutes, the "NORMAL SPEED" light turns off. b.) After about 3 minutes, the "FAIL" light turns on. c.) After about 3.5 minutes, the "FAIL" light turns off. d.) After about 6.5 minutes, the pump passes through a natural frequency and the pump makes a slight vibration noise.

21. Wait for at least 1 hour after shutting down the pump, before disconnecting or moving the pump to ensure it has stopped spinning.

22. After about 1 hour, close the valve on the turbo pump (switch from "OPEN" to "SHUT"). Disconnect the cryostat from the pump.

23. Turn off the AGC and disconnect from the AIM gage.

24. Both vacuum spaces (transfer line and cryostat) are ready for low temperature studies.

25. Connect the temperature controller to the cryostat using 10-pin feed-thru. Turn on the temperature controller. After initializing, the controller should read about 296 K.

26. Refer to Janis Research Manual for subsequent instructions for low temperature operation.

## E.4 Low Temperature PL Procedure

1. Mount sample. Using aluminum clip, place sample onto optical mount. Attach optical mount to cold finger and insert assembly into the vacuum jacket. Make certain to wear gloves when handling the optical mount.

2. Prepare monochromator and detector. Pour liquid nitrogen into detector and allow detector to cool to 140 K (cooling can take nearly an hour). Move grating to wavelength of interest. See "Operating the monochromator and detectors" for startup and shutdown procedure. [Note: After launching the software (Spectramax), the monochromator must be moved to a new wavelength before the CCD controller will register a temperature.]

3. Start laser. Initially the laser will be used to align the sample with the entrance slit of the monochromator. See "Operating the laser" for startup procedure. Make certain to allow enough time for the laser to warm up ($\sim$1 hour).

4. Adjust orientation of sample (within shroud) for optimum signal into the monochromator. Fasten clamp on shroud once sample is in place.

5. Perform RT PL to ensure proper alignment of sample for good signal. This will provide a good baseline for the low temperature data. Record the temperature from controller during experiment.

6. Use turbomolecular pump to evacuate cryostat vacuum jacket. The transfer line should already be evacuated. If not, evacuate transfer line prior to using. See section on cryostat for startup and shutdown procedure.
7. Refer to Janis Research Manual for subsequent instructions for low temperature operation.
8. Collect PL data for temperatures of interest. Afterward, shut down cryostat using instructions from Janis Research's operating manual.
9. Shut down spectrometer. See section on monochromator.
10. Shut down the laser. See section on $Ar^+$ laser.

# Appendix F

# Arrhenius Plot

The intensity $(I)$ for many of the luminescence peaks from ZnO varies with temperature $(T)$ according to Arrhenius' equation. This is expressed as:

$$I = Cexp\left(\frac{-E_A}{k_B T}\right) \tag{F.1}$$

where $E_A$ is the thermal activation energy and $C$ is a proportionality constant. Taking the natural logarithm of both sides results in:

$$\ln(I) = \hat{C} - \left(\frac{E_A}{k_B}\right)\frac{1}{T} \tag{F.2}$$

Comparing this result to an equation for a straight line, $y = mx + b$, we see that $\frac{E_A}{k_B}$ represents the slope of the natural logarithm of intensity $(I)$ as a function of inverse temperature $(1/T)$. From a plot of the natural logarithm of intensity $(I)$ as a function of inverse temperature $(1/T)$, we can then use the slope of the resulting linear portion of the data to determine an activation energy for any PL peak that is observed to be thermally quenched with increasing temperature.

# Appendix G

# FX Line Broadening

Using the notation developed in [102], the predicted difference in emission and absorption energy, as discussed in Chapter 2, is computed. The emission lineshape $\{R_{sp}\}$ is assumed to be proportional to the product of the absorption lineshape $\{S(\hbar\omega - E_x)\}$ and the exponential dependence of the luminescence lineshape $\{exp\,(-\hbar\omega/k_BT)\}$ [102], shown as Eqn. (G.1).

$$R_{sp} \propto S(\hbar\omega - E_x) exp\,(-\hbar\omega/k_BT) \tag{G.1}$$

## G.1 Lorentzian Lineshape

For a Lorentzian absorption lineshape as given by Eqn. (G.2),

$$S(\hbar\omega - E_x) = (\hbar\Gamma/2\pi)/\left\{[\hbar\omega - E_x]^2 + (\hbar\Gamma/2)^2\right\} \tag{G.2}$$

the emission lineshape, using Eqns. (G.1) and (G.2), is given by:

$$R_{sp} \propto exp\,[-\hbar\omega/k_BT]\,(\hbar\Gamma/2\pi)/\left\{[\hbar\omega - E_x]^2 + (\hbar\Gamma/2)^2\right\} \tag{G.3}$$

By taking the derivative of Eqn. (G.3) wrt $\hbar\omega$ and setting the result equal to zero, one obtains:

$$\left[(\hbar\omega - E_x)^2 + \left(\frac{\hbar\Gamma}{2}\right)^2\right]\left(-\frac{1}{k_BT}\right) = 2(\hbar\omega - E_x) \tag{G.4}$$

Solving for $\hbar\omega$, yields two solutions:

$$(\hbar\omega)_{1,2} = E_x - k_BT \pm \sqrt{(k_BT)^2 - \left(\frac{\hbar\Gamma}{2}\right)^2} \tag{G.5}$$

The solution $(\hbar\omega)_2 = E_x - k_BT - \sqrt{(k_BT)^2 - \left(\frac{\hbar\Gamma}{2}\right)^2}$ is discarded because it results in energy differences larger than the linewidth of emission peak at higher temperatures. Therefore, the predicted difference ($\delta$) between the energy of the measured free exciton emission peak ($\hbar\omega$) and the true (i.e., absorption) free exciton energy ($E_x$) is given by Eqn. (G.6)

$$\delta = \hbar\omega - E_x = -k_BT + \sqrt{(k_BT)^2 - \left(\frac{\hbar\Gamma}{2}\right)^2} \tag{G.6}$$

where the negative sign indicates that the energy of luminescence is less than the absorption energy for the FX peak.

## G.2 Gaussian Lineshape

For a Gaussian lineshape as given by Eqn. (G.7),

$$S(\hbar\omega - E_x) = \left(1/(2\pi)^{1/2}\sigma\right) exp\left[-(\hbar\omega - E_x)^2/2\sigma^2\right] \tag{G.7}$$

the emission lineshape, using Eqns. (G.1) and (G.7), is given by:

$$R_{sp} \propto exp\left[-\hbar\omega/k_BT\right] exp\left[-(\hbar\omega - E_x)^2/2\sigma^2\right] \tag{G.8}$$

By taking the derivative of Eqn. (G.8) wrt $\hbar\omega$ and setting the result equal to zero, one obtains:

$$\frac{1}{k_BT} = \frac{E_x - \hbar\omega}{\sigma^2} \tag{G.9}$$

Solving for $\hbar\omega - E_x$, yields:

$$\delta = \hbar\omega - E_x = -\frac{\sigma^2}{k_BT} \tag{G.10}$$

Using a value of $\sigma = 0.425\Gamma$ as quoted by [99] where $\Gamma$ is the FWHM of the measured peak, we obtain a predicted difference ($\delta$) between the measured free exciton energy ($\hbar\omega$) and the true (i.e.,

absorption) free exciton energy ($E_x$) of:

$$\delta = \hbar\omega - E_x = -\frac{0.181(\Gamma)}{k_B T} \tag{G.11}$$

where the negative sign indicates that the energy of luminescence is less than the absorption energy for the FX peak. These results suggest that the energy difference between the measured free exciton peak position and the true value of its position is a function of the absorption lineshape and temperature.

# Appendix H

# Temperature Dependent LO Phonon-assisted FX Luminescence

Momentum selection rules dictate that only those excitons with nearly zero kinetic energy can radiatively recombine [102]. Excitons with nonzero kinetic energy can recombine via exciton-phonon interaction, however. Emission from such transitions is referred to as phonon-assisted luminescence. For phonon-assisted FX luminescence, the peak position is a function of the number of phonon interactions (e.g., one or two) and temperature. Increased temperature is known to increase the total exciton kinetic energy. Because the total exciton energy depends in part on the exciton kinetic energy, the energy of the phonon-assisted FX transition ($\hbar\omega$) is increased by the kinetic energy distribution of the excitons ($uk_BT$) as given in Eqn. (H.1) [102].

$$\hbar\omega = E_x - m\hbar\omega_{LO} + uk_BT \tag{H.1}$$

where the value of $u$ is either 3/2 for a one LO phonon assisted transition ($m = 1$) or 1/2 for a two LO phonon assisted transition ($m = 2$) as shown below.

## H.1 One LO Phonon-assisted FX Luminescence

From Bebb and Williams [102], the spectral photon flux $F(\hbar\omega)$ for the emission from a one LO phonon assisted FX transition is:

$$F(\hbar\omega) \propto (\hbar\omega - E_x + \hbar\omega_{LO})^{3/2}\, exp\left(-\frac{\hbar\omega - E_x + \hbar\omega_{LO}}{k_B T}\right) \tag{H.2}$$

By setting the derivative of Eqn. (H.2) wrt $\hbar\omega$ equal to zero, one obtains:

$$\frac{3}{2}(\hbar\omega - E_x + \hbar\omega_{LO})^{1/2} = (\hbar\omega - E_x + \hbar\omega_{LO})^{3/2}\left(\frac{1}{k_B T}\right) \tag{H.3}$$

Solving for $\hbar\omega$ yields:

$$\hbar\omega = E_x - \hbar\omega_{LO} + \frac{3}{2}k_B T \tag{H.4}$$

## H.2 Two LO Phonon-assisted FX Luminescence

A similar analysis for the emission from a two LO phonon assisted transition can also be performed. Form Bebb and Williams [102], the spectral photon flux for the two LO phonon transition is:

$$F(\hbar\omega) \propto (\hbar\omega - E_x + 2\hbar\omega_{LO})^{1/2}\, exp\left(-\frac{\hbar\omega - E_x + 2\hbar\omega_{LO}}{k_B T}\right) \tag{H.5}$$

By setting the derivative of Eqn. (H.5) wrt $\hbar\omega$ equal to zero, one obtains:

$$\frac{1}{2}(\hbar\omega - E_x + 2\hbar\omega_{LO})^{-1/2} = (\hbar\omega - E_x + 2\hbar\omega_{LO})^{1/2}\left(\frac{1}{k_B T}\right) \tag{H.6}$$

Solving for $\hbar\omega$ yields:

$$\hbar\omega = E_x - 2\hbar\omega_{LO} + \frac{1}{2}k_B T \tag{H.7}$$

Figure H.1 illustrates the convergence of the FX and FX-1LO peak energies with increasing temperature. The energy separation between the FX and FX-2LO peaks exhibits only a weak temperature dependence.

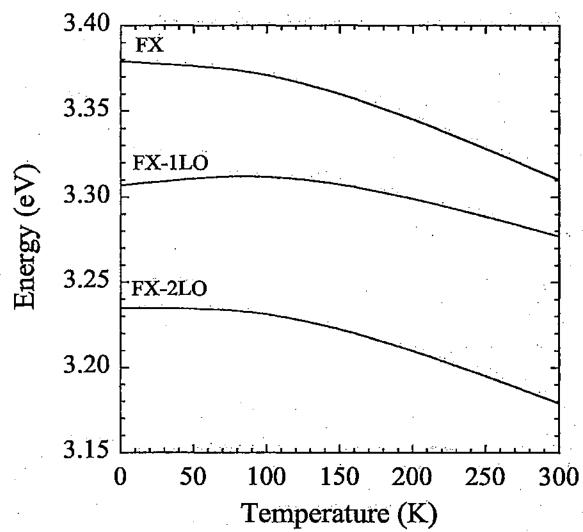


Figure H.1: Temperature dependent FX, FX-1LO and FX-2LO peak positions for 0-300 K. The FX curve is from Ref. [171], the FX-1LO and FX-2LO curves are from Eqns. (H.4) and (H.7), respectively.

# Appendix I

# Photoelectrochemical Etching

## I.1 Literature Review

Compared to dry etching techniques, photelectrochemical (PEC) wet etching has many advantages. First, material removal is achieved without damaging the near surface of the wafer. Whereas dry etching uses accelerated, high-energy ions coupled with a chemical etching component to remove material [195] resulting in layers of damaged material, PEC relies only on the oxidative dissociation of the semiconductor [196]. Second, the surface stoichiometry is preserved [197]. This is an important advantage as dry etching can result in significant stoichiometric changes in the near surface affecting device performance [198]. For these reasons, PEC wet etching has tremendous potential as either a complementary tool in the near surface characterization of ZnO or as a final surface preparation prior to epitaxy. PEC is currently used in the fabrication of many devices including waveguide filters [199], laser facets [200], and MESFETs [201] and has been used on a variety of compound semiconductors including GaN [202], GaAs [203], InP [203] and SiC [204]. The photoenhanced etching setup consists of a simple electrochemical cell, described in [196], a light source with energy above the band gap of the semiconductor (e.g., Hg lamp or $Ar^+$ laser), and a dilute concentration of an acid or base as the electrolyte. Typically, a portion of the sample is metalized to form an electrical contact to the material. The mask can also serve in the patterning of the substrate for depth characterization. A bias may also be applied to the sample to facilitate etching.

The earliest published work on PEC etching of GaN [202] compared the room temperature etching of GaN films in HCl:$H_2O$ (1:10) to that of the films in a solution of 45% KOH:$H_2O$ (1:3). The films were unintentionally doped n-type of thickness (1-2 $\mu$m) grown by MOCVD on sapphire substrates. The masking layer was formed from Ti (200 nm) and was annealed after deposition to form

a good contact with the film. No bias was applied during any of the etching experiments. Using a He-Cd laser (325 nm) with a power density of 0.57 $W/cm^2$, etch rates in HCl were reported to be 40 nm/min for the masked film compared to 1.5 nm/min for the unmasked film. Etch rates in KOH were 400 nm/min for masked films. The differences in etch rates for the masked versus the unmasked samples in HCl was attributed to the efficient extraction of electrons in the masked sample resulting in a substantial increase in the etch rate. Although the exact reactions for GaN remain unclear, etching was reported to take place photoelectrochemically with electrons and holes generated by the UV illumination enhancing the oxidation and reduction reactions in the cell. To verify the photoenhanced effect, a "dark" etch was performed using masked samples in HCl and KOH without UV illumination. No significant etching of either sample was observed. Experiments were also conducted using a sub-bandgap illumination (He-Ne laser) of the film in each electrolyte. No significant etching was observed. Lu et al. [205] used photoassisted anodic etching with a Hg lamp and an aqueous solution of tartaric acid and ethylene glycol to achieve etch rates of 2-160 nm/min for unintentionally doped n-type GaN. The samples were patterned with wax and attached to a polypropylene plastic sheet in the electrochemical cell. The roughness of the etched surface was reported to be 81.5 nm. "Dark" etch experiments were also conducted to verify the photoenhanced mechanism. No measurable etching was observed after the sample had been immersed for 24 hours without UV illumination. One significant advantage of the PEC etching technique on GaN is its high anisotropy. With an etching apparatus that consisted of a Teflon base for the sample, a Ni washer to fasten the sample to the base, and a Pt wire as the cathode in the electrochemical cell, Youtsey et al. [206] demonstrated highly anisotropic etch profiles (approximately 3.5 $\mu$m) with etch rates exceeding 300 nm/min on n-type GaN. The UV illumination was from an unfiltered Hg lamp (5-50 $mW/cm^2$ at 365 nm) and no bias was applied for the etching process. Using standard metal lift-off techniques, 100 nm of Ti was patterned on the surface of the GaN to provide electrical contact to the sample and an etch mask. In contrast to [202], the Ti metal contacts were not annealed. It was observed that less than 100 nA flowed without sample illumination, corresponding to a negligible etch rate ($<$10 nm after 12 h). After illuminating the sample with UV light, the photocurrent increased rapidly to approximately 30 mA, then steadily decreased (approximately exponentially) for the remainder of the etching process (30 min duration) and ceased when the light was removed. Using Faraday's law of electrolysis, it was reported that the current flow in the electrochemical cell was proportional to the reaction rate at the semiconductor/electrolyte interface, and therefore provided an instantaneous measure of the etch rate of the GaN film. One plausible explanation given for the decreasing current over time was a decrease in etch rate due to variations in material

quality of the epilayer at increasing depths. The anisotropy of the etching process was, in part, due to the collimation of the incident light, but may also have been due to the high density of vertical dislocations present in the film. Additionally, during etching, bubbles were observed on the sample surface. The authors believed that this was due to the release of $N_2$. No bubbles were reported in the absence of sample illumination. In a similar study, Peng et al. [207] studied the effect of varying the pH (-1 to 15) of the electrolyte (KOH and $H_3PO_4$) on the PEC etch process of n-type GaN using a deep UV (253.7 nm) light source. Peak etch rates of 125 and 90 nm/min were observed for $H_3PO_4$ (pH=0.75) and KOH (pH=14.25) solutions, respectively. From the SEM micrographs, the etched surfaces could be characterized as extremely rough. For PEC etching to become truly important and useful in the fabrication of devices it must be able to facilitate the characterization of defects in the semiconductor or it must exhibit a capability of rendering smooth surfaces while removing subsurface damage for subsequent film growth or laser facets. Recently, a comparison was made between conventional etching techniques for GaN (molten bases, hot $H_2SO_4/H_3PO_4$) and the PEC etching in aqueous KOH solutions as a means for defect characterization [208]. Whereas, the conventional methods result in the formation of etch pits on the dislocation sites, the PEC method results in the formation of protruding pillars instead of pits. Experiments were performed using single crystal GaN and homoepitaxial epilayers grown by MOCVD. The PEC technique used a 0.02 M KOH solution and a Hg lamp to illuminate the electrochemical cell. Subsequent characterization of etched samples was performed using differential interference contrast (DIC) optical microscopy, scanning electron microscopy (SEM), atomic force microscopy (AFM) and transmission electron microscopy (TEM). Initial PEC experiments performed on Ga- and N-polar heteroepitaxial films exhibited no substantial differences in the surface morphology. The density of the protruding etch pillars showed correlation with the density of dislocations established using cross-sectional TEM of the same material. It was suggested that the conventional etching techniques are more suitable for the study of defects within bulk GaN single crystals due to the low defect density. For the epilayers (particularly the heteroepitaxial films), the PEC method is preferable for revealing the dislocations. Others have also reported the usefulness of the PEC method for defect characterization. Youtsey [209] was one of the first to report this "whisker" formation on the surface of GaN after PEC etching. One possible mechanism for the whisker formation was related to the electrical activity at the dislocations. For example, the dislocations may introduce nonradiative recombination centers, resultant from dangling bonds or impurities gettered from the bulk, that locally decrease the hole concentration at the surface. This reduction in hole concentration then reduces the etch rate at dislocations. TEM analysis showed that dislocations inhibited the PEC etching of GaN. TEM anal-

ysis also showed good agreement of dislocation density with PEC etched whiskers. In a subsequent study, Youtsey [210] observed a one-to-one correspondence between the surface pits (prior to etching) identified by AFM, and the whiskers that were subsequently formed by photoenhanced wet etching of the identical region of the GaN sample. It was reported that the formation of the whiskers was associated with both edge and mixed character dislocations. The selective etching only occurred for very specific process conditions resulting in high etch selectivity at the dislocations. For electrolyte concentrations below the threshold (0.001 M KOH), strongly diffusion-limited etching would occur and result in a smooth etched surface (1.5 nm rms) [211]. The close correspondence between the etched pillars and threading dislocations was confirmed using TEM and AFM analysis. PEC etching shows promise in revealing different types of dislocations in epilayers. One advantage is that even those layers with high dislocation densities can be evaluated [208]. Another significant advantage of PEC etching is the smoothness of the resulting surfaces that achievable. This is particularly important when using this technique as a pre-growth subsurface preparation method for substrates.

As mentioned previously, for very specific processing parameters, namely the concentration of the electrolyte and the intensity of the illumination, very smooth surfaces are achievable using PEC etching. Using external bias voltage, Stocker and Schubert [212] demonstrated a reduction in surface roughness of PEC etched GaN surfaces from 170 nm (rms) to a minimum of 20 nm (rms) as the bias voltage was increased from 0 to 2.5 V and the KOH concentration was reduced from 1.0 to 0.01 M. Etch rates were reported as high as 400 nm/min at room temperature. Another novel technique for achieving smooth surfaces is the use of ultrasonic treatment after PEC etching to remove the whiskers mentioned above [213]. Etching rates were reported to be 20 nm/min with an rms surface roughness of 0.9 nm (after ultrasonic agitation) as compared to 0.98 nm obtained using RIE for the same $n$-GaN. The roughness is the best reported to date for PEC-etched surfaces and demonstrates the usefulness of the technique to achieve device quality etched surfaces over a large area.

## I.2 Preliminary Results

Our group is attempting to develop photoelectrochemical etching (PEC) as a means for damage depth profiling of the polished substrates, as well as for a possible final surface preparation technique prior to film growth. Initial studies of photoelectrochemical etching (PEC) have been performed. A typical electrolytic cell similar to the one reported in [206] and shown in Fig. I.1 was used. The cell includes ZnO as the working electrode (anode), Pt wire as the counter electrode (cathode) and a Ag/AgCl reference electrode to measure the applied bias to the working electrode. All three

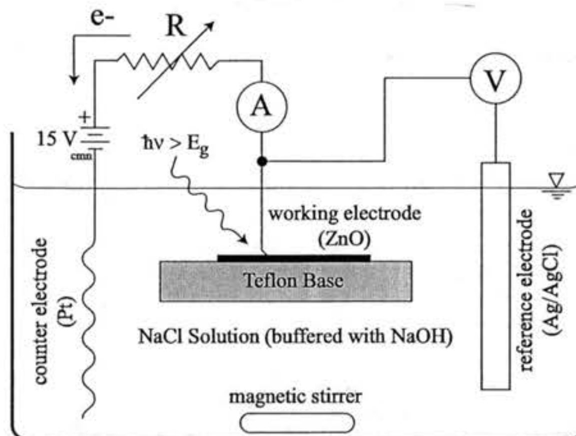


Figure I.1: PEC setup

electrodes are immersed in an aqueous solution (electrolyte) of a prescribed pH. UV excitation was used to create the needed minority carriers (holes) for etching. The variables investigated were: electrolyte type, electrolyte concentration, applied bias, electrolyte pH, and UV light intensity. Initial experiments were conducted to determine the best choice for electrolyte. Electrolytes selected for investigation in this study include aqueous solutions of KOH, $Na_2SO_4$, KCl, and NaCl with molarities ranging from 0.001 to 0.5 M. All chemicals used in this study were of reagent grade. Consistent with reports found in the literature [214], we have observed the best results using aqueous NaCl buffered with NaOH to a pH of about 12. Comparisons were then made for a range of UV light intensities from about 10-100 mW using either a Hg lamp, or a HeCd laser. Preliminary results indicate the best choice to be the Hg lamp with about 25 mW excitation power. The Hg lamp has a relatively smooth spatial intensity profile, as compared to the multimode HeCd laser, which has a highly non-uniform intensity profile. This uniform intensity profile of the Hg lamp lends itself to a more level etch. Whereas early results are mixed, we do believe anodic etching of the ZnO electrode has occurred. An increase in electrolytic cell current has been measured with exposure to UV light, indicative of the necessary photo-effect for PEC. Etching appears to be limited to the spot on the sample from the Hg lamp. Preliminary results indicate an etch rate of about 1 $\mu$m/min. Long etch times on the order of 30 minutes have resulted in extremely rough, pitted surfaces. Recently, we have observed a significant improvement of surface roughness by decreasing the amount of time the sample is etched. From a recent experiment, using NaCl as the electrolyte, a sample etched for only two minutes exhibited a surface roughness of about 13 nm rms as measured by atomic force microscopy (AFM). From scanning electron microscopy (SEM) results, for the same etched

sample, we observe a small amount of crystallographic (hexagonal) pitting near the edge of the etched region, with an even distribution of approximately 10 $\mu$m-sized features that initially appear to protrude from the surface. In between these apparent protrusions, however, the surface appears quite smooth. Further investigation is required to determine the nature of these 10 $\mu$m features and causes for pitting near the edge of the etch. Another important variable controlling etch rate and, perhaps, surface finish is the applied bias. By applying a bias to ZnO, the band bending at the surface can be manipulated, thereby controlling the diffusion of holes to the surface. These holes are believed to be the carriers that participate in the anodic etching of ZnO. We have observed a large increase in the measured current, which is related to the etch rate of ZnO, by increasing the applied bias to ZnO. Applied bias conditions have ranged from 0.5 V to 2 V resulting in 300 $\mu$A to 3 mA of current. Clearly much work in this area remains. Alternative methods for improving the ohmic contact between the cathode (Pt wire) wire and the anode (ZnO substrate) must be determined. In addition, new techniques for insulating the metal-to-semiconductor junction should be sought. We believe that improved ohmic contact and higher insulation for this junction will result in more consistent etch results. Future work should also include quantifying material removal rates for higher applied bias voltages and characterization of resulting etched surfaces using axial ion channeling, photoluminescence and scanning electrical techniques. With improved parameter selection and the proper control of all of the parameters, PEC wet etching has potential as a defect characterization tool as well as a complimentary technique for damage depth profiling. PEC also offers the possibility of a final substrate surface preparation technique prior to epitaxial growth.

# Appendix J

# PL of Si Implanted $SiO_2$

## J.1 Literature Review

Quoting from a very recent Nature addendum [215] "It is now becoming clear that crystalline silicon, when appropriately engineered, is capable of supporting efficient light emission, opening up many significant applications". Several methods have been employed to create silicon-based materials that luminescence in the visible. Such methods include: stain [216] and photochemical etching of Si [217] to create porous silicon (PS), boron implantation of Si [218], hydrogen implantation and annealing of Si [219] pressure annealing Si [220], and Si/Ge multilayers [221] among many others. Today much of the PS is created by etching in an HF solution referred to as stain etching. Observations of luminescence from PS layers have generated significant interest as researchers attempt to capitalize on the possibility of creating novel optoelectronic devices using current microchip fabrication techniques [216].

Whereas reports of visible luminescence from PS dominate the recent literature, PS does have some serious deficiencies that include fragility, high reactivity, spontaneous oxidation in air and unstable luminescence that degrades over time [222]. Creation of PS also poses serious health risks as poisonous $NO_x$ gas is created by the chemical reaction that forms PS [217]. Additionally, the luminescence mechanism for PS layers is still not clearly understood. Some researchers have reported that the visible luminescence is related to defects in the near surface [222], while others report quantum confinement [223] as the principal cause. There are reports in the literature of visible luminescence from Si other than PS. It has been demonstrated that ion implanted Si nanocrystals in a $SiO_2$ matrix exhibit visible luminescence [224–227]. The characteristic wavelength of emission has been shown to be a function of dosage of Si ions, but independent of annealing time and excitation

energy [224]. Other studies,however, have shown the characteristic luminescence wavelength to be dependent on the annealing conditions [228] and the size of the Si nanocrystals [229].

## J.2 Preliminary Results

In a collaborative investigation with LANL we have performed some initial experiments on Si implanted $SiO_2$ using RT PL as shown in Fig. J.1. Shown are RT PL curves for four implanted samples with different annealing conditions and an unimplanted sample. The four implanted samples are identified as follows: room temperature Si implanted $SiO_2$ without annealing (RT), hot temperature Si implanted $SiO_2$ without annealing (Hot), room temperature Si implanted $SiO_2$ annealed at 1000 C (RT1000), hot temperature Si implanted $SiO_2$ annealed at 1000 C (Hot1000). The specific experimental parameters are not reported, however from these preliminary results we can report some interesting observations. Most important, we do observe a dependence of the Si luminescence wavelength on annealing conditions, with the RT1000 sample exhibiting the strongest luminescence at about 1.6 eV, as compared to no luminescence at this same energy prior to annealing. Our results are consistent with those reported in the literature. Future work will focus on the variation of wavelength emission with Si nanocrystal size.

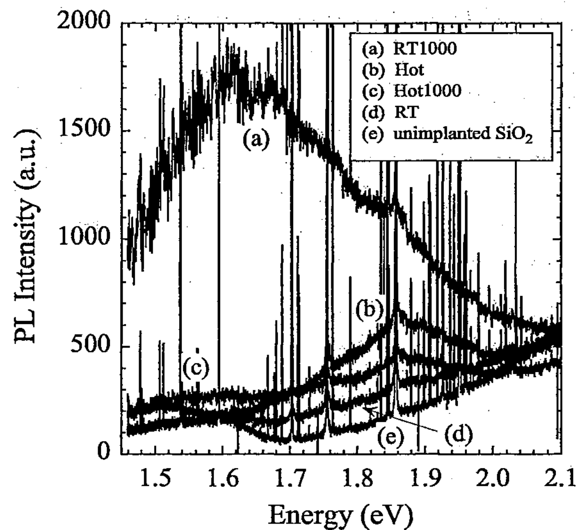


Figure J.1: RT PL comparison of four Si implanted, annealed $SiO_2$ samples.

# Appendix K

# List of Abbreviations

| | |
|---|---|
| AFM | atomic force microscopy |
| BX | bound exciton |
| CAIBE | chemically assisted ion beam etch |
| CCD | charge-coupled device |
| CL | cathodoluminescence |
| cw | continuous wave |
| DAP | donor-acceptor pair |
| DIC | differential interference contrast |
| DL | deep level |
| EHP | electron-hole pair |
| EP | Eagle-Picher Technologies |
| ERD | elastic recoil detection |
| FX | free exciton |
| GDMS | glow discharge mass spectrometry |
| HX | hot exciton |
| IR | infrared |
| LD | laser diode |
| LED | light emitting diode |
| LO | longitudinal optical |
| LPB | lower polariton branch |
| MOCVD | metal-organic chemical vapor deposition |
| MOVPE | metal-organic vapor-phase epitaxy |

| | |
|---|---|
| MW | Manoogian-Woolley |
| NBE | near band edge |
| PEC | photoelectrochemical |
| PL | photoluminescence |
| PS | porous silicon |
| RRS | resonant Raman scattering |
| RT | room temperature |
| SAW | surface acoustic wave |
| SCVT | seeded chemical vapor transport |
| SEM | scanning electron microscopy |
| TEM | transmission electron microscopy |
| TES | two-electron satellite |
| TO | transverse optical |
| UPB | upper polariton branch |
| UV | ultraviolet |
| XPS | X-ray photoelectron spectroscopy |

(2)

# VITA

David William Hamby

Candidate for the Degree of

Doctor of Philosophy

Thesis: EFFECTS OF SUBSURFACE DAMAGE ON THE PHOTOLUMINESCENCE OF ZnO

Major Field: Mechanical Engineering

Biographical:

Personal Data: Born in Dodge City, Kansas, February 23, 1969. Married to Jennifer Anne McMurtry on October 5, 1996. Proud father of Emily Anne Hamby, born September 2, 2002.

Education: Graduated from Putnam City West High School, Oklahoma City, Oklahoma, in May 1987. Received the Bachelor of Science degree in Mechanical Engineering from Oklahoma State University in July, 1991. Received the Master of Science degree in Mechanical Engineering from Virginia Polytechnic Institute and State University in August, 1993. Completed the requirements for the Doctor of Philosophy degree with a major in Mechanical Engineering at Oklahoma State University in December, 2003.

Experience: Open-hole logging engineer, Halliburton Energy Services, 1993-1995; mechanical engineer, Electric Submersible Pumps, Inc., 1995-1997; graduate research assistant, Oklahoma State University, August 1997 to December 2003.

Professional Memberships: Student Member of American Society for Precision Engineering, Student member of Sigma Xi